Geochemical characteristics of West Molokai shield- and postshield-stage lavas: Constraints on Hawaiian plume models

Guangping Xu, Frederick Frey, David Clague, Wafa Abouchami, Janne Blichert-Toft, Brian Cousens, Marshall Weisler

Geochemistry Geophysics Geosystems G3
AN ELECTRONIC JOURNAL OF THE EARTH SCIENCES
Published by AGU and the Geochemical Society

Article
Volume 8, Number 8
21 August 2007
Q08G21, doi:10.1029/2006GC001554
ISSN: 1525-2027

Geochemical characteristics of West Molokai shield- and postshield-stage lavas: Constraints on Hawaiian plume models

Guangping Xu and Frederick A. Frey
Department of Earth, Atmospheric, and Planetary Sciences, Massachusetts Institute of Technology, Room 54-1226, Cambridge, Massachusetts 02139, USA (gpxu@mit.edu)

David A. Clague
Monterey Bay Aquarium Research Institute, 7700 Sandholdt Road, Moss Landing, California 95039, USA

Wafa Abouchami
Max-Planck-Institut für Chemie, Postfach 3060, D-55020 Mainz, Germany

Now at An der Sandflora 5, D-55122 Mainz, Germany

Janne Blichert-Toft
Ecole Normale Superieure de Lyon, UMR CNRS 5570, Lyon, France

Brian Cousens
Ottawa-Carleton Geoscience Centre, Department of Earth Sciences, Carleton University, Ottawa, Ontario, Canada K1S 5B6

Marshall Weisler
School of Social Science-Archaeology Program, University of Queensland, St Lucia, Queensland 4072, Australia

[1] There are systematic geochemical differences between the <2 Myr Hawaiian shields forming the subparallel spatial trends, known as Loa and Kea. These spatial and temporal geochemical changes provide insight into the spatial distribution of geochemical heterogeneities within the source of Hawaiian lavas, and the processes that create the Hawaiian plume. Lavas forming the ~1.9 Ma West Molokai volcano are important for evaluating alternative models proposed for the spatial distribution of geochemical heterogeneities because (1) the geochemical distinction between Loa and Kea trends may end at the Molokai Fracture Zone and (2) West Molokai is a Loa-trend volcano that has exposures of shield and postshield lavas. This geochemical study (major and trace element abundances and isotopic ratios of Sr, Nd, Hf, and Pb) shows that the West Molokai shield includes lavas with Loa- and Kea-like geochemical characteristics; a mixed Loa-Kea source is required. In contrast, West Molokai postshield lavas are exclusively Kea-like. This change in source geochemistry can be explained by the observed change in strike of the Pacific plate near Molokai Island so that as West Molokai volcano moved away from a mixed Loa-Kea source it sampled only the Kea side of a bilaterally zoned plume.

Components: 21,199 words, 19 figures, 9 tables.

Keywords: West Molokai; shield stage; postshield stage; Sr, Nd, Hf, Pb isotopes; trace element.

Index Terms: 1037 Geochemistry: Magma genesis and partial melting (3619); 1038 Geochemistry: Mantle processes (3621); 1025 Geochemistry: Composition of the mantle.

Received 12 December 2006; **Revised** 13 June 2007; **Accepted** 21 June 2007; **Published** 21 August 2007.

Xu, G., F. A. Frey, D. A. Clague, W. Abouchami, J. Blichert-Toft, B. Cousens, and M. Weisler (2007), Geochemical characteristics of West Molokai shield- and postshield-stage lavas: Constraints on Hawaiian plume models, *Geochem. Geophys. Geosyst.*, *8*, Q08G21, doi:10.1029/2006GC001554.

Theme: Hawaii Scientific Drilling Project
Guest Editors: D. DePaolo, E. Stolper, and D. Thomas

1. Introduction

[2] The processes that create long-lived sources of hot spot-derived magma, i.e., a mantle plume, are reflected in the geochemical characteristics of the magmas. First order results are the well known geochemical differences between ocean island and mid-ocean ridge basalts and the geochemical diversity of ocean island basalts [e.g., *Hofmann*, 2004]. Most recently the recognition of systematic spatial and temporal geochemical variations in Hawaiian basalts have provided constraints on the processes that create the Hawaiian plume [*Abouchami et al.*, 2005; *Bryce et al.*, 2005; *Ito and Mahoney*, 2005; *Ren et al.*, 2005].

[3] Recent Hawaiian volcanoes define two subparallel trends, Kea and Loa, and according to *Jackson et al.* [1972], East Molokai is on the Kea trend while West Molokai is a Loa trend volcano (Figure 1a). *Hieronymus and Bercovici* [2001] evaluated the physical parameters that lead to subparallel chains of volcanoes and the spacing of volcanoes along these chains. They argued that a double chain of volcanoes, the Kea and Loa trends, can form during periods of high plume flux, i.e., a wide plume stress region. Alternatively, a double chain of volcanoes can arise from an off axis volcanic load created by a change in relative motion of the hot spot and overriding plate [*DePaolo et al.*, 2001; *Hieronymus and Bercovici*, 2001].

[4] Lavas forming Loa- and Kea-trend volcanoes differ in major and trace element abundances and isotopic ratios of Sr, Nd, Hf and Pb [e.g., *Lassiter et al.*, 1996]; one of the most reliable discriminants is higher $^{208}Pb/^{204}Pb$ at a given $^{206}Pb/^{204}Pb$ for Loa volcanoes compared with Kea volcanoes [e.g., *Tatsumoto*, 1978; *Abouchami et al.*, 2005]. A popular hypothesis is that Loa and Kea volcanoes sample different parts of a plume that is geochemically zoned in cross section [e.g., *Lassiter et al.*, 1996; *Abouchami et al.*, 2005; *Bryce et al.*, 2005] (Figure 2), but *Blichert-Toft et al.* [2003] emphasized that vertical heterogeneities within the plume are also important. A complication to the zoned models (Figure 2) is that Loa-like lavas occur in at least two Kea volcanoes: Mauna Kea [e.g., *Eisele et al.*, 2003] and Haleakala [*Ren et al.*, 2006]. To explain this complexity, *Ren et al.* [2005] and *Herzberg* [2005] proposed that on a <1 km scale, both Loa and Kea sources are present but that on ~20 km scale, depending upon location, either Loa or Kea sources dominate (Figure 2d).

[5] Previously, we showed that lavas erupted at East Molokai volcano have Kea-like geochemical characteristics [*Xu et al.*, 2005]. On the basis of Kea-like Pb isotopic ratios of a dredged sample inferred to be from West Molokai (sample D8-1 in Figure 1b), *Abouchami et al.* [2005] concluded that West Molokai volcano is also Kea-like and that the isotopic differences between Loa and Kea trend lavas do not extend to Molokai Island (Figure 1a). However, *Tanaka et al.* [2002] noted that Sr-Nd-Pb isotopic ratios of three subaerially erupted shield lavas from West Molokai [*Stille et al.*, 1986; *West et al.*, 1987] overlap with the field for Mauna Loa lavas, and concluded that the West Molokai shield includes lavas with both Kea- and Loa-like geochemical characteristics. However, these data for subaerial shield lavas, obtained more than 20 years ago, have large uncertainties compared to modern techniques, especially for determination of Pb isotopic ratios, and no Hf isotope data exist. In

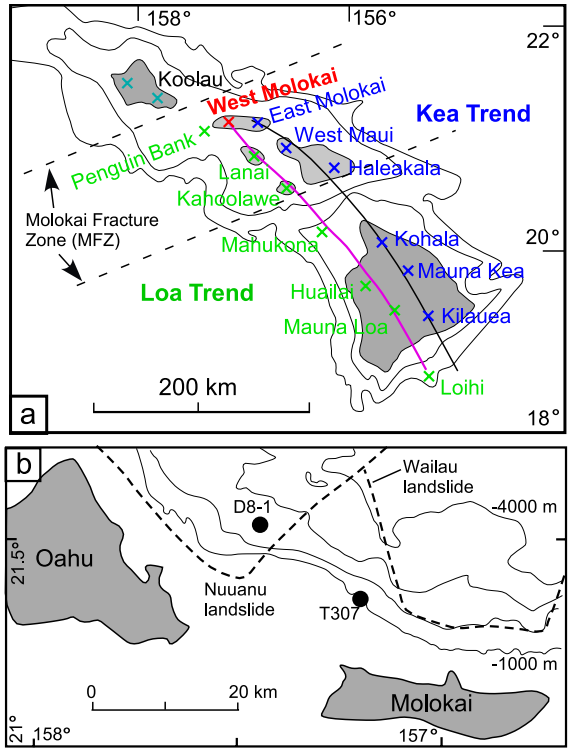

Figure 1. (a) Young, ≤2 Ma Hawaiian volcanoes, i.e., from Molokai Island to Loihi seamount, define the subparallel spatial trends, known as Loa and Kea. Although *Jackson et al.* [1972] included Koolau volcano on the Loa-trend, West Molokai is the oldest Loa-trend volcano on the subparallel portion of the Loa- and Kea-trends. The Molokai Fracture Zone crosscuts the Hawaiian Ridge in the vicinity of Molokai Island but is a complex feature consisting of two separate bands [*Searle et al.*, 1993]. (b) Map showing the location of dredged sample D8-1 which was interpreted to be from West Molokai [*Tanaka et al.*, 2002] and dive T307 samples relative to the boundaries of the Nuuanu and Wailau landslides derived from the Koolau and East Molokai shield, respectively [after *Moore and Clague*, 2002].

this study we focused on West Molokai lavas and find that this shield includes basalt with diverse geochemical characteristics, ranging from lavas similar to the extreme Loa end-member (i.e., Koolau (Makapuu stage) [*Huang and Frey*, 2005b]) to Kea-like samples. The presence of Kea- and Loa-like lavas in West Molokai is consistent with small-scale Kea and Loa heterogeneities in the source (Figure 2d).

[6] An important aspect of understanding Hawaiian magmatism is that a typical Hawaiian volcano evolves through four petrologically defined stages [e.g., *Clague and Dalrymple*, 1987]: alkalic pre-shield stage (~3% of volcano volume, observed at Loihi seamount [*Moore et al.*, 1982], Kilauea [*Sisson and Lipman*, 2002], and Hualalai [*Coombs et al.*, 2006; *Hammer et al.*, 2006] and assumed to be present at all Hawaiian volcanoes); main tholeiitic shield stage (~95–98% of the volume, present in all volcanoes); alkalic postshield stage (~1% of the volume, present at some volcanoes); alkalic rejuvenated stage (<1% of the volume, present at some volcanoes). Postshield-stage and rejuvenated-stage lavas are geochemically distinct from associated shield lavas [e.g., *Chen and Frey*, 1985]; therefore they are important in documenting changes in magmatic processes and sources as a Hawaiian volcano matures. Previous studies [*Gaffney et al.*, 2004; *Xu et al.*, 2005] used the overlap of Sr, Nd, and Pb isotope ratios in late shield/postshield lavas from Mauna Kea (<350 ka), West Maui and East Molokai (~1.5 Ma) to show that the portion of the hot spot sampled by Kea-trend late shield/postshield lavas had long-term geochemical continuity (Figure 1a). Do Loa-trend volcanoes also maintain their distinct isotopic characteristics as they transit from shield-stage to postshield-stage volcanism? Among Loa-trend volcanoes Hualalai, Kahoolawe and West Molokai have postshield lavas. Hualalai postshield lavas have a Loa-trend Pb isotopic signature [*Cousens et al.*, 2003; *Xu et al.*, 2005], while Kahoolawe postshield and shield lavas overlap in Sr and Nd isotopic ratios [*Huang et al.*, 2006]. Another objective of this study is to compare the isotopic characteristics of shield- and postshield-stage lavas from West Molokai. In contrast to Hualalai and Kahoolawe, we find that postshield lavas at West Molokai are Kea-like in their isotopic signature.

2. Geology

[7] Molokai was part of Maui Nui, a single large island at about 1.2 Ma that included the present-day islands of Maui, Kahoolawe, Molokai and Lanai, an area 50% larger than the Big Island of Hawaii today (Figure 1a) [*Price and Elliott-Fisk*, 2004]. West Molokai, the older of the two volcanoes on the island of Molokai, has a peak height of only 421 m. East Molokai volcano, which rises 1515 m above sea level, forms the eastern two-thirds of the island and overlies lavas of West Molokai volcano. West Molokai has received little attention owing to its poorly dissected condition and extensive soil cover. Shield-stage lava flows

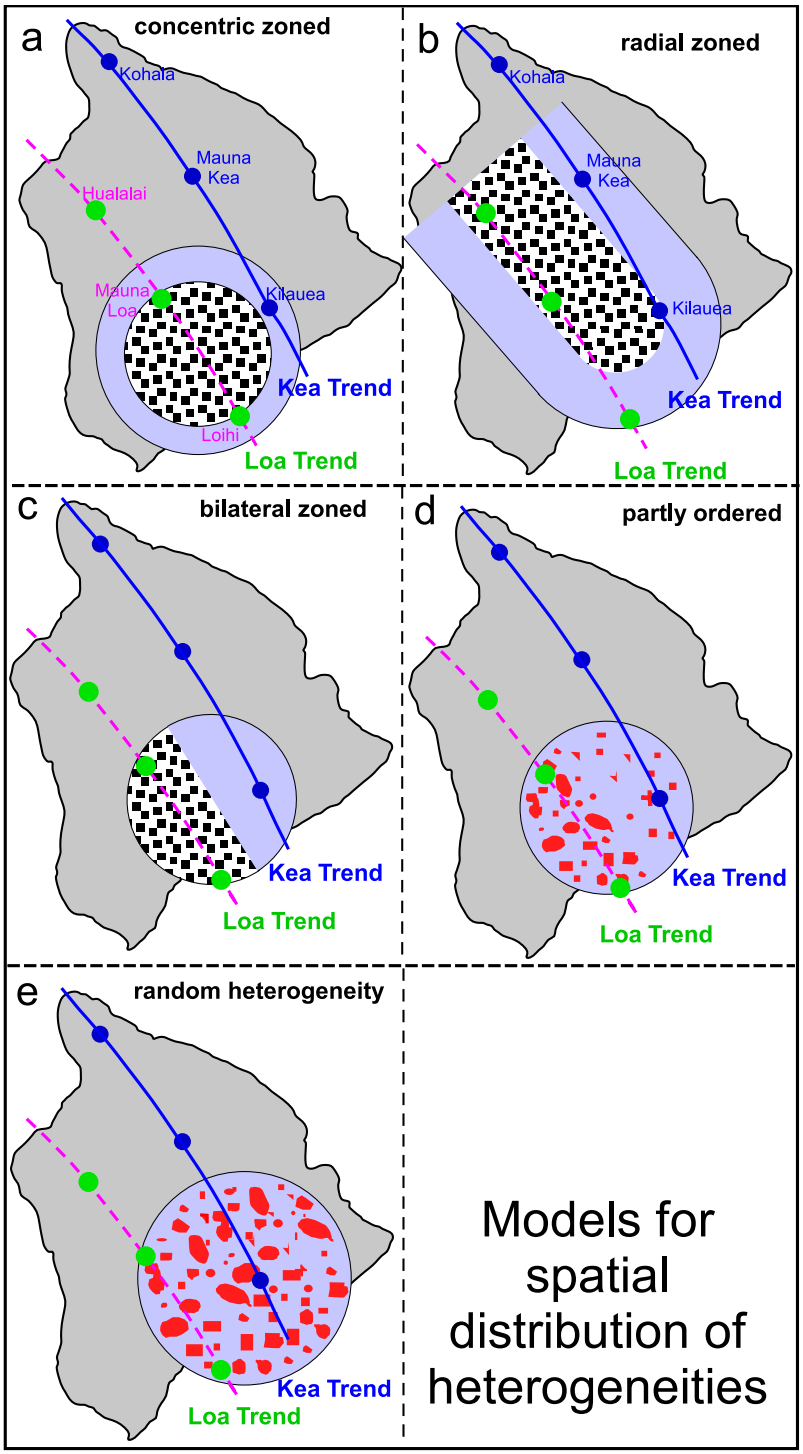
a
concentric zoned
Kohala
Mauna Kea
Hualalai
Mauna Loa
Kilauea
Kea Trend
Loihi
Loa Trend
b
radial zoned
Kohala
Mauna Kea
Kilauea
Kea Trend
Loa Trend
c
bilateral zoned
Kea Trend
Loa Trend
d
partly ordered
Kea Trend
Loa Trend
e
random heterogeneity
Kea Trend
Loa Trend
Models for spatial distribution of heterogeneities

Figure 2

dip 2 to 10 degrees away from the principal southwest and subordinate northwest rift zones, which join near the summit (Figure 3). Some dikes are exposed where coastal erosion has cut into the rift zones. Unlike East Molokai or most other Hawaiian volcanoes, there is no evidence of a summit caldera. About 16 small spatter and cinder cones are preserved on the surface of West Molokai, particularly in the northwest quadrant of the volcano; those that have been sampled (Figure 3) range in composition from alkalic basalt to hawaiite. These cones and the flows erupted from them constitute the alkalic postshield stage. No rejuvenated-stage lava is known at West Molokai. Beneath the sea, West Molokai extends west-southwest to Penguin Bank, which has a flat surface at a depth of 55 m below sea level. Penguin Bank may be a subsided portion of the southwest rift zone of West Molokai volcano but is more likely to be a separate shield volcano (Figure 1a).

[8] Three samples of postshield-stage alkalic basalt and hawaiite were dated using K-Ar techniques in the U.S. Geological Survey laboratory at Menlo Park by G. B. Dalrymple. The samples are from the western flank (Figure 3). The results, presented in Table 1 show that the postshield lavas erupted between 1.72 ± 0.08 and 1.81 ± 0.08 Ma; they are statistically indistinguishable and could all have erupted at 1.76 ± 0.06 Ma, which we take as the age of the postshield stage. *Clague* [1987] previously reported this age, but the analytical data were not published. This age postdates by about 0.13 Ma the end of the shield stage, represented by a highly fractionated tholeiitic flow exposed near the summit (our samples 71WMOL-1, 74WMOL-3, and 74WMOL-5 are from the same unit; see Figure 3) that *McDougall* [1964] dated at 1.89 ± 0.06 Ma (corrected to modern decay constants). The time period between the shield tholeiitic and postshield alkalic stages is therefore inferred to be on the order of several hundred thousand years, but could be much shorter.

3. Sample Location

[9] Fifty-four whole-rock samples collected from West Molokai were studied including 14 samples which experienced postmagmatic REE-Y enrichment [*Clague*, 1987] similar to that documented at Kahoolawe volcano [*Fodor et al.*, 1992]. Samples with REE-Y enrichment were not chosen for isotopic studies.

[10] Forty-seven whole-rock samples were collected from the subaerial surface of West Molokai volcano; locations are shown in Figure 3. Many of the tholeiitic lavas (20) were collected along highway 460 northwest of Puu Nana. Most of the alkalic lavas (15 of the 18 alkalic basalts and hawaiites) are from the northwest part of West Molokai (Figure 3).

[11] Glasses were collected from the margins of three tholeiitic dikes (89FDD, WMO-11 and WFD) southeast (<500 m) of Puu Nana and an alkalic dike (89KAA-1) from near the north coast at Kaa Gulch (Figure 3).

[12] Seven breccia samples were collected by the remotely operated vehicle (Tiburon) ~10 km from the submarine north coast of West Molokai (T307 in Figure 1b). On the basis of their location, these samples originated from the West Molokai shield. They were collected while traversing upward along a sediment-covered slope with outcrops of thin breccia units. Samples R1 and R2 are from a lower breccia unit with R1 below R2, samples R3 and R4 are loose blocks, samples R6 and R7 are from the

Figure 2. Five different plume models proposed to explain the geochemical differences between Loa and Kea shields. (a) The concentrically zoned model assumes that Loa-trend volcanoes sample the core of the plume whereas Kea-trend volcanoes sample the margin of the plume [e.g., *Lassiter et al.*, 1996]. (b) The radially zoned plume model is a variant of the concentrically zoned plume model [*Bryce et al.*, 2005], which includes downstream distortion of the plume by interaction with the Pacific lithosphere. In this model, Loa volcanoes never sample the margin of the plume. (c) The bilaterally zoned plume model [*Abouchami et al.*, 2005] assumes that the southwest side of the plume is geochemically distinct from the northeast side of the plume. (d) The partly ordered zonation model [e.g., *Herzberg*, 2005] has the proportion of randomly distributed heterogeneities (in red) varying systematically from the Loa to Kea parts of the plume. (e) The randomly distributed heterogeneity model has no systematic zonation [*Huang and Frey*, 2005a; *Ren et al.*, 2005]. As drawn, Loa volcanoes sample a higher proportion of heterogeneities with low solidii, perhaps recycled oceanic crust and sediment (red color), whereas Kea volcanoes which are at the plume center sample a higher proportion of components (blue background) with high solidii. Note that all of these models emphasize the lateral zonation of the plume (i.e., horizontal heterogeneity) and do not consider vertical heterogeneities; *Blichert-Toft et al.* [2003] argued that because of the inferred high upwelling velocity of the plume, vertical heterogeneities are also important and should not be neglected.

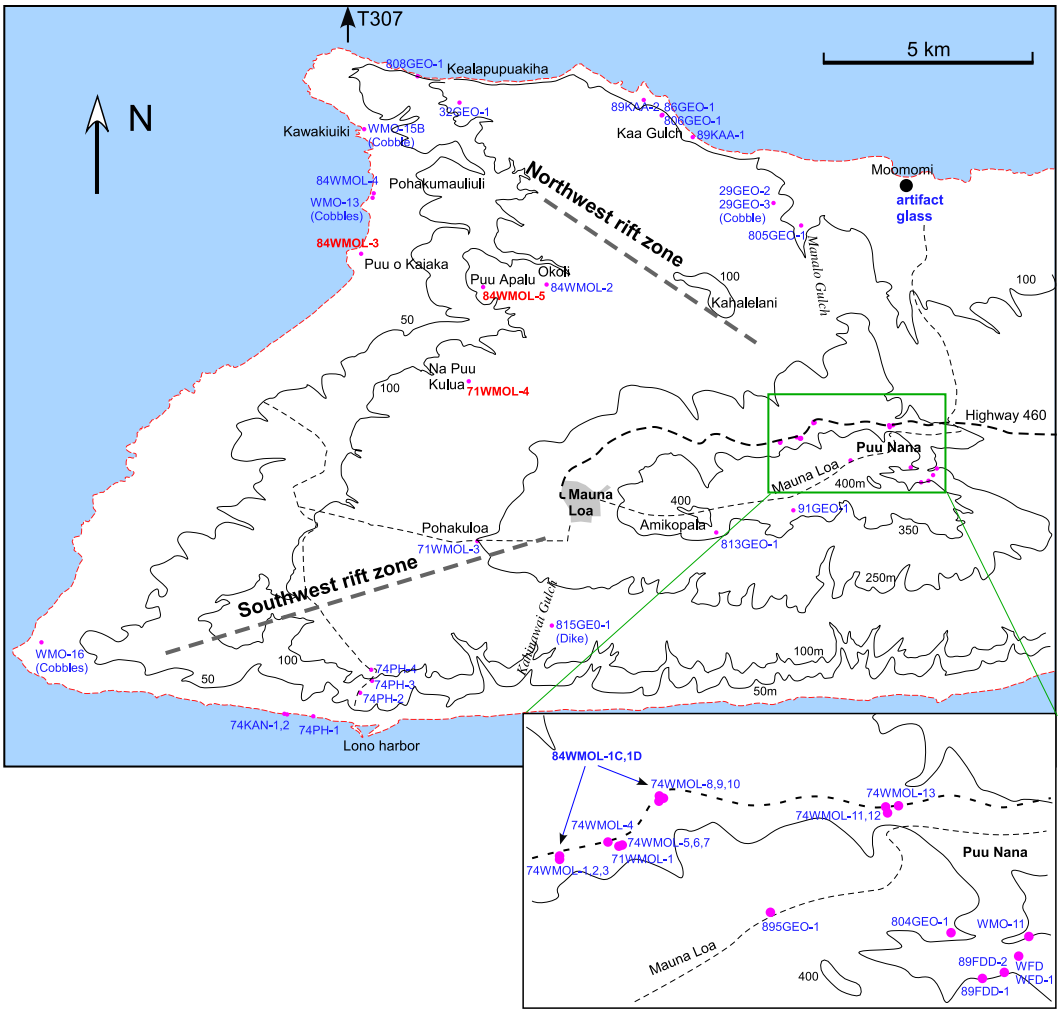

Figure 3. Map of western Molokai Island showing locations of the studied samples. The inset is for the cluster of samples collected along highway 460. The thick dashed lines represent the southwest and northwest rift zones. The dive samples (T307) were collected from ~10 km north of the West Molokai coast (Figure 1b). Most of the tholeiitic lavas were collected along highway 460 northwest of Puu Nana. Samples 84WMOL-1C and 84WMOL-1D were collected along highway 460 between the two arrows. Five tholeiitic glass samples (WMO-11, 89FDD-1, 89FDD-2, WFD, and WFD-1) were collected from three dikes southeast (<500 m) of Puu Nana. An alkalic glass from a dike (89KAA-1) was collected near the north coast at Kaa Gulch. All the other glass samples are artifacts from settlement sites near Moomomi on the north coast. Most alkalic basalt and hawaiite were sampled from the northwest West Molokai, i.e., beach cobbles, near western coastal outcrops from Kawakiuiki to Puu o Kaiaka, and cones, Okoli, Puu Apalu, and Nau Puu Kulua, close to the 100 m contour. Three alkalic samples (in red) were analyzed for K-Ar ages (Table 1).

same outcrop of an overlying unit and sample R8 is from an upper breccia unit. Probably, but not certainly, the sequence R1 to R8 is a chronologic sequence of decreasing age.

[13] In addition to basaltic clasts, glasses from the submarine breccia slope were also analyzed; they include glass grains in sediment cores, glass from rinds on basalt clasts in samples R4 and R8, glass from the breccia matrix of samples R2 and R7, glass in crack-filling hyaloclastite in sample R8, and glass inclusions in olivine from sample R8. Several of these glasses, including rinds on basalt clasts in R4 and R8 are relatively undegassed, i.e., S contents > 0.056 wt% (Table 2), indicating that they were derived from submarine flows [*Dixon et al.*, 1991]. However, melt inclusions in olivine from the uppermost sample, R8, include degassed and undegassed glass (Table 2). Mixing of subaerially and submarine-erupted magmas is implied; a likely scenario is that subaerially erupted, hence

Table 1. K-Ar Age Data for West Molokai Alkalic Lavas[a]

Sample	K_2O, wt%	Weight, g	$^{40}Ar^*$, mol/g	$^{40}Ar^*$%	Age, Myr	σ
84WMOL-5 (Puu Apalu)	1.030 ± 0.005	12.389	2.73×10^{-12}	21.8	1.838	0.092
		11.392	2.46×10^{-12}	15.8	1.658	0.083
Weighted mean age					**1.74**	**0.13**
71WMOL-4 (Na Puu Kulua)	1.489 ± 0.012	9.761	3.59×10^{-12}	19.4	1.673	0.084
		9.883	3.80×10^{-12}	28.0	1.771	0.089
Weighted mean age					**1.72**	**0.08**
84WMOL-3 (Puu o Kaiaka)	1.361 ± 0.010	9.776	3.62×10^{-12}	12.0	1.847	0.093
		9.570	3.48×10^{-12}	22.2	1.776	0.089
Weighted mean age					**1.81**	**0.08**

[a] Isotopic abundance and decay constants for ^{40}K are $\lambda_\beta = 4.962 \times 10^{-10}$/yr, $\lambda_e = 0.581 \times 10^{-10}$/yr, and $^{40}K/K = 1.167 \times 10^{-4}$ [*Steiger and Jager*, 1977]. Errors are estimates of analytical precision at 68% confidence level, whereas the errors for weighted mean ages are at 95% confidence level. Means are weighted by the inverse of the variances. Analyses done at the U.S. Geological Survey in 1985–1986 by G. B. Dalrymple.

degassed, magma retreated into a magma reservoir (the 1959 Kilauea Iki eruption is an example [*Dixon et al.*, 1991]), was incorporated into olivine and subsequently included in a submarine-erupted magma. An important implication is that West Molokai existed as a subaerial shield when this submarine breccia formed.

4. Sample Preparation

[14] The subaerial whole-rock samples were coarse crushed and pieces were hand-picked using a binocular microscope in order to avoid highly altered portions and sawed surfaces. The freshest pieces (~4–6 gram) were washed in an ultrasonic bath three times (5 min each) using MQ-H_2O; they were dried on a hotplate and crushed into fine powder in an agate shatterbox. These powders were used for trace element analyses by inductively coupled plasma mass spectrometry (ICP-MS) and after acid leaching, isotopic analyses were determined by thermal ionization mass spectrometry (TIMS) and multicollector ICP-MS (see Appendix A for analytical methods).

[15] Altered surface of the glass from the three dikes was removed using a minisaw before coarsely crushing to less than 2 mm pieces. Fresh glass was picked from the greater than 0.5 mm but less than 2 mm fraction. This glass was coarsely crushed inagate and fresh pieces were selected using a binocular microscope before crushing to fine powders for trace element analysis by ICP-MS.

[16] Basaltic clasts from the submarine breccia slope were crushed in an agate mortar for trace element and isotopic analyses and in steel for major element analysis. Major and trace element abundances were determined at the Geoanalytical Laboratory at Washington State University, and Sr, Nd, Hf and Pb isotopic ratios were determined at Carleton University, Ecole Normale Supérieure in Lyon and Max-Planck-Institut fur Chemie (see Appendix A for analytical methods).

5. Petrography

[17] Many of the West Molokai shield-stage tholeiitic lava flows are less than 50 cm thick. The subaerial lavas have 3% to 25% vesicles and are sparsely porphyritic (<2%) with olivine, plagioclase, clinopyroxene and orthopyroxene phenocrysts, but lavas from the submarine breccia slope have abundant olivine phenocrysts (>10%) except T307-R2 with less than 2%. The postshield-stage alkalic lavas, dominantly hawaiite with subordinate alkalic basalt, are typically aphyric.

6. Geochemical Results

6.1. Major Element Compositions

[18] Lavas from West Molokai range from older, tholeiitic basalt and basaltic andesite (hereafter referred to as highly fractionated tholeiite) forming the shield to younger alkalic basalt and hawaiite forming the postshield (Figure 4).

6.1.1. Glasses

[19] Glass from West Molokai has been used to infer a local origin of artifacts from the Moomomi region on the north flank of the shield (Figure 3). Specifically *Weisler and Clague* [1998] showed that these artifacts are compositionally similar, either to glass margins on tholeiitic dikes found

Table 2. Glass Compositions for Rinds and Sand Grains[a]

Sample	Analysis Number	SiO_2	TiO_2	Al_2O_3	FeO	MnO	MgO	CaO	Na_2O	K_2O	P_2O_5	S	Cl	Total
Glass in Breccia Matrix														
T307-R2	1, 3–5	51.65	2.45	13.90	10.99	0.16	6.79	11.04	2.28	0.30	0.22	**0.076**	0.012	99.88
Glass Rinds on Basaltic Clast in Breccia														
T307-R4	1–6	51.31	2.45	13.96	10.55	0.17	7.17	11.11	2.22	0.30	0.22	**0.093**	0.011	99.56
Sand Grains in Hyaloclastite														
T307-R7	1–2	51.17	2.29	13.21	11.07	0.13	9.14	10.67	2.10	0.27	0.21	**0.096**	0.026	100.51
T307-R7	3–4	51.71	2.52	14.07	11.45	0.18	6.55	10.98	2.27	0.32	0.24	**0.102**	0.013	100.55
T307-R7	5	52.09	2.57	13.87	11.81	0.15	6.54	11.24	2.21	0.29	0.26	0.017	0.008	101.06
T307-R7	6	52.23	2.20	13.96	10.93	0.11	7.01	11.62	2.17	0.23	0.19	0.014	0.007	100.70
T307-R7	7	51.97	2.34	14.23	11.02	0.18	6.89	11.41	2.24	0.27	0.23	0.006	0.013	100.80
Glass Inclusion in Olivine														
T307-R8	12	51.07	2.50	13.57	11.83	0.11	7.42	11.06	2.04	0.28	0.23	0.034	0.007	100.14
T307-R8	13	50.82	2.48	13.20	12.46	0.16	7.14	11.01	1.98	0.27	0.25	0.013	0.015	99.80
T307-R8	5	51.46	2.26	13.75	11.10	0.11	7.45	10.94	2.09	0.28	0.20	**0.067**	0.006	99.71
Glass Rinds														
T307-R8	1–2, 4, 11	51.48	2.31	13.74	11.00	0.14	7.51	10.98	2.10	0.27	0.22	**0.056**	0.012	99.81
Sand Grains in Hyaloclastite Filling Lava Crack														
T307-R8	6–10	51.67	2.60	13.74	11.92	0.15	6.38	10.97	2.20	0.30	0.25	0.004	0.009	100.18
Glass in Push Core (PC) Sediment, Collected From the Bottom of the Dive at 3451 mbsl														
T307-PC65	1	51.41	2.57	14.31	10.85	0.20	6.57	11.13	2.27	0.30	0.25	**0.104**	0.014	100.13
T307-PC65	2	51.34	2.98	13.35	12.70	0.22	5.83	10.47	2.43	0.52	0.35	0.017	0.015	100.25
T307-PC65	3	51.13	2.72	13.86	11.67	0.18	6.24	10.65	2.30	0.33	0.27	**0.122**	0.014	99.67
T307-PC65	4	51.72	2.97	13.32	12.61	0.22	5.86	10.63	2.48	0.51	0.34	0.017	0.009	100.70
T307-PC65	5	51.58	2.93	13.34	12.48	0.20	5.81	10.46	2.43	0.50	0.37	0.013	0.008	100.13
T307-PC65	6	51.30	2.91	13.27	12.72	0.15	5.77	10.40	2.44	0.51	0.32	0.024	0.014	99.86
T307-PC65	7	51.37	2.57	14.27	10.90	0.17	6.59	11.07	2.32	0.29	0.25	**0.110**	0.010	100.07
T307-PC65	8	51.78	2.33	14.13	10.64	0.15	7.15	11.11	2.28	0.33	0.22	0.014	0.014	100.18
T307-PC65	9	50.75	2.37	13.73	10.83	0.16	8.00	10.98	2.12	0.28	0.24	**0.083**	0.012	99.67
T307-PC65	10	51.23	2.98	13.35	12.75	0.15	5.84	10.41	2.37	0.51	0.33	0.008	0.010	99.96
T307-PC65	11	51.33	2.83	13.96	12.07	0.16	6.18	10.82	2.28	0.32	0.26	**0.107**	0.014	100.50
T307-PC65	12	51.46	2.77	13.96	11.94	0.14	6.21	10.80	2.38	0.35	0.29	**0.110**	0.016	100.57
T307-PC65	13	51.38	2.98	13.35	12.87	0.24	5.75	10.58	2.28	0.51	0.36	0.014	0.007	100.33
T307-PC65	14	51.73	2.42	14.31	10.64	0.19	6.93	11.09	2.30	0.34	0.22	0.010	0.008	100.19
T307-PC65	15	51.40	3.03	13.20	12.96	0.20	5.68	10.37	2.51	0.51	0.34	0.010	0.007	100.22
T307-PC65	16	51.48	3.00	13.38	12.69	0.18	5.83	10.42	2.51	0.49	0.36	0.016	0.005	100.39
Glass Grains in Sediment, Collected From the Top of the Dive at 3337 mbsl														
T307-PC76	1	51.73	2.92	13.35	12.69	0.18	6.73	10.55	2.39	0.50	0.35	0.012	0.005	101.43
T307-PC76	2	51.73	2.90	13.28	12.63	0.17	5.80	10.55	2.36	0.50	0.34	0.011	0.006	100.29
T307-PC76	3	51.70	2.94	13.35	12.82	0.20	5.89	10.48	2.39	0.48	0.34	0.017	0.012	100.65
T307-PC76	4	51.62	2.88	13.45	12.58	0.17	5.89	10.67	2.37	0.52	0.36	0.016	0.018	100.58
T307-PC76	5	51.94	2.95	13.37	12.60	0.20	5.82	10.52	2.43	0.51	0.35	0.014	0.013	100.74
T307-PC76	6	51.77	2.94	13.41	12.71	0.18	5.89	10.52	2.36	0.50	0.34	0.012	0.011	100.64
T307-PC76	7	51.77	2.96	13.18	12.85	0.22	5.85	10.44	2.43	0.53	0.37	0.011	0.006	100.63

[a] Glass compositions are in wt%. Glass with S contents > 0.05 wt% (in bold) are submarine erupted, and the others are degassed and erupted subaerially [*Dixon et al.*, 1991]. The locations for T307-PC65 and T307-PC76 are (−157.1168, 21.4307) and (−157.1204, 21.4301), respectively. Locations for T307R2, R4, R7, and R8 are in Table 3.

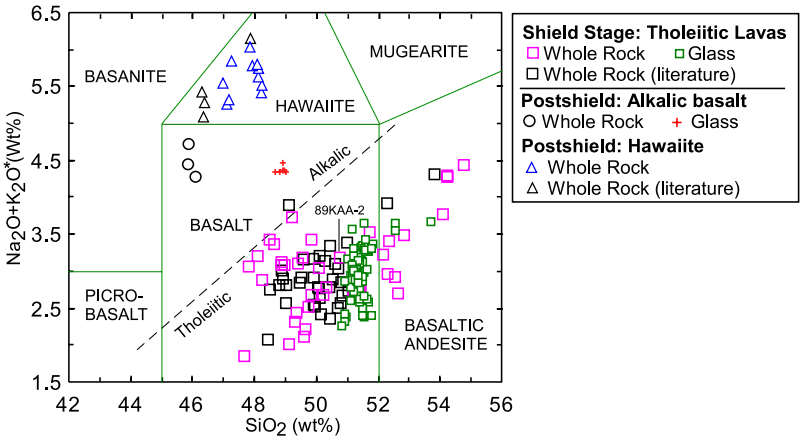

Figure 4. $Na_2O + K_2O$ versus SiO_2 classification plot showing that the West Molokai whole rocks and glass range from tholeiitic to alkalic basalt and hawaiite. The alkalic-tholeiitic dividing line is from *Macdonald and Katsura* [1964]. Major element data were adjusted to a $Fe^{3+}/(Fe^{2+} + Fe^{3+})$ molar ratio of 0.10. Whole rock samples with K_2O/P_2O_5 less than 1.21 were corrected for K_2O loss during alteration (see Figure A2). Most whole-rock (54 samples) and glass data are from this paper, but also plotted are literature data from *Macdonald and Katsura* [1964] (2 samples) and *Shinozaki et al.* [2002] (36 samples).

near the summit or on the north shore dike of alkalic basalt (Figure 5 and Table A1).

[20] A new result is that glasses from the submarine breccia slope (T307 in Figure 1b) are tholeiitic basalt (Table 2), but they are compositionally distinct from glass margins on the dikes and artifact glasses; specifically, at a given MgO content submarine glasses are offset to higher CaO and lower Na_2O and P_2O_5 (not shown), but they have similar SiO_2 contents (Figures 5a, 5b, and 5c); also in a Al_2O_3/CaO versus TiO_2/Na_2O plot the artifact and dike glasses overlap the Mauna Loa field, whereas the submarine glasses overlap the Mauna Kea field (Figure 5d). Relative to tholeiitic glasses, the alkalic glasses have lower CaO and SiO_2 and higher Na_2O contents (Figure 5a, 5b, and 5c).

6.1.2. Whole Rock

[21] The tholeiitic whole-rock compositions (Table 3) overlap the tholeiitic glass compositions (Figure 6). For lavas with MgO > 7% (basaltic clasts from the submarine breccia slope; see Table 3) the contents of CaO, SiO_2, TiO_2, Al_2O_3, Fe_2O_3* and P_2O_5 increase with decreasing MgO which is consistent with olivine fractionation and accumulation (Figure 6). For the basaltic lavas with MgO < 7%, CaO content is positively correlated with MgO thereby indicating the important role of clinopyroxene fractionation (Figure 6a). Some highly fractionated tholeiitic samples range to high SiO_2 (>53%) at low MgO contents (4–5%); these samples have higher SiO_2, P_2O_5, and lower CaO, Al_2O_3, Fe_2O_3* and TiO_2 at a given MgO than other tholeiitic samples (Figure 6), indicating fractionation of clinopyroxene + plagioclase + Fe-Ti oxides. Such highly evolved tholeiitic lavas have previously been described from distant parts of rift zones where isolated magma chambers cooled and fractionated [*Helz and Wright*, 1992; *Clague et al.*, 1995; *Yang et al.*, 1999]. However, at West Molokai and Waianae [*Sinton*, 1987] these fractionated tholeiitic lavas erupted near the summit, perhaps produced as the sub-caldera reservoir filled with tholeiitic melt cooled and crystallized as magma supply rate waned at the end of shield stage.

[22] Compared to tholeiitic lavas, at a given MgO content, alkalic basalt lavas have lower CaO and SiO_2 and higher TiO_2, Fe_2O_3* and P_2O_5 (Table 3 and Figure 6). These differences are consistent with the commonly inferred decrease in extent of melting that accompanies the transition from shield to postshield stages [e.g., *Yang et al.*, 1996].

[23] Relative to basalt, hawaiites from the Kea volcanoes (such as Mauna Kea and East Molokai) are characterized by relatively high SiO_2 (>49%), low Fe_2O_3* (<12%) and low TiO_2 (<3%) (Table 3 and gray shaded fields in Figures 6b, 6c, and 6e). These features can be explained by Fe-Ti oxide segregation [*West et al.*, 1988; *Frey et al.*, 1990]. In contrast, West Molokai hawaiites trend to relatively low SiO_2 and high Fe_2O_3 and TiO_2 contents showing that Fe-Ti oxide fractionation was less

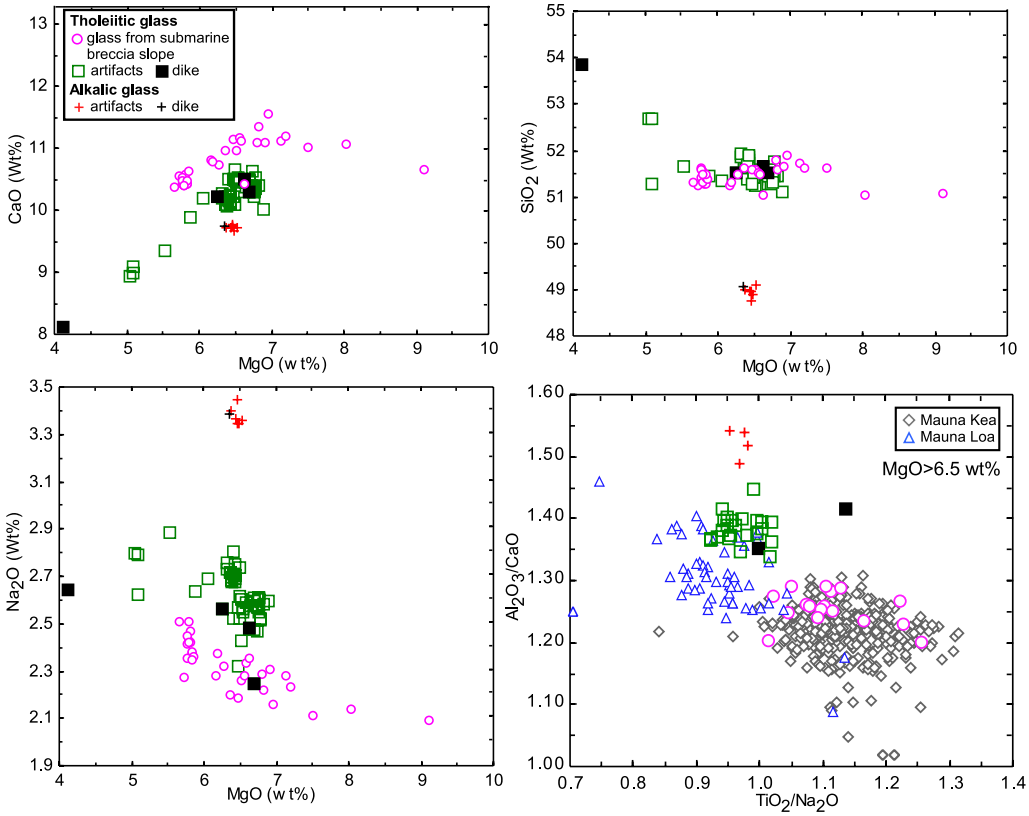

Figure 5. MgO versus CaO, SiO_2, and Na_2O and TiO_2/Na_2O versus Al_2O_3/CaO for West Molokai glasses. The alkalic glasses of artifacts are identical to that of the alkalic dike, and they are distinguished from tholeiitic glasses by lower CaO and SiO_2 but higher Na_2O at a given MgO content. Note that at a given MgO content tholeiitic glasses from the submarine breccia slope have higher CaO and lower Na_2O than tholeiitic glasses from the artifacts and dikes. To avoid the effects of clinopyroxene and plagioclase fractionation, Figure 5d shows data only for glasses with MgO > 6.5%. Fields for a typical Loa volcano (Mauna Loa) and a typical Kea volcano (Mauna Kea) are distinct; submarine West Molokai glasses overlap with the Mauna Kea field, and the West Molokai artifacts and dike glasses overlap with the Mauna Loa field. Data sources: West Molokai, this study; Mauna Kea, *Garcia et al.* [1995] and *Stolper et al.* [2004]; Mauna Loa, *Garcia et al.* [1989, 1995], *Garcia* [1996], *Moore and Clague* [1987, 1992], and *Moore et al.* [1995].

important in the formation of West Molokai hawaiite (Figure 6).

6.2. Trace Element Abundances

[24] Trace element data are reported in Table 4. Thorium content is positively correlated with abundances of other immobile, incompatible elements (e.g., Nb and Zr) in tholeiitic lavas (Figure 7). Three of the four fractionated tholeiitic lavas with relatively low CaO, Fe_2O_3* and TiO_2 are offset to lower Nb/Th, Sr/Nb and Eu/Th ratios (Figure 7), which is consistent with Fe-Ti oxides and plagioclase in the fractionating mineral assemblage that led to these tholeiitic lavas; i.e., Nb is compatible in Fe-Ti oxides [*Jang and Naslund*, 2003] and Sr and Eu are compatible in plagioclase relative to clinopyroxene and olivine [e.g., *Bindeman et al.*, 1998; *Blundy and Dalton*, 2000; *Bedard*, 2005].

[25] Relative to tholeiitic lavas, at a given MgO content, alkalic basalts have higher contents of incompatible elements such as Th (Figure 7f), but they have similar contents of heavy rare earth elements (e.g., Lu in Figure 7e). These differences are consistent with the interpretation that the parental magmas of alkalic basalt were derived by lower extents of melting with significant residual garnet [e.g., *Yang et al.*, 1996]. Hawaiites have the highest abundances of Th, Nb, Zr, Sr and Eu (Figure 7) and relatively low Sc and Ni contents (Table 4). These characteristics are expected for low MgO lavas derived from an alkalic parental magma by extensive fractionation of a clinopyroxene-rich and plagioclase-poor assemblage. This scenario,

Table 3. Major Element Compositions of West Molokai Lavas[a]

Sample[b]	Longitude[c]	Latitude[c]	Lab[d]	SiO_2	TiO_2	Al_2O_3	Fe_2O_3	FeO	Fe_2O_3*[e]	FeO*[e]	MnO	MgO	CaO	Na_2O	K_2O	P_2O_5	LOI	H_2O^+	H_2O^-	CO_2	Total
Postshield-Stage Lavas																					
Hawaiite																					
71WMOL-4	−157.2304	21.1573	USGS	47.30	3.66	16.00				12.20	0.30	4.73	7.52	4.03	1.45	0.95					98.14
71WMOL-4	−157.2304	21.1573	UMASS	47.49	3.66	16.08			13.48		0.26	4.83	7.49	4.16	1.49	0.94	0.24				99.88
74PH-2	−157.2500	21.0937	UMASS	47.35	4.07	16.55			14.85		0.17	3.52	6.72	4.35	1.35	0.90	1.46				99.83
74PH-3	−157.2474	21.0966	USGS	46.40	4.15	15.50				13.30	0.15	3.81	6.73	4.10	1.31	0.79					96.24
74PH-4	−157.2479	21.0985	UMASS	46.45	4.50	17.61			15.99		0.82	2.16	5.45	4.32	1.41	0.94	3.74				99.65
84WMOL-2	−157.2163	21.1773	USGS	46.10	4.52	16.00				14.20	0.16	3.30	7.41	4.22	1.20	0.78					97.89
84WMOL-3	−157.2496	21.1835	USGS	47.60	3.71	15.40				12.70	0.19	4.99	7.72	4.01	1.32	0.88					98.52
84WMOL-4	−157.2473	21.1954	USGS	46.10	4.10	15.50				13.40	0.18	4.50	7.95	3.93	1.20	0.79					97.65
WMO-13	−157.2475	21.1943	USGS	46.70	4.15	15.30	7.51	6.65			0.18	5.06	7.91	3.98	1.26	0.81		0.41	0.35	0.01	100.3
WMO-15B	−157.2491	21.2079	USGS	47.30	3.77	15.70	6.99	6.49			0.18	4.12	7.74	4.07	1.34	0.89		0.75	0.54	0.02	99.9
806-GEO-1	−157.1970	21.2102	USGS	47.50	3.76	15.80	5.94	7.07			0.19	4.95	7.75	4.30	1.42	0.91		0.37	0.15	0.08	100.2
86GEO-1	−157.1970	21.2102	UMASS	47.30	3.73	15.83			13.63		0.20	4.92	7.55	4.53	1.42	0.89	0				100.0
Alkalic basalt																					
84WMOL-5	−157.2285	21.1767	USGS	45.50	4.63	15.00				14.20	0.19	5.69	8.50	3.64	1.03	0.68					99.06
29-GEO-2	−157.1776	21.1938	USGS	44.60	4.35	15.60	3.87	11.10			0.19	6.41	8.57	3.38	0.87	0.67		0.62	0.12	0.03	100.4
29-GEO-3	−157.1776	21.1938	USGS	46.53	4.16	16.12				14.35	0.18	5.98	8.44	3.37	0.92	0.64					100.7
Shield-Stage Lavas																					
Subaerial tholeiite																					
71WMOL-1	−157.1729	21.1453	USGS	53.61	2.93	14.05	2.31	9.06			0.16	3.92	7.90	3.10	1.13	0.70		0.89	0.22	0.01	99.99
71WMOL-3	−157.2297	21.1245	USGS	51.15	2.63	13.98	1.79	9.72			0.17	6.58	10.35	2.36	0.54	0.31		0.31	0.12	0.01	100.0
74WMOL-1	−157.1768	21.1445	USGS	46.90	3.44	15.50	4.80	9.00			0.18	5.60	8.75	2.30	0.12	0.51		1.30	0.82	0.01	99.23
74WMOL-2	−157.1768	21.1450	USGS	47.90	2.77	14.90	6.95	5.00			0.29	5.69	9.51	2.00	0.10	0.34		3.00	2.20	0.01	100.27
74WMOL-3	−157.1768	21.1450	USGS	48.80	2.48	14.30	3.50	8.10			0.26	6.68	9.99	2.19	0.10	0.31		1.20	0.77	0.01	98.69
74WMOL-4	−157.2304	21.1573	USGS	53.10	2.94	13.70	3.00	8.30			0.16	4.17	7.81	3.14	1.04	0.71		1.20	0.47	0.01	99.75
74WMOL-5	−157.1729	21.1453	USGS	53.50	2.90	13.40	2.65	8.60			0.16	4.03	7.53	3.13	1.18	0.72		1.30	0.42	0.01	99.53
74WMOL-6	−157.1729	21.1453	USGS	47.30	2.62	14.60	7.49	5.23			0.25	5.81	9.72	1.97	0.08	0.26		1.78	1.97	0.20	99.28
74WMOL-7	−157.1729	21.1453	USGS	47.20	3.19	14.60	4.19	9.10			0.19	5.96	10.40	2.21	0.13	0.38		0.93	0.68	0.30	99.46
74WMOL-8	−157.1702	21.1485	USGS	49.60	2.51	13.80	5.15	6.90			0.16	6.41	9.31	2.32	0.30	0.28		1.50	0.95	0.01	99.2
74WMOL-9	−157.1702	21.1485	USGS	48.20	3.35	14.00	3.35	9.50			0.18	5.72	9.70	2.93	0.15	0.45		1.40	0.45	0.01	99.39
74WMOL-10	−157.1702	21.1485	USGS	49.00	3.35	14.30	5.20	8.30			0.16	5.23	9.27	2.62	0.13	0.46		1.00	0.97	0.01	100
74WMOL-11	−157.1571	21.1479	USGS	47.30	3.39	14.10	4.85	8.60			0.18	5.83	9.79	2.54	0.20	0.50		1.50	0.59	0.01	99.38
74WMOL-12	−157.1571	21.1479	USGS	47.30	2.66	14.30	4.80	7.50			0.17	6.55	10.30	2.50	0.09	0.29		1.40	0.79	0.01	98.66
74WMOL-13	−157.1562	21.1480	USGS	50.30	2.45	13.90	3.00	8.64			0.17	6.55	10.50	2.15	0.34	0.28		0.35	0.88	0.08	99.59
74KAN-1	−157.2631	21.0897	USGS	48.30	2.39	13.60	4.20	7.20			0.17	7.04	10.60	2.45	0.12	0.30		1.30	0.66	0.08	98.41
74KAN-2	−157.2627	21.0899	USGS	46.90	3.29	14.10	4.72	8.98			0.20	6.20	10.50	2.24	0.14	0.48		0.99	0.90	0.16	99.8
74PH-1	−157.2586	21.0893	USGS	48.00	2.74	14.30	6.99	5.50			0.18	6.04	10.20	2.08	0.15	0.31		1.23	1.59	0.15	99.46
84WMOL-1C (S)[f]	−157.1729	21.1453	UMASS	48.95	3.11	14.26			13.84		0.19	5.96	10.19	2.52	0.25	0.38	0.74				99.65
84WMOL-1D (S)	−157.1729	21.1453	UMASS	48.21	3.38	15.53			14.83		0.18	5.20	9.36	2.67	0.14	0.41	2.38				99.91
84WMOL-1C (NW)	−157.1729	21.1453	UMASS	48.41	3.35	15.10			14.65		0.18	5.57	9.75	2.54	0.14	0.31	1.66				100.0
84WMOL-1C (NE)	−157.1729	21.1453	UMASS	48.33	3.27	15.23			14.49		0.18	5.51	9.75	2.62	0.14	0.29	1.78				99.81

Table 3. (continued)

Sample[b]	Longitude[c]	Latitude[c]	Lab[d]	SiO_2	TiO_2	Al_2O_3	Fe_2O_3	FeO	Fe_2O_3*[e]	FeO*[e]	MnO	MgO	CaO	Na_2O	K_2O	P_2O_5	LOI	H_2O^+	H_2O^-	CO_2	Total
84WMOL-1D (N)	−157.1729	21.1453	UMASS	50.55	2.63	13.81			13.14		0.19	6.21	10.29	2.36	0.36	0.31	0.75				99.85
89KAA-2	−157.2005	21.2137	UMASS	50.13	2.89	13.94			12.77		0.17	6.14	10.34	2.60	0.53	0.38	0.01				99.89
WMO-16	−157.3087	21.1037	USGS	49.10	2.78	14.20	4.66	8.23			0.17	6.46	10.60	2.53	0.14	0.34		0.60	0.57	0.01	100.4
32-GEO-1	−157.2320	21.2132	USGS	50.60	3.13	13.90	5.12	7.45			0.15	5.26	9.78	2.70	0.65	0.42		0.78	0.39	0.01	100.3
804-GEO-1	−157.1514	21.1389	USGS	52.80	3.43	13.10	3.46	8.32			0.17	4.63	8.65	2.62	1.01	0.56		1.03	0.28	0.01	100.1
805-GEO-1	−157.1739	21.1881	USGS	49.80	2.44	13.90	5.41	6.20			0.15	6.76	10.60	2.25	0.12	0.30		0.69	1.58	0.01	100.2
808-GEO-1	−157.2400	21.2187	USGS	50.80	2.95	13.80	5.23	7.17			0.15	5.54	9.82	2.57	0.63	0.39		0.60	0.66	0.01	100.3
813-GEO-1	−157.1874	21.1263	USGS	51.30	2.41	14.10	3.26	8.23			0.16	6.31	9.91	2.32	0.48	0.31		0.85	0.46	0.01	100.1
815-GEO-1	−157.2158	21.1077	USGS	51.30	3.24	13.20	4.21	8.72			0.17	5.42	9.49	2.68	0.66	0.43		0.43	0.24	0.01	100.2
895-GEO-1	−157.1642	21.1413	USGS	51.40	2.76	13.70	3.66	8.50			0.16	6.15	9.86	2.34	0.53	0.35		0.70	0.28	0.01	100.4
91-GEO-1	−157.1752	21.1316	USGS	51.90	2.54	13.80	3.00	8.64			0.17	6.61	10.30	2.28	0.44	0.30		0.53	0.10	0.02	100.6
Tholeiitic basalt clasts from submarine breccia slope																					
T307R1[g]	−157.1190	21.4309	WSU	49.6	2.086	12		11.36			0.166	12.66	9.66	1.99	0.32	0.283					100.1
T307R2	−157.1193	21.4313	WSU	52.59	2.122	13.87		10.26			0.15	7.46	9.17	2.85	0.61	0.304					99.39
T307R3	−157.1196	21.4305	WSU	49.05	1.888	11.09		11.3			0.166	14.38	8.9	1.9	0.4	0.221					99.30
T307R4	−157.1197	21.4296	WSU	49.48	2.124	11.79		10.82			0.166	13.06	9.62	1.92	0.27	0.195					99.45
T307R6	−157.1227	21.4294	WSU	48.76	1.812	10.52		10.42			0.164	16.74	8.52	1.77	0.22	0.167					99.09
T307R7	−157.1228	21.4294	WSU	49.16	1.853	10.84		10.26			0.162	15.5	8.89	1.84	0.24	0.172					98.92
T307R8	−157.1245	21.4289	WSU	47.45	1.693	9.57		10.99			0.166	19.68	7.86	1.6	0.24	0.152					99.40

[a] Major element compositions are in wt%. Volatile-free compositions were used in all diagrams involving major elements. They were determined by recalculation of total iron as Fe_2O_3, subtracting H_2O and CO_2, and then normalizing to 100 percent.

[b] Samples with prefix of "71WMOL" were collected by D. Jackson and M. Beeson in 1971, and "GEO," "WMO," and "89KAA-2" samples were collected by M. Weisler; all the other samples were collected by D. Clague.

[c] The latitude and longitude for subaerial samples are approximate only since their locations were digitized from field maps of USGS quadrangles in old Hawaiian coordinates that were then adjusted to modern geographic coordinates (WGS84).

[d] Lab indicates analytical facility: United States Geological Survey (USGS), University of Massachusetts of Amherst (UMASS), and Washington State University (WSU).

[e] Fe_2O_3* and FeO* stand for the total Fe reported as Fe_2O_3 and FeO, respectively.

[f] N, NW, NE, and S after the sample names for 84WMOL-1 indicate the relative direction of the road outcrop.

[g] Submarine samples T307R1, 2, 3, 4, 6, 7, and 8 were collected from 3451.1, 3424.7, 3422.9, 3404.9, 3243.9, 3243.9, and 3133.1 meters below sea level, respectively.

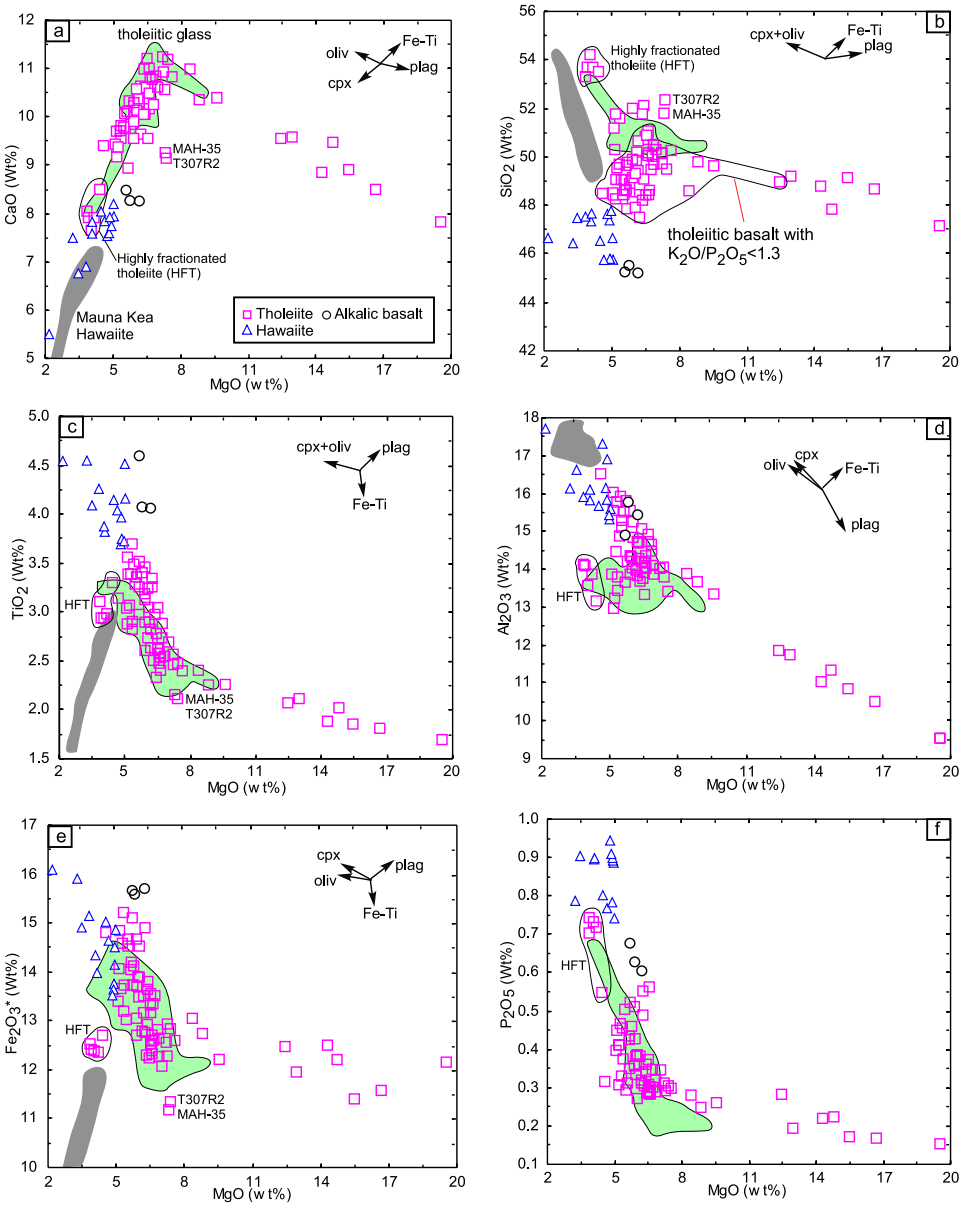

Figure 6. MgO versus CaO, SiO_2, TiO_2, Al_2O_3, Fe_2O_3*, and P_2O_5 for West Molokai whole rocks. For comparison, tholeiitic glass data in which the total iron was converted to Fe_2O_3* are shown as green fields. Also shown for comparison are dark gray fields for Mauna Kea hawaiite. The arrows in Figures 6a, 6b, and 6d show the effect of olivine, plagioclase, clinopyroxene, and Fe-Ti oxide fractionation. Two West Molokai samples, MAH-35 [*Shinozaki et al.*, 2002] and T307R2 (this paper, Table 3), which have Koolau (Makapuu-stage)-like major element compositions (i.e., high SiO_2, low CaO, TiO_2, and Fe_2O_3* at a given MgO content) are labeled. Five samples with high SiO_2 contents (>53%) (designated as highly fractionated tholeiites (HFT)) which have experienced fractionation of clinopyroxene, plagioclase, and Fe-Ti are grouped. In Figure 6b, lavas with $K_2O/P_2O_5 < 1.3$ which have lost K are labeled as a field. The whole-rock data from this study and literature data (2 samples from *Macdonald and Katsura* [1964] and 36 samples from *Shinozaki et al.* [2002]) were plotted using the same symbols for clarity.

plagioclase and olivine-dominated fractionation of shield-stage tholeiitic basalt followed by higher pressure clinopyroxene-dominated fractionation of postshield alkalic lavas is evident at Mauna Kea volcano [*Frey et al.*, 1990].

6.3. Sr, Nd, Hf, and Pb Isotopic Ratios

[26] Isotopic data, Sr, Nd, Hf and Pb for West Molokai lavas are given in Table 5; in addition, Hf isotopic data for previously studied East Molokai

Table 4. Trace Element Compositions of West Molokai Lavas[a]

Sample	Cs	Rb	U	Ba	Th	Nb	Ta	Zr	Hf	Sr	Pb	La	Ce	Pr	Nd	Sm	Eu	Gd	Tb	Dy	Ho	Er	Tm	Yb	Lu	Y	Sc	Ni*
Postshield-Stage Lavas																												
Hawaiite																												
71WMOL-4	0.27	26.1	0.99	486	2.83	42.8	2.63	429	9.81	912	2.35	40.6	91.4	13.8	61.9	14.3	4.47	13.53	2.00	10.57	1.92	4.66	0.63	3.60	0.49	57.1	14.8	28
74PH-2	0.25	23.6	0.85	419	2.62	38.3	2.36	376	8.87	823	2.39	39.7	83.6	13.1	58.9	14.0	4.40	13.69	2.01	10.53	1.93	4.59	0.62	3.42	0.46	55.2	15.6	
74Ph-3	0.13	21.8	0.74	357	2.35	35.8	2.21	350	8.15	805	2.23	38.4	74.1	12.8	59.7	14.6	4.71	14.72	2.14	11.43	2.18	5.28	0.73	3.99	0.55	67.5	15.6	12
74PH-4	0.15	23.0	0.91	436	2.60	37.3	2.34	372	8.95	758	2.17	34.2	77.7	12.0	56.5	13.8	4.54	13.56	1.96	10.49	2.07	5.27	0.76	4.54	0.67	65.3	16.2	
84WMOL-2	0.20	20.8	0.81	360	2.22	31.5	1.94	321	7.60	797	2.11	30.9	69.5	10.8	49.5	12.2	3.91	11.86	1.77	9.34	1.72	4.23	0.57	3.17	0.44	48.7	17.1	45
84WMOL-3	0.21	24.1	0.84	460	2.60	38.4	2.34	378	8.75	799	2.48	34.6	79.3	11.7	52.6	12.8	4.02	11.99	1.79	9.35	1.74	4.10	0.56	3.17	0.42	50.6	15.4	40
84WMOL-4	0.12	19.8	0.77	354	2.29	35.8	2.24	343	8.16	828	2.03	31.5	74.5	11.1	50.5	12.3	3.87	11.58	1.76	9.33	1.72	4.22	0.58	3.29	0.45	48.7	15.7	32
WMO-13	0.55	26.1	0.78	346	2.29	35.0	2.27	339	8.12	824	2.17	32.4	71.4	11.8	55.7	13.7	4.48	13.82	2.04	10.81	2.00	4.84	0.66	3.65	0.50	56.4	15.7	
WMO-15B	0.31	24.9	0.76	386	2.72	37.8	2.35	378	8.88	789	2.53	36.3	81.1	12.7	57.4	13.7	4.36	13.04	1.93	10.20	1.83	4.39	0.59	3.31	0.45	52.7	15.3	
806GEO-1	0.26	25.2	0.90	389	2.64	39.2	2.46	393	9.22	827	2.50	36.2	79.1	12.4	56.0	13.3	4.19	12.48	1.86	9.74	1.80	4.30	0.59	3.33	0.45	53.3	14.9	1
86GEO-1	0.26	24.8	0.87	378	2.59	39.0	2.40	389	9.10	793	2.48	36.2	75.5	12.4	56.1	13.2	4.15	12.50	1.86	9.73	1.81	4.37	0.59	3.32	0.45	54.1	14.6	
Alkalic basalt																												
84WMOL-5	0.43	21.9	0.68	304	2.04	31.8	1.96	308	7.34	772	1.92	27.4	65.0	9.5	42.9	10.4	3.35	10.01	1.53	8.02	1.48	3.59	0.48	2.77	0.37	42.5	17.8	53
89KAA-1 (glass)	0.25	16.4	0.58	227	1.70	22.8	1.44	268	6.47	584	2.38	21.8	54.3	7.9	36.3	9.3	2.88	8.76	1.32	7.10	1.29	3.15	0.44	2.39	0.33	36.2	24.6	
29-GEO-2	0.21	14.8	0.61	238	1.68	26.1	1.68	296	7.07	730	1.77	24.1	60.4	9.1	41.5	10.4	3.21	9.97	1.50	8.06	1.49	3.62	0.50	2.80	0.38	41.5	18.4	67
29-GEO-3*		14.0		229		29.0		277		765		25.0	66.0													38.0	21.0	64
Shield-Stage Lavas																												
Tholeiite																												
71WMOL-1	0.22	18.2	0.60	206	1.98	23.4	1.48	360	8.80	392	2.58	26.3	65.3	9.9	45.9	11.6	3.38	11.59	1.80	10.01	1.93	4.86	0.70	3.97	0.56	55.4	23.7	47
71WMOL-3*		14.0		110		15.0		163		383		14.0	32.0													31.0	29.0	120
74WMOL-4	0.24	16.0	0.57	192	2.04	23.9	1.52	368	9.16	399	2.26	27.6	65.2	10.3	48.0	12.1	3.58	12.29	1.90	10.71	2.06	5.23	0.75	4.22	0.59	58.8	23.8	19
74WMOL-5	0.22	19.3	0.61	210	2.04	24.4	1.52	376	9.15	399	2.34	27.7	68.0	10.4	48.0	12.0	3.54	12.04	1.89	10.27	1.98	5.03	0.73	4.11	0.58	57.5	23.8	22
74WMOL-9	0.03	0.2	0.17	103	1.21	17.8	1.15	246	6.05	427	1.60	18.3	42.0	6.9	33.3	8.8	2.90	9.22	1.44	8.13	1.60	4.02	0.59	3.31	0.47	46.8	32.8	98
74WMOL-11	0.04	0.5	0.27	90	1.29	18.5	1.21	269	6.75	415	3.41	18.9	48.8	7.5	36.3	9.6	3.10	9.81	1.56	8.74	1.66	4.26	0.61	3.47	0.49	47.4	32.5	68
74WMOL-13	0.07	5.5	0.22	84	0.71	10.6	0.70	162	3.99	370	1.05	11.2	29.4	4.5	21.7	5.9	1.96	6.19	0.98	5.61	1.07	2.76	0.39	2.22	0.32	30.9	31.7	93
74KAN-1	0.02	0.5	0.14	54	0.73	11.0	0.72	163	4.10	392	1.05	11.6	28.8	4.6	22.0	6.0	2.00	6.42	1.01	5.77	1.13	2.88	0.40	2.32	0.33	34.3	31.9	85
74KAN-2	0.03	1.2	0.26	60	1.05	15.9	1.01	227	5.67	401	1.42	15.8	41.3	6.3	30.0	8.1	2.64	8.35	1.32	7.46	1.43	3.64	0.51	2.92	0.41	40.7	33.1	70
74PH-1	0.02	0.4	0.17	101	0.84	11.9	0.77	175	4.41	375	1.06	12.4	30.7	4.9	23.5	6.4	2.12	6.73	1.08	6.13	1.18	3.02	0.43	2.48	0.34	34.1	32.8	75
84WMOL-1C (S)	0.06	1.3	0.26	99	1.08	15.9	1.01	225	5.58	404	1.40	14.8	37.1	6.0	29.0	7.9	2.60	8.32	1.32	7.46	1.44	3.68	0.53	2.99	0.42	40.9	33.8	
84WMOL-1D (S)	0.09	0.4	0.23	92	1.35	18.5	1.20	269	6.68	414	1.71	18.1	44.7	7.3	34.7	9.1	2.98	9.38	1.47	8.13	1.53	3.95	0.57	3.19	0.44	45.1	32.1	
84WMOL-1C (NW)	0.12	0.5	0.25	68	1.11	16.0	1.05	226	5.83	394	1.41	15.8	36.3	6.1	28.8	7.9	2.56	8.30	1.31	7.46	1.46	3.75	0.55	3.07	0.43	43.5	32.7	
84WMOL-1C (NE)	0.05	0.5	0.21	83	1.29	18.1	1.15	259	6.47	407	1.59	13.8	36.9	6.0	28.8	8.2	2.77	8.45	1.35	7.54	1.47	3.80	0.56	3.17	0.46	41.1	31.9	
84WMOL-1D (N)	0.09	4.5	0.23	95	0.83	12.5	0.80	177	4.37	378	1.10	14.1	34.0	5.4	25.2	6.7	2.24	7.16	1.12	6.37	1.25	3.32	0.47	2.58	0.37	39.7	32.2	
89KAA-2	0.14	7.6	0.30	151	1.01	15.6	1.00	193	4.81	438	1.28	14.2	36.1	5.4	25.6	6.9	2.24	7.00	1.09	6.09	1.17	2.91	0.42	2.36	0.33	33.1	30.8	

Table 4. (continued)

Sample	Cs	Rb	U	Ba	Th	Nb	Ta	Zr	Hf	Sr	Pb	La	Ce	Pr	Nd	Sm	Eu	Gd	Tb	Dy	Ho	Er	Tm	Yb	Lu	Y	Sc	Ni*
89FDD-1 (glass)	0.12	8.4	0.27	109	0.80	11.9	0.77	167	4.21	394	2.07	12.1	31.2	4.7	22.2	6.0	2.01	6.21	0.99	5.58	1.06	2.71	0.38	2.21	0.31	29.9	31.4	
89FDD-2 (glass)	0.11	7.4	0.25	96	0.73	11.0	0.73	159	4.06	366	1.81	11.0	29.1	4.4	21.0	5.8	1.92	6.00	0.96	5.43	1.03	2.67	0.38	2.20	0.31	29.5	30.6	
804GEO-1	0.19	18.3	0.51	235	1.52	20.2	1.28	303	7.33	411	1.83	22.6	57.7	8.8	41.8	11.2	3.51	11.63	1.83	10.38	1.98	5.13	0.73	4.05	0.58	58.7	29.4	170
808GEO-1	0.13	10.6	0.34	142	1.02	15.4	0.98	200	5.01	437	1.22	14.5	35.6	5.6	26.2	6.9	2.29	6.96	1.10	6.11	1.15	2.87	0.41	2.35	0.32	32.9	31.7	67
815GEO-1	0.20	11.5	0.37	144	1.08	15.9	1.01	220	5.42	387	1.42	16.2	37.8	6.4	30.9	8.4	2.81	8.89	1.40	7.93	1.53	3.93	0.55	3.16	0.45	44.1	30.3	58
Tholeiitic basalt clasts from submarine breccia slope																												
T307R1	0.05	3.8	0.66	43	0.42	8.0	0.51	116	3.13	278	0.63	7.8	19.6	3.0	15.0	4.4	1.53	4.86	0.77	4.39	0.83	2.14	0.29	1.77	0.26	24.4	29.0	442
T307R2	0.10	7.5	0.57	97	0.58	9.7	0.60	140	3.67	420	1.21	11.9	27.9	4.1	19.4	5.4	1.76	5.43	0.81	4.49	0.82	2.06	0.28	1.69	0.25	24.1	25.4	167
T307R3	0.11	5.7	0.14	65	0.47	8.6	0.54	110	2.99	294	0.74	8.6	20.8	3.1	14.8	4.3	1.47	4.65	0.72	4.08	0.76	1.96	0.27	1.63	0.24	22.1	27.4	543
T307R4	0.05	4.2	0.15	53	0.47	9.8	0.63	114	3.10	240	0.54	8.2	20.2	3.1	14.8	4.4	1.50	4.92	0.78	4.50	0.86	2.13	0.30	1.83	0.28	24.7	29.8	500
T307R6	0.05	3.3	0.11	35	0.38	8.2	0.52	98	2.66	208	0.47	6.8	16.9	2.6	12.5	3.8	1.35	4.39	0.68	3.99	0.76	1.97	0.28	1.66	0.25	22.4	27.3	786
T307R7	0.10	3.4	0.23	38	0.38	8.1	0.51	97	2.62	232	0.47	6.8	16.8	2.6	12.4	3.8	1.33	4.33	0.69	3.98	0.75	1.96	0.28	1.67	0.25	22.4	27.5	743
T307R8	0.10	3.3	0.11	27	0.35	7.4	0.48	87	2.39	181	0.50	6.3	15.4	2.3	11.4	3.4	1.16	3.75	0.60	3.49	0.65	1.66	0.23	1.42	0.21	19.2	24.6	840
REE-Y enriched tholeiite																												
74WMOL-1*		4		110	1.45	15		249	6.80	340		42.0	61.0		88.5	27.6	9.74	30.3	3.69				1.85	9.05	1.13	108	32	79
74WMOL-2*		4		284	0.90	10		164	4.30	368		51.0	35.0		41.0	9.8	3.48	19.3	1.66				1.07	4.75	0.74	150	31	118
74WMOL-3*		4		140	0.90	8		154	4.10	388		48.0	116.0		79.5	22.8	7.79	29.0	3.01				1.46	8.00	1.02	88	31	120
74WMOL-6	0.29	0.5	0.17	100	0.71	11.7	1.51	160	4.82	359	1.06	40.2	83.9	23.4	151	54.0	21.2	93.4	15.4	96.1	20.9	56.4	8.02	42.8	6.60	662	32.1	139
74WMOL-7*		2		73	1.10	17		204	5.20	382		43.0	45.0		62.0	15.9	5.25	21.4	3.81				1.68	8.90	1.28	204	30	99
74WMOL-8*		7		91	0.90	16		158	3.95	364		24.5	30.0		39.5	10.9	3.68	14.9	1.56				0.86	4.45	0.59	56	31	135
74WMOL-10*		7		86	1.30	14		227	6.25	432		48.5	47.0		56.0	14.3	5.08	20.6	2.11				1.09	6.60	0.96	118	31	84
74WMOL-12	0.04	0.2	0.19	55	0.79	12.1	0.78	178	4.48	386	1.09	15.4	30.4	5.5	26.7	7.2	2.48	8.51	1.31	7.56	1.53	3.97	0.55	2.94	0.42	56.0	33.3	92
WMO-16	0.03	0.6	0.19	88	0.84	11.6	0.81	172	4.49	400	1.15	20.7	30.1	7.2	36.0	9.8	3.49	12.64	1.98	11.74	2.52	6.70	0.93	4.88	0.76	85.0	31.9	
32GEO-1*		12		161		18		200		452		45.0	89.0													132	31	59
805GEO-1*		3		41		12		152		381		21.0	33.0													122	36	92
813GEO-1*		11		89		12		156		377		26.0	54.0													68	33	74
895GEO-1*		10		95		14		170		369		80.0	175.0													172	35	75
91GEO-1	0.12	7.5	0.23	96	0.69	10.3	0.66	156	3.90	355	1.04	12.8	32.0	5.2	25.9	7.3	2.71	8.80	1.35	7.79	1.60	4.16	0.55	2.94	0.43	57.8	31.2	73

[a] Trace element compositions are in ppm. All data determined by ICP-MS at MIT and Washington State University (T307- samples) except that Ni data for all samples were determined by XRF, and REE and Sc in 29GEO-3, 71WMOL-3, and 10 REE-Y enriched tholeiitic basalt (designated by *) were determined by INAA.

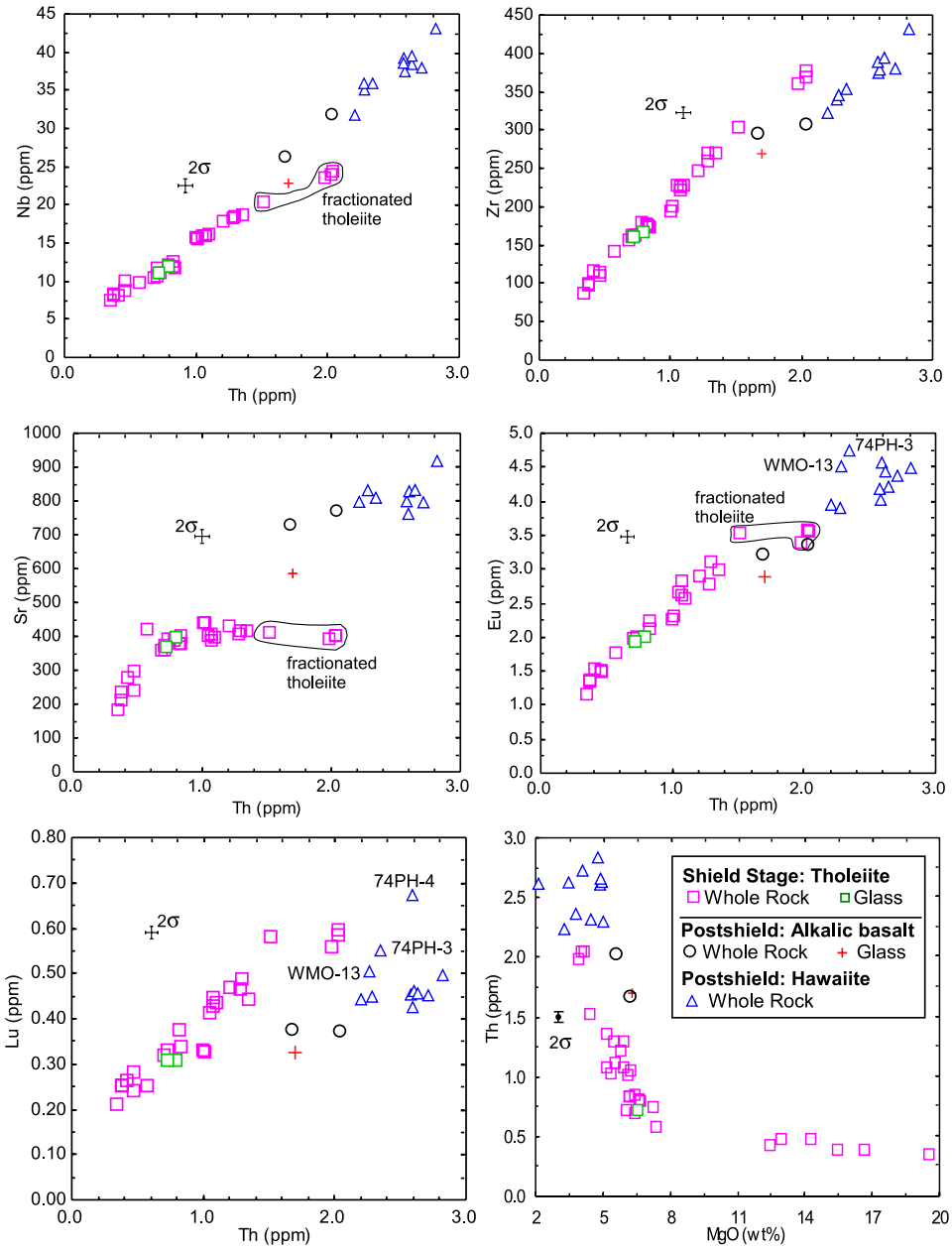

Figure 7. Th abundance versus Nb, Zr, Sr, Eu, Lu, and MgO abundances for West Molokai lavas. Tholeiitic basalts with REE-Y enrichment are not shown in the Th-Eu and Th-Lu panels. The 2 sigma uncertainties for the trace elements analyzed by ICP-MS are ±3%.

lavas [*Xu et al.*, 2005] are listed in Table 6. West Molokai tholeiitic and alkalic lavas define inverse trends in $^{87}Sr/^{86}Sr$ versus $^{143}Nd/^{144}Nd$ and $^{176}Hf/^{177}Hf$ plots (Figure 8). At the low $^{87}Sr/^{86}Sr$ and high $^{143}Nd/^{144}Nd$ and $^{176}Hf/^{177}Hf$ end, West Molokai tholeiitic lavas overlap with the field for Kea shield lavas, but other West Molokai tholeiitic lavas extend to higher $^{87}Sr/^{86}Sr$ and lower $^{143}Nd/^{144}Nd$ and $^{176}Hf/^{177}Hf$ overlapping with Loa shield lavas; the extreme is sample T307R2, which is similar to the Hawaiian end-member defined by Koolau (Makapuu stage) lavas (Figure 8). Two postshield West Molokai alkalic basalts and five hawaiites, are nearly homogenous in terms of Sr, Nd and Hf isotopic ratios (Figure 8). Two tholeiitic basalts, 89KAA-2 and T307R4, have isotopic ratios of Sr and Nd similar to these postshield lavas (Figure 8). Sample 89KAA-2 is from Kaa Gulch where alkalic basalt and hawaiite

Table 5. Sr, Nd, Hf, and Pb Isotope Data for West Molokai Samples[a]

Sample[b]	$^{87}Sr/^{86}Sr$[c]	2σ[g]	$^{143}Nd/^{144}Nd$[c]	2σ	$^{176}Hf/^{177}Hf$[d]	2σ	$^{206}Pb/^{204}Pb$[e]	2σ	$^{207}Pb/^{204}Pb$[e]	2σ	$^{208}Pb/^{204}Pb$[e]	2σ
Postshield-Stage Lavas												
Hawaiite												
71 WMOL-4	0.703662	10	0.512985	6	0.283109	4	18.419	1	15.489	1	37.985	3
74 PH-2	0.703635	10	0.512998	9	0.283113	5	18.402	3	15.503	2	37.986	5
84 WMOL-3	0.703638	8	0.512992	6	0.283116	5	18.378	2	15.474	2	37.897	4
84 WMOL-4	0.703636	13	0.513001	8	0.283108	4	18.409	2	15.510	2	38.012	5
84 WMOL-4 Rep	0.703648	7										
84 WMOL-4 TS							18.3962	23	15.4914	29	37.9642	93
86 GEO-1	0.703662	10	0.513000	8	0.283105	4	18.423	2	15.492	2	37.983	4
Alkalic basalt												
84 WMOL-5	0.703631	8	0.512984	8	0.283115	5	18.371	2	15.469	2	37.878	5
84 WMOL-5 TS							18.3911	21	15.4878	26	37.9482	84
29 GEO-2	0.703622	14	0.513005	6	0.283113	4	18.426	3	15.487	2	37.957	5
Shield-Stage Lavas												
Subaerial tholeiite[f]												
71WMOL-1*	0.70378	5	0.512930	28			18.133	17	15.455	18	37.751	59
71WMOL-3*	0.70376	5	0.512940	22			18.167	18	15.460	19	37.754	58
74 WMOL-5	0.703762	10	0.512932	7	0.283082	5	18.092	1	15.447	1	37.777	2
74 WMOL-5 Rep	0.703772	8										
74 WMOL-5 TS							18.1020	25	15.4588	31	37.8221	102
74 WMOL-13	0.703815	10	0.512933	18	0.283072	4	18.080	2	15.469	2	37.849	4
74 WMOL-13 Rep	0.703816	10										
74 WMOL-13 Dup							18.071	2	15.458	2	37.810	6
74 WMOL-13 TS							18.0688	19	15.4560	24	37.8153	78
74 KAN-1	0.703777	7					18.094	4	15.453	3	37.793	8
74 PH-1	0.703705	8					18.170	4	15.442	3	37.788	8
74 PH-1 TS							18.1783	23	15.4578	29	37.8490	93
84 WMOL-D(N)	0.703968	8	0.512867	7	0.283030	4	18.105	2	15.470	2	37.912	5
84 WMOL-D(N) Rep	0.703973	8										
84 WMOL-D(N) Dup	0.703972	8					18.085	2	15.444	2	37.831	4
84 WMOL-D(N) TS							18.0952	32	15.4575	40	37.8874	131
89 KAA-2	0.703592	8	0.512996	7	0.283110	4	18.234	3	15.485	3	37.874	8
89 KAA-2 Dup	0.703593	10										
804 GEO-1	0.703757	10	0.512949	6	0.283082	5	18.118	2	15.464	2	37.834	5
808 GEO 1	0.703720	8	0.512958	7	0.283086	4	18.237	2	15.487	2	37.921	5
808 GEO 1 Rep	0.703725	8										
808 GEO 1 TS							18.2316	19	15.4736	25	37.8886	80
815 GEO-1	0.703733	10	0.512949	6	0.283084	4	18.123	2	15.465	2	37.816	4
Tholeiitic basalt clasts from submarine breccia slope												
T307R1	0.703697 (C)	13	0.512954 (C)	4	0.283110	4	18.225 (C)	5	15.459 (C)	4	37.850 (C)	10
T307R1 TS			0.512976	6	0.283119 (L)	3	18.2285	22	15.4651	22	37.8985	64
T307R2	0.704098	8	0.512706	5	0.282956 (L)	4	17.8427	24	15.4349	29	37.7415	91

Table 5. (continued)

Sample[b]	$^{87}Sr/^{86}Sr$[c]	2σ[g]	$^{143}Nd/^{144}Nd$[c]	2σ	$^{176}Hf/^{177}Hf$[d]	2σ	$^{206}Pb/^{204}Pb$[e]	2σ	$^{207}Pb/^{204}Pb$[e]	2σ	$^{208}Pb/^{204}Pb$[e]	2σ
T307R4	0.703666 (C)	12	0.513003 (C)	4	0.283141	4	18.438 (C)	18	15.470 (C)	15	38.003 (C)	37
T307R4			0.513009	4	0.283143 (L)	3						
T307R6			0.513002	5	0.283138 (L)	3	18.3740	23	15.4623	27	38.0107	85
T307R7			0.512997	7	0.283144 (L)	5	18.3774	35	15.4646	43	38.0209	140
T307R8			0.513005	6	0.283136 (L)	4	18.4358	47	15.4731	47	38.0996	134

[a] Most Sr, Nd, and Pb isotopic data were obtained at MIT. Exceptions are (1) 71WMOL-1 and −3 Sr, Nd, and Pb data from *Stille et al.* [1986]; (2) T307R1 and R4 Sr, Nd, and Pb data obtained at Carleton University by B. Cousens; (3) Nd data for T307 samples obtained at Ecole Normale Supérieure in Lyon (ENSL) by J. Blichert-Toft; and (4) Pb data by the triple-spike technique (TS) obtained at Max-Planck-Institut fur Chemie (MPI) by W. Abouchami. In figures the Sr result with smaller error, and the Nd data from Ecole Normale Supérieure in Lyon were used when there are duplicates and the average of duplicates for Pb are plotted. The leached Hf data were used when both leached and unleached data exist.

[b] Samples with postfix "Dup" are full procedural duplicates, i.e., separate aliquot of powder. Samples with postfix "Rep" are duplicate runs on TIMS. Samples with postfix "TS" designate Pb data obtained by triple-spike technique.

[c] Sr data were normalized to $^{86}Sr/^{88}Sr = 0.1194$ and Nd were normalized to $^{146}Nd/^{144}Nd = 0.7219$. Mean measured $^{87}Sr/^{86}Sr$ for NBS987 during the course of study at MIT was 0.710240 ± 13 (2σ, n = 27), and $^{143}Nd/^{144}Nd$ for JNdi-1 in-house standard was 0.512103 ± 8 (2s, n = 12). This standard value is generally lower by 0.000013 compared with JNdi-1 value of 0.512115 [*Tanaka et al.*, 2002]. Therefore all the Nd reported were corrected for interlaboratory bias to JNdi-1 of 0.512115. Two samples, T307R1 and R4, analyzed at Carleton University ("(C)" following value) were also corrected on the basis of measured Sr standard NBS987 of 0.710251 and Nd La Jolla standard of 0.511846.

[d] All the Hf isotopic ratios were analyzed at Ecole Normale Supérieure in Lyon. Most samples were not acid-leached; analyses of leached ("(L)" following value) and unleached aliquots for T307R1 and R4 are not significantly different in $^{176}Hf/^{177}Hf$. The Hf data are reported relative to JMC-475 Hf standard of 0.282160.

[e] The Pb analyses are corrected for fractionation using the NBS-981 standard. The average ratios measured for NBS-981 by conventional TIMS at MIT are $^{206}Pb/^{204}Pb = 16.896 \pm 0.016$, $^{207}Pb/^{204}Pb = 15.437 \pm 0.022$, and $^{208}Pb/^{204}Pb = 36.527 \pm 0.070$ (2 sigma) on the basis of 61 runs during the course of this study. The fractionation correction is $0.12 \pm 0.03\%$/amu. The average ratios measured for NBS-981 by conventional TIMS at Carleton are $^{206}Pb/^{204}Pb = 16.890 \pm 0.012$, $^{207}Pb/^{204}Pb = 15.429 \pm 0.014$, and $^{208}Pb/^{204}Pb = 36.502 \pm 0.048$ (2 sigma) on the basis of 73 runs during the course of the study. The fractionation correction is 0.13%/amu. The average ratios measured for NBS-981 by triple-spike method are $^{206}Pb/^{204}Pb = 16.9447 \pm 0.0015$, $^{207}Pb/^{204}Pb = 15.5024 \pm 0.0015$, and $^{208}Pb/^{204}Pb = 36.7350 \pm 0.0034$ (2 sigma) on the basis of 12 runs during the course of this study. The reported Pb data, conventional TIMS, and triple-spike are normalized to the value of *Galer and Abouchami* [1998] for NBS-981, which requires fractionation correction of 0.135%/amu for conventional TIMS.

[f] The asterisk (*) for 71WMOL-1 and 71WMOL-3 indicates data from *Stille et al.* [1986]; the Sr and Nd isotopic data are plotted in the figures but Pb isotopic data are not used due to large uncertainties.

[g] Indicated 2σ are in-run uncertainties and apply to the last decimal places.

Table 6. Hf and Nd Isotopic Data for East Molokai Samples[a]

Sample	$^{176}Hf/^{177}Hf$	2σ	$^{143}Nd/^{144}Nd$
Late Shield/Postshield Lavas			
71PELE-19	0.283120	5	0.513017
71PELE-21	0.283137	4	0.513029
71WAIK-14F	0.283133	4	0.513015
71WAIK-10F	0.283137	5	0.513039
MT 5.3 + 375F	0.283121	5	0.513021
MT 4.6F	0.283107	4	0.513006
71HALW-4	0.283113	4	0.513012
Rejuvenated-Stage Lavas			
74KAL-1	0.283175	5	0.513068
P5-252-2	0.283182	5	0.513063
P5-253-9	0.283172	3	0.513057
P5-253-11B	0.283174	4	0.513064
P5-253-12	0.283180	4	0.513072

[a] Reported 2σ applies to the last decimal place. Nd data are from *Xu et al.* [2005].

were also sampled (Figure 3); sample T307R4 is from a loose block on a submarine slope of sediment-covered thin breccia units (see section 3); therefore it is possible that these tholeiitic basalts were intercalated with alkalic basalts erupted in the postshield stage as observed at Mauna Kea [*Frey et al.*, 1991].

[27] On an εNd-εHf plot, West Molokai lavas define a linear trend (Figure 9). Alkalic postshield and some shield tholeiitic lavas overlap with the field for Kea shield lavas; most of the West Molokai shield lavas overlap with the field for Mauna Loa lavas. The two most extreme West Molokai lavas (84WMOL-1D(N) and T307R2) are close to or overlap the field defined by lavas forming the Lanai and Koolau (Makapuu-stage) shields.

[28] In εNd versus εHf plot, East Molokai late shield/postshield lavas overlap with the field for other Kea shields, such as Mauna Kea (Figure 9). Like other rejuvenated-stage lavas, East Molokai rejuvenated-stage lavas are offset form the shield trend to higher εHf at a given εNd; this offset has been interpreted as evidence for a non-MORB (mid-ocean ridge basalt) related, depleted component in the plume source [*Bizimis et al.*, 2005; e.g., *Frey et al.*, 2005; *Salters et al.*, 2006].

[29] West Molokai lavas range widely in $^{206}Pb/^{204}Pb$ ratios (17.84–18.44) and define elongated trends in $^{206}Pb/^{204}Pb$ versus $^{208}Pb/^{204}Pb$ and $^{207}Pb/^{204}Pb$ space (Figure 10). The West Molokai alkalic lavas have relatively high Pb isotopic ratios and overlap with the field for late shield and postshield lavas from East Molokai; in contrast, most West Molokai tholeiitic shield lavas have low Pb isotopic ratios (except for submarine samples T307R4, R6, R7 and R8), and their trend extends to the fields for Koolau (Makapuu-stage) and Lanai shield lavas with sample T307R2 at the low $^{206}Pb/^{204}Pb$ extreme (Figure 10). Relative to other West Molokai tholeiitic lavas, samples 84WMOL-1D(N) and especially T307R2, which have distinctly high $^{87}Sr/^{86}Sr$, and low $^{143}Nd/^{144}Nd$ and $^{176}Hf/^{177}Hf$ (Figures 8 and 9), are offset to higher $^{208}Pb/^{204}Pb$ at a given $^{206}Pb/^{204}Pb$; i.e., they have the highest $^{208}Pb^*/^{206}Pb^*$ (defined as $(^{208}Pb/^{204}Pb\text{-}29.475)/(^{206}Pb/^{204}Pb\text{-}9.307)$), which is a characteristic of Loa-trend lavas [*Abouchami et al.*, 2005].

7. Discussion

[30] A major objective of this study is to determine if West Molokai lavas have dominantly Loa- or Kea-trend geochemical characteristics, and in particular, to determine if the geochemical distinction between Loa- and Kea-trend lavas terminated at Molokai Island as proposed by *Abouchami et al.* [2005]. Although a minority of lavas at some volcanoes are exceptions, most shield-forming lavas of Kea- and Loa-trend volcanoes can be distinguished by differences in major and trace element abundances and isotopic ratios [e.g., *Frey and Rhodes*, 1993; *Frey et al.*, 1994; *Lassiter et al.*, 1996; *Abouchami et al.*, 2005]. In the following discussion, we use each of these data sets to determine whether West Molokai shield lavas are Kea- or Loa-like. Because the magmatic characteristics of West Molokai lavas have been variably affected by postmagmatic alteration, we first determined the geochemical effects of such alteration (see Appendix A, section A2). On the basis of Appendix A, section A2, our discussion of magmatic characteristics uses the major element composition of glasses, the trace element ratios Zr/Nb, Sr/Nb and La/Nb (screened for La/Nb < 1.25) and isotopic ratios of Sr, Nd, Hf and Pb.

7.1. Loa or Kea? Constraints From the Major Element Contents of West Molokai Tholeiitic Glass

[31] Glasses are useful in showing major element differences between Loa- and Kea-trend volcanoes because they represent unaltered, quenched melt. A difficulty with using the major element composition of glasses is that, like West Molokai glasses,

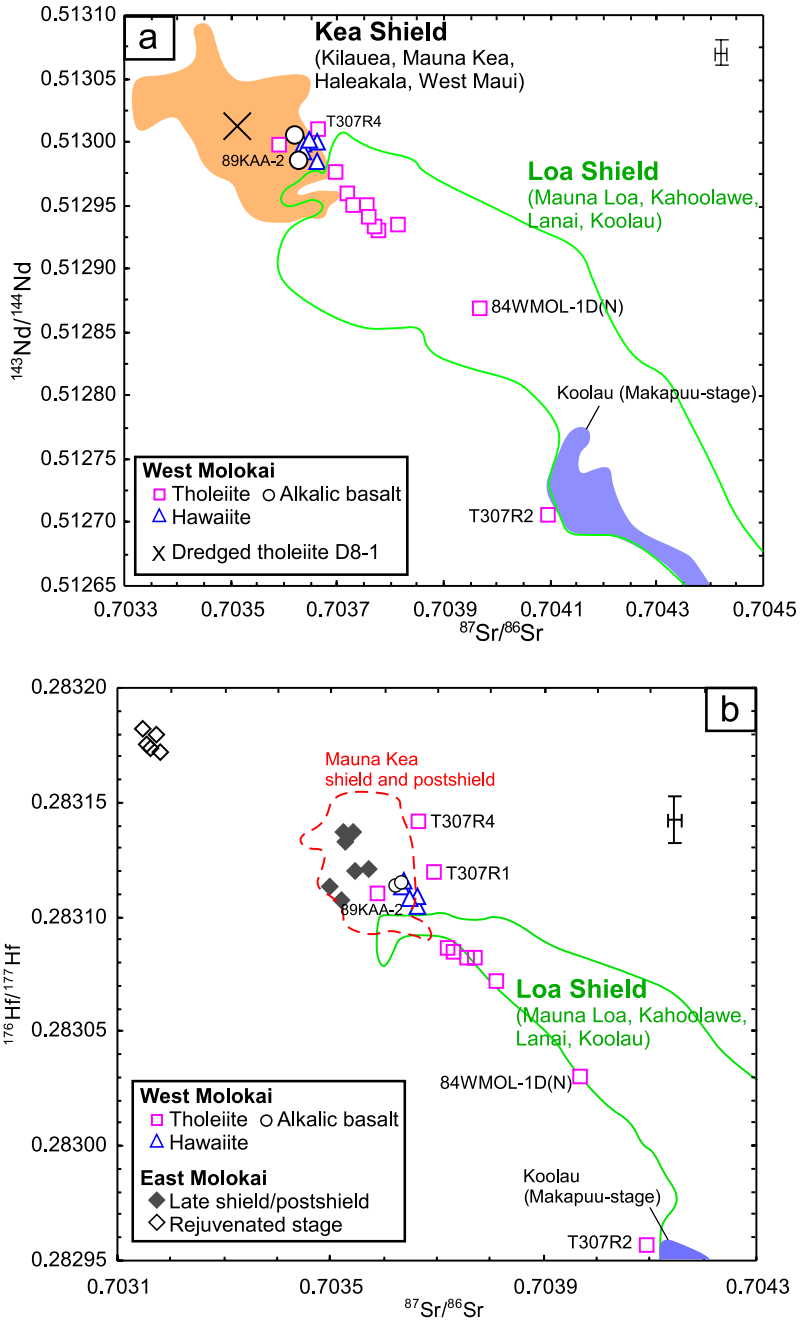

Figure 8. $^{87}Sr/^{86}Sr$ versus (a) $^{143}Nd/^{144}Nd$ and (b) $^{176}Hf/^{177}Hf$ for West Molokai and East Molokai lavas. For comparison, the fields are shield-stage lavas from Kea and Loa volcanoes in Figure 8a and Mauna Kea shield and postshield lavas and Loa shield lavas in Figure 8b. Only acid-leached Sr and Nd isotopic data were used to define fields for Kea and Loa volcanoes. The error bars are 2σ calculated for the means of 27 analyses of the NBS 987 Sr standard, 12 analyses of the JNdi-1 Nd standard, and 28 analyses of the JMC-475 Hf standard. Data sources: East Molokai, this study, *Xu et al.* [2005], and *Basu and Faggart* [1996]; West Molokai, this study (note that sample D8-1 (Figure 8a) is a dredged sample inferred to be erupted at West Molokai [*Tanaka et al.*, 2002], but it has Sr and Nd isotopic ratios distinct from all of our data for West Molokai samples); Mauna Loa, *Abouchami et al.* [2000], *Blichert-Toft and Albarède* [1999], *Cohen et al.* [1996], *DePaolo et al.* [2001], *Hauri et al.* [1996], *Kurz et al.* [1995], *Rhodes and Hart* [1995], and *Stracke et al.* [1999]; Mauna Kea, *Abouchami et al.* [2000], *Blichert-Toft and Albarède* [1999], *Blichert-Toft et al.* [2003], *Bryce et al.* [2005], *Kennedy et al.* [1991], and *Lassiter et al.* [1996]; Kilauea, *Chen et al.* [1996] and *Pietruszka and Garcia* [1999]; Kahoolawe, *West et al.* [1987] and *Huang et al.* [2005b]; Haleakala, *Ren et al.* [2006]; West Maui, *Gaffney et al.* [2004]; Lanai, *Gaffney et al.* [2005]; Koolau, *Roden et al.* [1994] and *Blichert-Toft et al.* [1999].

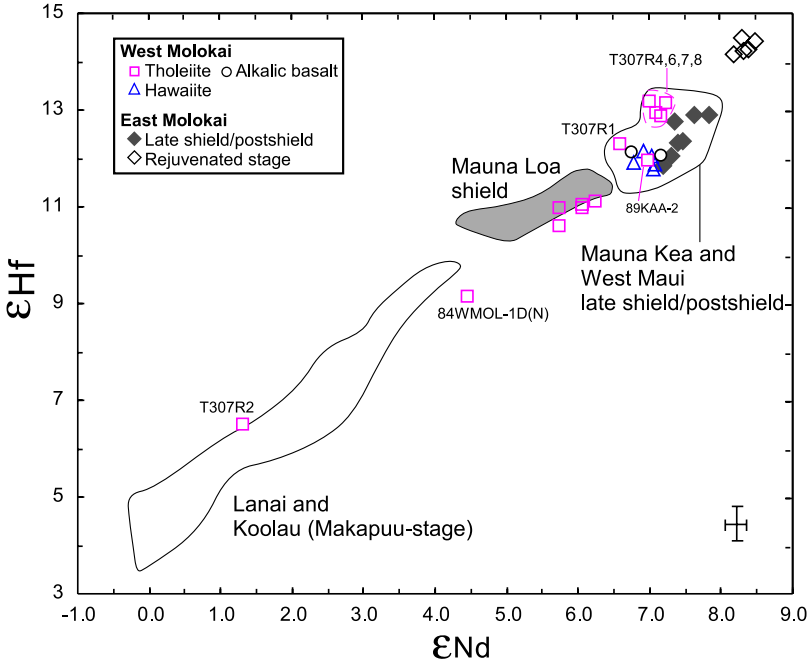

Figure 9. εNd (defined as 10000*(^{143}Nd/^{144}Nd/0.512638-1)) versus εHf (defined as 10000*(^{176}Hf/^{177}Hf/0.282772-1)) for East Molokai and West Molokai lavas. Also shown are fields for late shield/postshield lavas from Kea volcanoes (Mauna Kea, West Maui) and fields for shield lavas from Mauna Loa, Lanai, and Koolau (Makapuu stage). Tholeiitic basalts 89KAA-2, T307R1, R4, R6, R7, and R8 that have Nd and Hf isotopic ratios overlapping with the Kea field are labeled on the figure. Tholeiitic basalt 84WMOL-1D(N) and T307R2 with the most unradiogenic Nd and Hf isotopic ratios are also labeled. Data sources are the same as for Figure 8.

they typically have relatively low MgO contents (<7%) (Figure 5). Consequently, they have been affected by fractionation of clinopyroxene and plagioclase; for example, West Molokai glasses with <6.5% MgO clearly show the effects of clinopyroxene fractionation, i.e., a positive CaO-MgO trend (Figure 5a). Therefore it is necessary to use an MgO filter, >6.5%, to show the differences between Loa- and Kea-trend volcanoes. For example, the large data sets for glasses from Mauna Kea (HSDP core [*Garcia*, 1996; *Stolper et al.*, 2004]) and Mauna Loa [*Moore and Clague*, 1987, 1992; *Garcia et al.*, 1989, 1995; *Moore et al.*, 1995; *Garcia*, 1996] show that, relative to Mauna Kea glasses, Mauna Loa glasses range to higher Al_2O_3/CaO and lower TiO_2/Na_2O (Figure 5d). The West Molokai glasses collected during dive T307 and glass collected subaerially (i.e., artifacts and dikes) differ significantly in that the submarine glasses have higher CaO at a given MgO and lower Al_2O_3/CaO (Figures 5a and 5d). Therefore the submarine glasses are Kea-like, whereas subaerial glasses (i.e., artifacts and glasses on dike margins) are Loa-like (Figure 5d).

7.2. Loa or Kea? Constraints From Trace Element Ratios in West Molokai Whole Rocks and Glasses

[32] Relatively young, <100 ka Mauna Loa shield lavas define a Zr/Nb versus Sr/Nb field that is distinct from the field for shield and postshield lavas from Mauna Kea (Figure 11). A complication to this Loa-Kea dichotomy is that some older, >100 ka, Mauna Loa lavas [*Kurz et al.*, 1995; *Morgan et al.*, 2007], overlap with the Mauna Kea field; i.e., 15 of the entire data set (158 samples) for Mauna Loa are within the Mauna Kea field. Nevertheless, in general these trace element abundance ratios in Hawaiian lavas are correlated with isotopic ratios (e.g., Figure 12); therefore the Loa-Kea trace element differences in Figure 11 are interpreted to reflect Loa-Kea source differences [e.g., *Frey and Rhodes*, 1993; *Huang and Frey*, 2003; *Ren et al.*, 2005].

[33] Shield tholeiitic lavas from West Molokai range from 11.6 to 15.3 in Zr/Nb. Subaerial tholeiitic whole rocks and glasses with MgO > 6.5% have Zr/Nb > 14 and plot within the field for Mauna Loa lavas (Figure 11). Submarine breccia

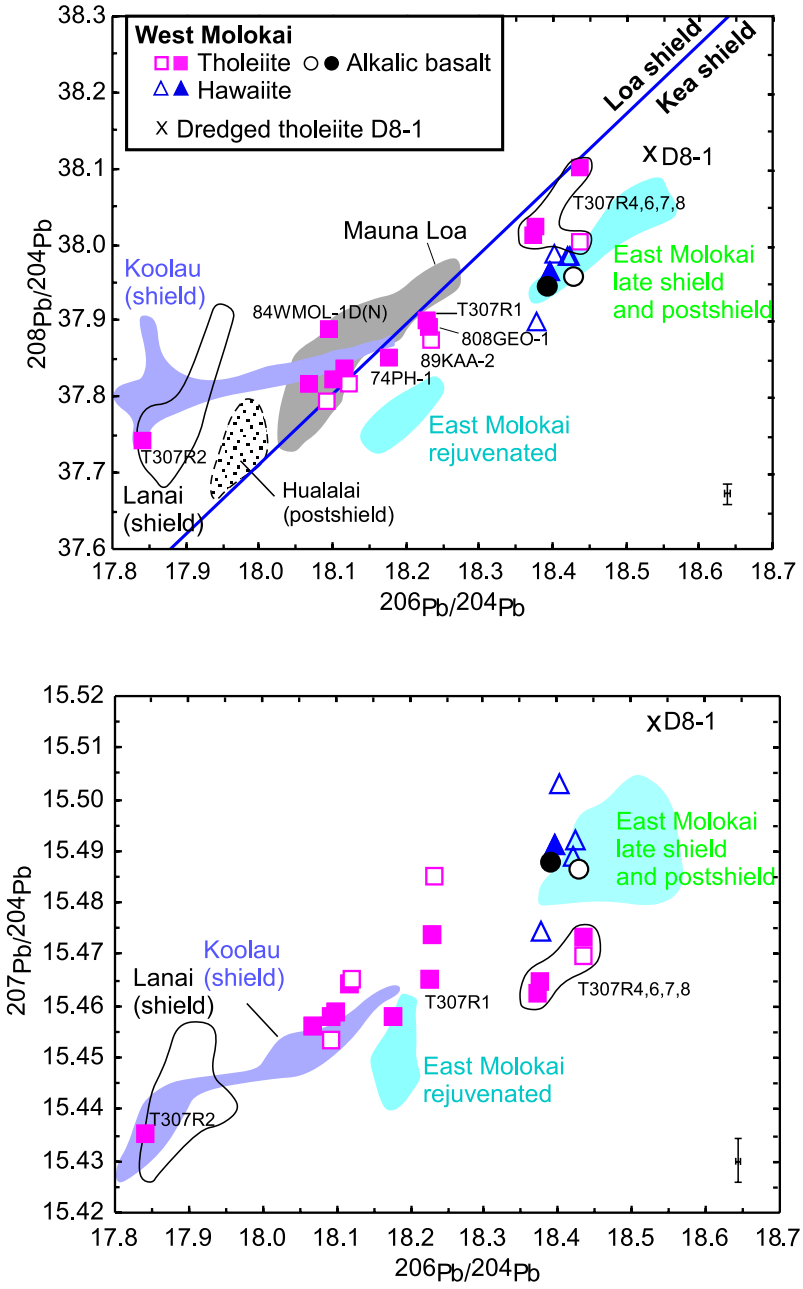

Figure 10. $^{206}Pb/^{204}Pb$ versus $^{208}Pb/^{204}Pb$ and $^{207}Pb/^{204}Pb$ for West Molokai lavas and sample D8-1 (see Figure 8 caption). Fields for East Molokai, Mauna Loa, Lanai, and Koolau (Makapuu stage and KSDP) are shown. Filled symbols are for triple-spike data, and open symbols are for traditional TIMS data. West Molokai lavas straddle the Loa-Kea boundary line defined by *Abouchami et al.* [2005]. Data sources: this study as well as *Abouchami et al.* [2000, 2005], *Fekiacova et al.* [2007], *Wanless et al.* [2006], *Tanaka et al.* [2002], and *Xu et al.* [2005]. The 2 sigma errors shown are the maximum in-run uncertainties for triple-spike data and conventional TIMS (Table 5).

clast samples (T307R1, R2 and R3, all with MgO > 7.4%) from the lower part of the north slope also have high, Mauna Loa-like Sr/Nb and Zr/Nb ratios, whereas samples collected farther upslope (T307R4, R6, R7 and R8) have low, Mauna Kea-like ratios (Figure 11). If eruption age decreases upward on this submarine breccia slope a Loa- to Kea-like temporal trend is inferred from the breccia clasts. However, glasses from this submarine breccia slope with diverse origins, such as glass rinds on basaltic clasts and glass grains in sediment (Table 2), have Kea-like major element character-

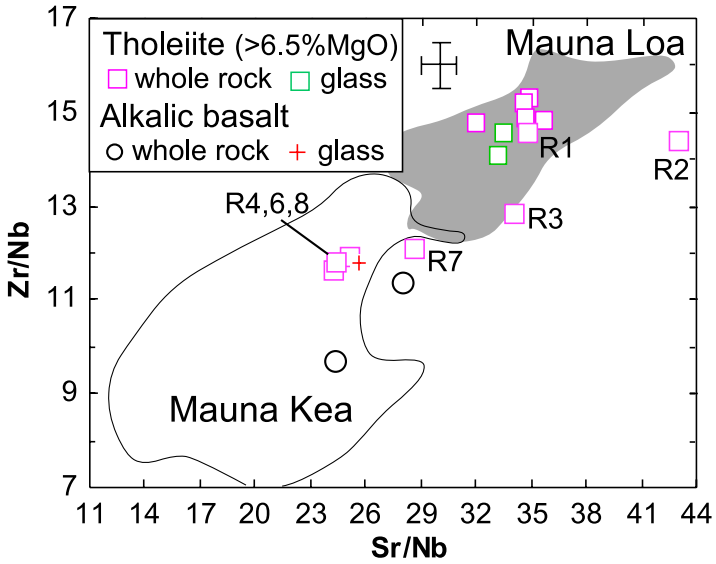

Figure 11. Sr/Nb versus Zr/Nb for West Molokai lavas. Fields for lavas from Mauna Kea and <100 ka lavas from Mauna Loa are shown for comparison. Only lavas with major element data and with MgO > 6.5% are included to minimize the effect of clinopyroxene, plagioclase, and Fe-Ti oxide fractionation on Sr/Nb and Zr/Nb ratios. Nevertheless, there are a few outlier samples, such as Mauna Kea sample SR129-5.10 from the HSDP core which is a plagioclase cumulate (13% plagioclase phenocryst [*DePaolo et al.*, 1999]) resulting in anomalously high Sr/Nb (33.2 [*Huang and Frey*, 2003]) at a MgO content of 6.9% [*Rhodes and Vollinger*, 2004]. The 2 sigma uncertainties are 3%. Subaerially exposed West Molokai shield lavas overlap the Mauna Loa field, but postshield lavas overlap the Mauna Kea field. Samples (Rx) from the north breccia slope range from Loa-like at the bottom (R2) to Kea-like at the top (R4, R6, R7, and R8). Data sources: Mauna Kea, *Frey et al.* [1990, 1991], *Rhodes* [1996], and *Huang and Frey* [2003]; Mauna Loa, *Rhodes* [1995, 1996], *Rhodes and Hart* [1995], and *Rhodes and Vollinger* [2004].

istics (Figure 5). Consequently, the robust result is that major and trace element compositions of the West Molokai shield lavas show that both Loa- and Kea-like compositions are present.

7.3. Loa or Kea? Constraints From Sr-Nd-Hf-Pb Isotopic Ratios of West Molokai Lavas

[34] Sr, Nd and Hf isotopic ratios for the West Molokai shield lavas range widely (Figures 8 and 9). At one extreme, samples are close to (84WMOL-1D(N)) or within (T307R2) the field for the Loa end-member defined by Makapuu-stage lavas of the Koolau shield. *Abouchami et al.* [2005] proposed that Pb isotopic ratios are the best geochemical discriminant between Loa and Kea lavas. In particular, Loa lavas have high $^{208}Pb/^{204}Pb$ at a given $^{206}Pb/^{204}Pb$, as measured by $^{208}Pb^*/^{206}Pb^*$. Consistent with their Loa-like Sr, Nd and Hf isotopic ratios, samples 84WMOL-1D(N) and T307R2 have relatively low $^{206}Pb/^{204}Pb$ and the highest $^{208}Pb^*/^{206}Pb^*$ (Figures 10 and 13). At the other extreme, samples 89KAA-2 and T307R4, R6, R7 and R8 have Kea-like isotopic ratios very similar to those of the West Molokai alkalic postshield lavas.

[35] In summary, West Molokai lavas shifted from a shield containing both Loa- and Kea-like lavas to a postshield with only Kea-like geochemical characteristics. However, among the studied subaerial- and submarine-erupted West Molokai shield lavas, age constraints are not sufficient to assess if there was a systematic temporal trend, such as Loa to Kea, during growth of the West Molokai shield. On the basis of existing data we infer a temporally random sampling of Loa- and Kea-like sources. In support of this inference a sample (MAH-35) studied by *Shinozaki et al.* [2002] collected from close to the summit of West Molokai has a major element composition very similar to T307R2, notably relatively low CaO and Fe_2O_3 and high SiO_2 at a given MgO (Figure 6). Consequently, Loa-like samples occur low in the submarine breccia section and near the summit.

[36] Also sample D8-1, dredged approximately 40 km from the West Molokai coastline (see Figure 1b and *Tanaka et al.* [2002]), has considerably lower $^{87}Sr/^{86}Sr$, higher $^{143}Nd/^{144}Nd$ and more radiogenic Pb isotopic ratios than any West

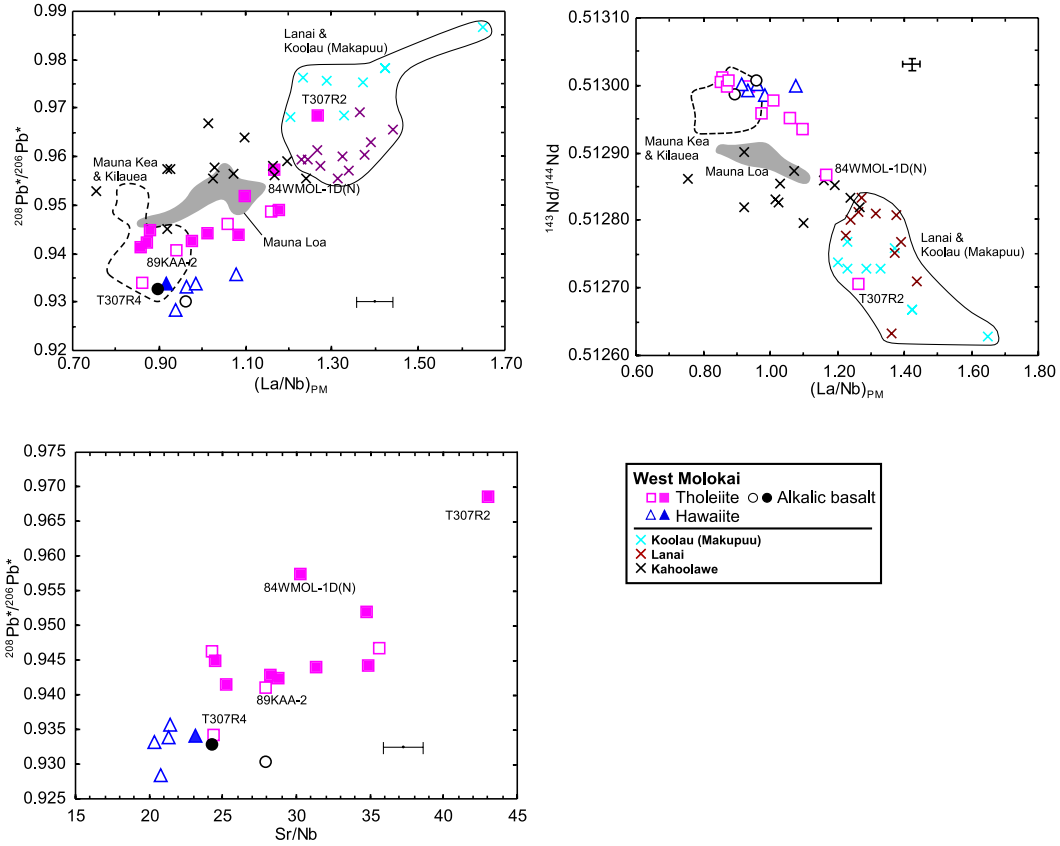

Figure 12. La/Nb and Sr/Nb versus $^{208}Pb^*/^{206}Pb^*$ and La/Nb versus $^{143}Nd/^{144}Nd$ for West Molokai lavas. Fields for Mauna Kea and Kilauea, Mauna Loa, and Lanai and Koolau (Makapuu stage) are shown for comparison. Filled symbols are for triple-spike Pb data, and open symbols are for traditional TIMS Pb data. Samples which experienced fractionation of plagioclase and Fe-Ti oxide are not plotted. These trace element ratios in West Molokai shield lavas are correlated with radiogenic isotopic ratios and trend from the Loa to Kea fields. Therefore we infer that La/Nb, Sr/Nb, and Zr/Nb (not shown) are source related. La/Nb is shown because this ratio is less sensitive than Zr/Nb and Sr/Nb to processes such as partial melting and crystallization. Data sources: *Abouchami et al.* [2005], *Eisele et al.* [2003], *Gaffney et al.* [2005], *Huang and Frey* [2003, 2005b], *Pietruszka and Garcia* [1999], *Rhodes and Hart* [1995], and *Wanless et al.* [2006].

Molokai lava in this study (Figures 8a and 9); it overlaps in these ratios with the field of Nuuanu landslide samples that are inferred to be early, Kea-like lavas of the Koolau shield (Kalihi-stage) [*Tanaka et al.*, 2002]. In this case the West Molokai and Koolau shields have sampled the full isotopic range expressed by younger Loa- and Kea-trend volcanoes. Alternatively, we note that the dredge location of sample D8-1 is within or close to the proposed boundary of the Nuuanu landslide which is inferred to originate from Koolau volcano (Figure 1c) [*Moore and Clague*, 2002; *Shinozaki et al.*, 2002]. Hence it is possible that this dredge sample erupted at Koolau volcano rather than at West Molokai.

7.4. Effects of the Molokai Fracture Zone on Hawaiian Volcanism

[37] Previous geochemical studies suggested that the Molokai Fracture Zone (MFZ) had an important influence on Hawaiian volcanism [e.g., *Basu and Faggart*, 1996; *Abouchami et al.*, 2005]. The MFZ, a large-offset fracture zone in the northeast Pacific Ocean, was named from its intersection with the Hawaiian island chain in the vicinity of Molokai Island [*Menard*, 1962]. It is considerably more complex than a simple offset of oceanic crust with different ages because it consists of several ENE-WSW tectonic lineaments forming two major bands, the Oahu and Maui strands, which cross the Hawaiian island chain (Figure 1a) [*Searle et al.*, 1993]. Oceanic lithosphere on opposite sides of the

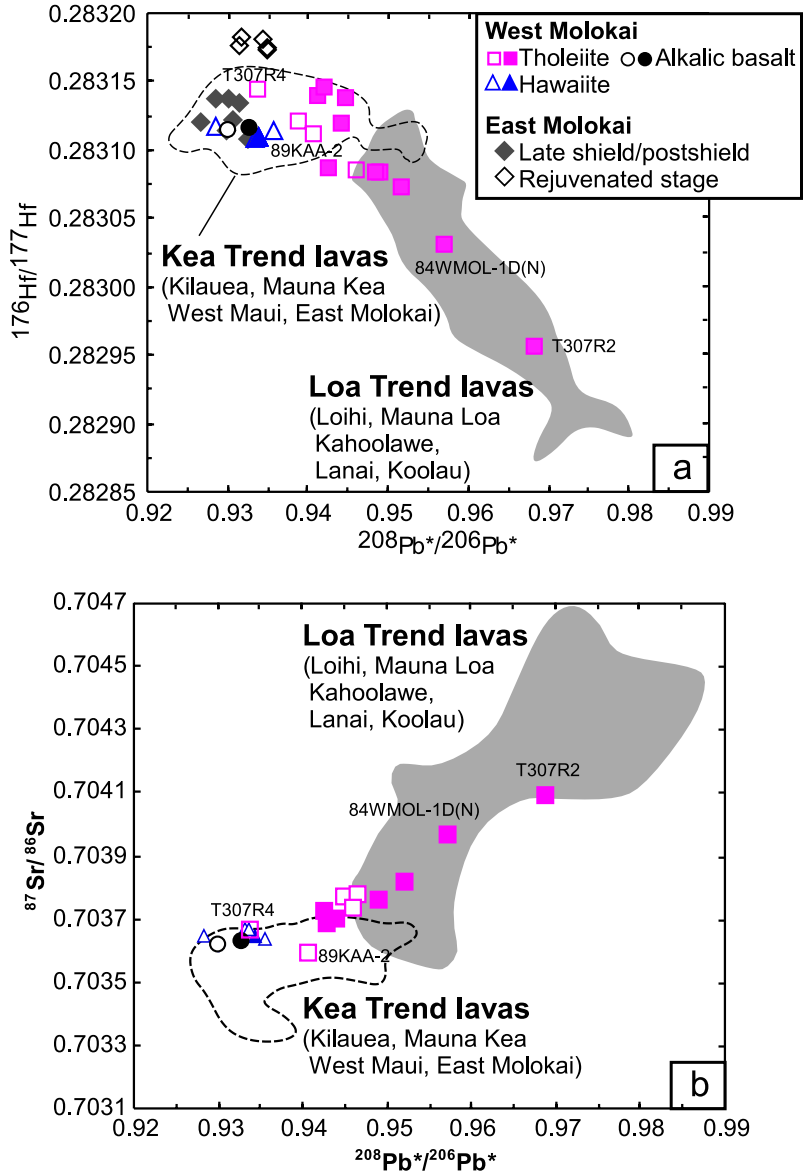

Figure 13. (a) $^{208}Pb^*/^{206}Pb^*$ versus $^{176}Hf/^{177}Hf$ for West Molokai and East Molokai lavas and (b) $^{208}Pb^*/^{206}Pb^*$ versus $^{87}Sr/^{86}Sr$ for West Molokai lavas. Fields for lavas from Kea and Loa volcanoes are shown for comparison. Filled symbols are for triple-spike Pb data, and open symbols are for traditional TIMS Pb data. Only literature data with Pb isotopes analyzed by triple-spike and MC-ICP-MS are used in defining the fields for Loa and Kea lavas. Using this filter, the fields for lavas from Loa and Kea volcanoes overlap only slightly; the region of overlap is defined by lavas from Loihi and the low SiO_2 group of shield lavas at Mauna Kea. West Molokai shield lavas include Loa- and Kea-like lavas, whereas postshield alkalic basalt and hawaiite are Kea-like. Data sources are the same as Figure 8.

strands has different ages and thicknesses [*ten Brink and Brocher*, 1988; *Searle et al.*, 1993]. For example, the Pacific crust south of Oahu is older by ~15 Myr. *Hieronymus and Bercovici* [2001] noted that such differences should be evident in the volcanism on opposite sides of the fracture zone, but the small inferred difference in lithospheric thickness, only a few kilometers, is an unlikely explanation for the dramatic increase in volume at ~2 Ma at Maui Nui. More likely explanations are temporal variation in plume flux [*Robinson and Eakins*, 2006].

[38] *Basu and Faggart* [1996] argued that the MFZ enabled influx of a lower mantle plume component represented by the Hawaiian geochemical end-

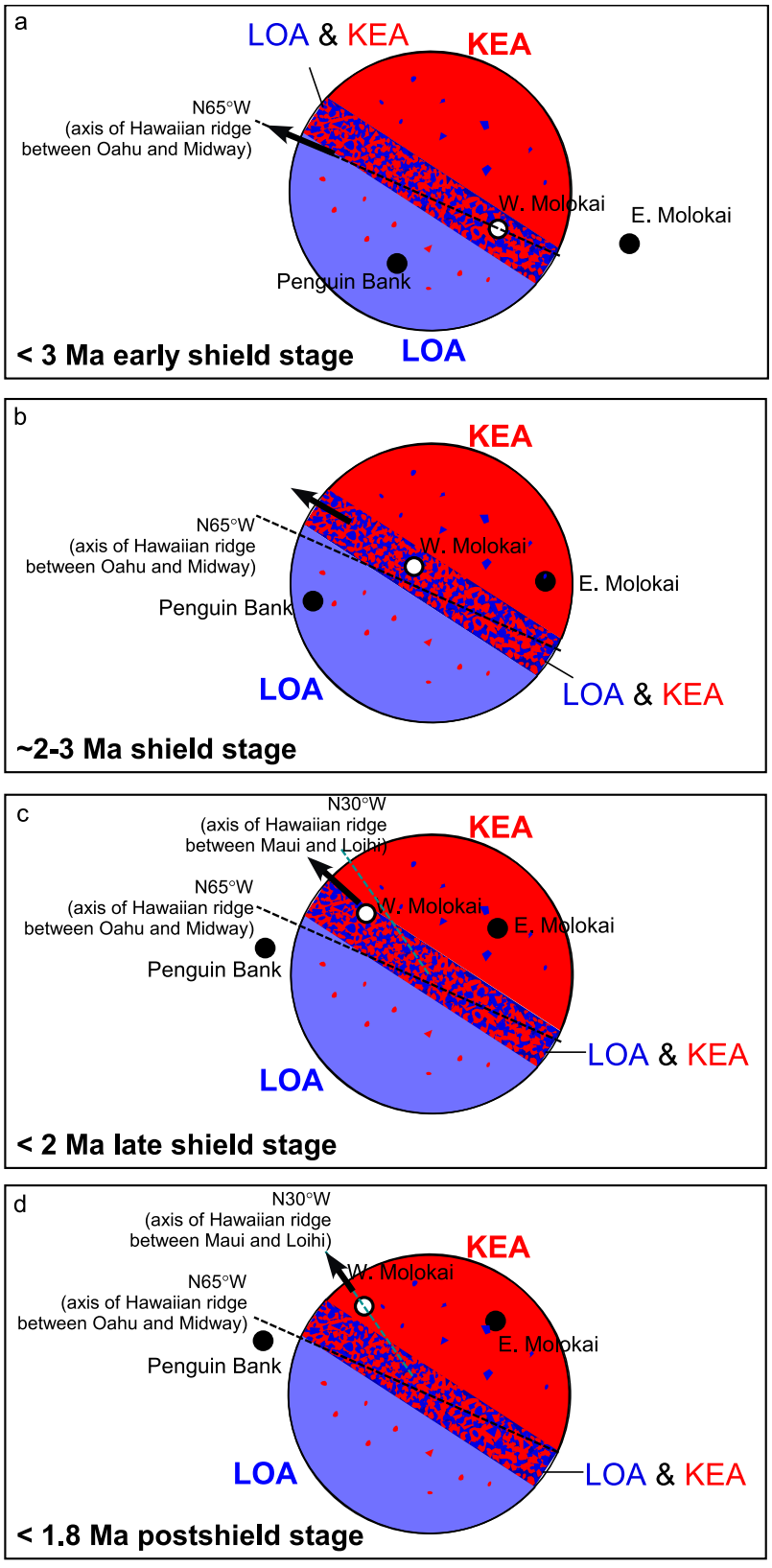
a
LOA & KEA
KEA
N65°W
(axis of Hawaiian ridge
between Oahu and Midway)
W. Molokai
E. Molokai
Penguin Bank
< 3 Ma early shield stage
LOA
b
KEA
N65°W
(axis of Hawaiian ridge
between Oahu and Midway)
W. Molokai
E. Molokai
Penguin Bank
LOA
LOA & KEA
~2-3 Ma shield stage
c
N30°W
(axis of Hawaiian ridge
between Maui and Loihi)
KEA
N65°W
(axis of Hawaiian ridge
between Oahu and Midway)
W. Molokai
E. Molokai
Penguin Bank
LOA & KEA
LOA
< 2 Ma late shield stage
d
N30°W
(axis of Hawaiian ridge
between Maui and Loihi)
KEA
W. Molokai
N65°W
(axis of Hawaiian ridge
between Oahu and Midway)
E. Molokai
Penguin Bank
LOA
LOA & KEA
< 1.8 Ma postshield stage

Figure 14

member defined by the Koolau (Makupuu stage), Lanai and Kahoolawe shields. If the MFZ influenced sampling of the plume source, this component should be abundant in the West Molokai shield which is located between the Lanai and Koolau shields (Figure 1a). Although we do not know the volumetric proportion, the occurrence of two West Molokai shield lavas at disparate locations that have the geochemical signature of Koolau (Makapuu-stage) lavas (i.e., high $^{87}Sr/^{86}Sr$, low $^{143}Nd/^{144}Nd$, $^{176}Hf/^{177}Hf$ and $^{206}Pb/^{204}Pb$ and high $^{208}Pb^*/^{206}Pb^*$) is consistent with the MFZ facilitating sampling of this Loa end-member.

7.5. Spatial Distribution of Geochemical Heterogeneities in the Hawaiian Plume

[39] Geochemical heterogeneities in Hawaiian lavas provide constraints on the origin of the plume and the processes that lead to plume-related volcanism. For example, geochemical differences between shield lavas erupted on the spatial Kea- and Loa-trends have been used to propose alternative models for the spatial distribution of geochemical heterogeneities within the plume. These alternatives include (1) concentric zonation created during plume ascent (Figure 2a), perhaps distorted by physical interaction between the plume and migrating oceanic lithosphere (Figure 2b); (2) bilateral asymmetry in the form of geochemically distinct, <50 km wide streaks that are vertically continuous for possibly hundreds of kilometers (Figure 2c) (these streaks were created as a plume ascends after sampling geochemical heterogeneities in the lower mantle); and (3) a random distribution of geochemical heterogeneities with different solidi that are sampled in different proportions in the core to margin temperature gradient within the plume (Figure 2e).

7.5.1. Constraints From Geochemical Changes During Shield-Stage Volcanism

[40] The geochemically zoned plume hypotheses for the Hawaiian plume (Figure 2) arose to explain the geochemical differences between shields dominated by Loa- and Kea-like volcanoes, but some shields are composed of both Loa- and Kea-like lavas, e.g., West Molokai (this paper), Koolau [*Tanaka et al.*, 2002; *Haskins and Garcia*, 2004; *Huang and Frey*, 2005b], Haleakala [*Ren et al.*, 2006; *Abouchami and Frey*, 2006] and Mauna Kea [e.g., *Blichert-Toft et al.*, 2003; *Eisele et al.*, 2003; *Huang and Frey*, 2003; *Kurz et al.*, 2004; *Rhodes and Vollinger*, 2004].

[41] A new constraint on the distribution of Loa- and Kea-like heterogeneities in the plume arises from studies of Molokai Island; all subaerially erupted samples from East Molokai volcano are Kea-like [*Xu et al.*, 2005]. In contrast, ~20 km to the west, West Molokai lavas, both subaerially and submarine erupted, require localized Loa- and Kea-like heterogeneities in the source. The extreme model for explaining such short-term isotopic variability is a locally heterogeneous source [e.g., *Zindler et al.*, 1984]. These local heterogeneities may vary in proportion with location (Figure 2d), in particular, dominantly Kea-like in the source of East Molokai lavas to both Kea- and Loa-like sources in the source of West Molokai shield lavas to dominantly Loa-like in the source of Penguin Bank lavas, erupted west of the West Molokai shield (Figure 1a) (D. A. Clague et al., manuscript in preparation, 2007). This spatial zonation can be explained if East Molokai and Penguin Bank sampled the Kea and Loa sides, respectively, of a bilaterally zoned plume, whereas the West Molokai shield sampled a transition zone where Kea- and Loa-like sources were both abundant (Figure 14a).

Figure 14. Sampling of a bilateral asymmetrically zoned plume which is dominantly Kea component in the northeast (red) and dominantly Loa component in the southwest (blue); but a few Kea-like heterogeneities are in the Loa region and vice versa. These two portions are separated by a central zone that has similar amounts of Loa and Kea components. The latter zone was sampled by the West Molokai shield, which includes both Loa- and Kea-like lavas. The black arrow in each panel indicates the direction of the Pacific plate movement, ~N65°W in Figure 14a gradually changing to ~N30°W in Figure 14d. Figure modified from *Abouchami et al.* [2005]. (a) At ~3 Ma the Pacific Plate is striking N65°W over the hot spot; East and West Molokai and Penguin Bank are in the preshield or early shield stages. (b) At 2 to 3 Ma the strike of the Pacific plate is more northerly and starting to change from N65°W (the strike from Oahu to Midway Island) to N30°W (the strike from Maui Island to Loihi seamount). West Molokai volcano is centered over the hot spot and sampling a central region where Loa- and Kea-like heterogeneities are both abundant. (c) At ~2 Ma the strike of the Pacific Plate is farther to the north as West Molokai volcano enters the late shield stage. (d) At 1.8 Ma the strike of the Pacific plate is now N30°W, as defined by volcanoes from Maui to Loihi. West Molokai volcano has entered the postshield stage and is now sampling the dominantly Kea part of the plume.

Table 7a. Predicted Shield to Postshield Geochemical Changes Based on Simple Models for the Spatial Distribution of Geochemical Heterogeneities in Hawaiian Plume

		Predicted Geochemical Characteristics	
	Model	Shield	Postshield
1	Concentrically zoned (Figure 2a)	Kea Loa	Kea Kea
2	Radially zoned with distortion arising from lithosphere interaction (Figure 2b)	Kea Loa	Kea Loa
3, 4	Bilaterally zoned (Figures 2c and 2d)	Kea Loa	Kea Loa
5	Random heterogeneity (Figure 2e) sampled differently at different temperatures with the Kea component having a higher solidus than the Loa component (see text)	Kea Loa	Loa Loa

7.5.2. Constraints From Geochemical Changes Accompanying the Shield to Postshield Transition

[42] The models in Figure 2 lead to different predictions for the temporal geochemical variation during the transition from the shield to postshield stage (Table 7a). Specifically, a concentrically zoned model predicts that a Loa-like shield should change to a Kea-like postshield as the Loa volcano migrates from the core to margin of the plume, whereas a Kea shield formed at the plume margin is expected to retain a Kea-signature as it enters the postshield stage. However, if a radially zoned plume is distorted by physical interaction with the lithosphere (e.g., Figure 2b and Figure 17 of *Bryce et al.* [2005]), the postshield stage of a Loa volcano may not sample the presumed Kea-like margin. The temporal evolution, Kea-like shield and postshield and Loa-like shield and postshield, is expected for the asymmetrically zoned models (Figures 2c and 2d) providing that the Loa-Kea compositional boundary is aligned with the direction of plate motion [see *Abouchami et al.*, 2005, Figure 3]. In contrast, the randomly distributed heterogeneity model (Figure 2e) predicts that different proportions of components in magma arise because the components have different solidus temperatures; for example, lavas derived from the hotter plume core should have a higher proportion of the component with a high solidus temperature than lavas derived from the plume margin, such as postshield lavas.

[43] An important question is, which component, Loa or Kea, has the lower solidus? *Huang et al.* [2005a] proposed that the Loa component has the lowest solidus because the extreme Loa end-member, represented by Koolau shield (Makapuu stage) originated from recycled oceanic crust and sediment [*Huang and Frey*, 2005b]. This inference is consistent with the relatively high Ni and SiO_2 contents of Makapuu lavas that led *Sobolev et al.* [2005] to propose a dominantly pyroxenite source for Makapuu lavas; a hypothesis supported by the recent Pb isotope study on Koolau Volcano [*Fekiacova et al.*, 2007]. However, if the Loa component has a relatively low solidus temperature it should be the dominant contributor to all postshield magmas.

[44] Postshield lavas have been studied at the Kea-trend volcanoes, Mauna Kea, Kohala, Haleakala and East Molokai. In each case the decreasing magma flux is accompanied by a change from tholeiitic to alkalic lavas, consistent with a decrease in extent of melting as the volcano migrated to the lower temperature plume margin. Generally, relative to shield lavas, Kea postshield lavas have lower $^{87}Sr/^{86}Sr$ and higher $^{143}Nd/^{144}Nd$, and post-

Table 7b. Observed Geochemical Characteristics in Loa Volcanoes

	Predicted Geochemical Characteristics	
Model	Shield	Postshield
West Molokai	Loa and Kea	Kea
Kahoolawe	Loa	Loa
Hualalai	Loa	Loa

shield lavas from the different Kea volcanoes define overlapping fields in Sr-Nd isotopic space [*Xu et al.*, 2005]. Therefore a depleted (i.e., lower $^{87}Sr/^{86}Sr$ and higher $^{143}Nd/^{144}Nd$) component becomes important as a Kea volcano samples the plume margin [*Xu et al.*, 2005]. In contrast, relative to shield lavas, the associated postshield lavas may have higher (Kohala) or lower (Mauna Kea) $^{206}Pb/^{204}Pb$. Regardless, the Kea-like $^{208}Pb^*/^{206}Pb^*$ (<0.95) occurs in Kea shield and postshield lavas. This Pb isotopic similarity of Kea shield and postshield lavas has been used to argue that the Kea component has persisted for 1.5 Ma [*Gaffney et al.*, 2004; *Abouchami et al.*, 2005; *Xu et al.*, 2005]. The persistence of the Kea signature from shield to postshield lavas is consistent with models 1 to 4 (Table 7a and Figures 2a, 2b, 2c, and 2d) but inconsistent with model 5 in Table 7a and Figure 2e if the Loa component has a lower solidus temperature.

[45] At the Loa-trend volcanoes, Hualalai and Kahoolawe, the postshield lavas retain the Loa-like Pb isotopic signature ($^{208}Pb^*/^{206}Pb^* > 0.95$) [*West et al.*, 1987; *Cousens et al.*, 2003, and references therein; *Hanano et al.*, 2005; *Xu et al.*, 2005; *Huang et al.*, 2006] (Table 7b). This observation is inconsistent with the concentrically zoned model (Figure 2a and model 1 in Table 7a), but consistent with the distorted radial zonation [*Bryce et al.*, 2005] and bilaterally zoned [*Abouchami et al.*, 2005] models, i.e., Figures 2b, 2c, and 2d and models 2, 3, and 4 in Table 7a.

[46] In summary, models 2, 3, and 4 (Table 7a) are consistent with existing data for the shield to postshield evolution of Loa and Kea trend volcanoes. None of these models, however, explains the trend to lower $^{87}Sr/^{86}Sr$ and higher $^{143}Nd/^{144}Nd$ during the shield to postshield transition of Kea-trend volcanoes. Nevertheless, we ask, can the West Molokai data distinguish between radially and bilaterally zoned models? We suggest that the change at West Molokai volcano from a shield composed of Loa- and Kea-like lavas to a Kea-like postshield can be best explained by a bilaterally zoned model if the direction of Pacific plate motion changed relative to the strike of the bilateral zonation axis [e.g., *Abouchami et al.*, 2005, Figure 3]. Specifically, the Pacific plate motion changed at 2–3 Ma, between Oahu and Molokai Islands in the vicinity of the Molokai Fracture Zone (Figure 1) and subsequent volcanism created the distinct Loa and Kea trends [*Wessel and Kroenke*, 1997; *Hieronymus and Bercovici*, 2001]. This change in plate motion from N65°W at Oahu to N30°W at Maui [*DePaolo et al.*, 2001] would affect the sampling of a bilaterally zoned plume. That is, the West Molokai shield sampled a central region of the plume core composed of significant amounts of Loa and Kea components, but because the strike of the Pacific plate changed from N65°W to N30°W the postshield stage of West Molokai sampled the Kea part of the zoned plume (Figure 14).

8. Conclusions

[47] At West Molokai, a Hawaiian volcano on the Loa spatial trend, both shield tholeiitic basalt and postshield alkalic lavas are exposed. Geochemical data for these lavas and associated glasses lead to the following conclusions:

[48] 1. Compared to postshield hawaiite from Kea-trend volcanoes (Mauna Kea, Kohala, Haleakala), hawaiites from West Molokai have lower SiO_2 and higher Fe_2O_3* and TiO_2 contents. Fractionation of Fe-Ti oxides was more important in the fractionation process that led to hawaiites at these Kea-trend volcanoes than at West Molokai.

[49] 2. Tholeiitic glasses associated with West Molokai shield-stage lavas range widely in major element compositions; artifact glasses and their presumed sources, glassy dike margins, are Loa-like (e.g., low CaO at a given MgO content); in contrast submarine glasses collected from a sediment-covered breccia slope have Kea-like compositions.

[50] 3. Most West Molokai tholeiitic shield basalts have high Zr/Nb (>13) and Sr/Nb (>32) ratios overlapping the Mauna Loa field, but some shield and all postshield lavas have lower Zr/Nb and Sr/Nb ratios that overlap the Mauna Kea field.

[51] 4. Most West Molokai shield-stage lavas have higher $^{87}Sr/^{86}Sr$ and $^{208}Pb^*/^{206}Pb^*$, lower $^{143}Nd/^{144}Nd$, $^{176}Hf/^{177}Hf$ and $^{206}Pb/^{204}Pb$ than postshield lavas; they overlap the field defined by Mauna Loa lavas and one sample is like the extreme Hawaiian geochemical end-member represented by Koolau (Makapuu-stage) lavas. In contrast, four shield and all postshield lavas plot in the field of Kea-trend lavas.

[52] 5. We infer that the West Molokai shield was derived from a bilaterally zoned plume source, Kea in the northeast, Loa in the southwest, with a

central zone composed of Loa- and Kea-like components. The change to exclusively Kea-like characteristics in the West Molokai postshield reflects the change in strike of the Pacific plate in the vicinity of Molokai Island.

Appendix A

A1. Analytical Methods

[53] Glass major element compositions were analyzed by electron microprobe at the U.S. Geological Survey in Menlo Park (Table 2 and Table A1) using natural and synthetic standards as described by *Clague and Frey* [1982]. Major element contents for whole-rock samples, except 10 samples, were analyzed by X-ray fluorescence (XRF) with FeO, H_2O^+, H_2O^-, and CO_2 analyzed by classical wet chemical techniques at the U.S. Geological Survey (USGS) laboratories in Denver, Colorado, and Menlo Park, California, respectively (Table 3). Ten additional samples were analyzed by XRF at University of Massachusetts, Amherst (Table 3). Data for one sample, 71WMOL-4, analyzed by both laboratories (Univ. Mass and USGS) agree within 3% except for MnO (Table 3).

[54] Trace elements for the seven dive samples (T307Rx) were analyzed at the Geoanalytical Laboratory at Washington State University. Information on methods, precision, and accuracy for samples analyzed at this facility are available at http://www.wsu.edu/~geolab/. Trace element abundances for all the other samples were determined at MIT by ICP-MS (Table 4) using a Fisons VG Plasmaquad 2 + S with both internal and external drift monitors. Trace element results are reported as the mean of duplicate analyses obtained on different days. The chemical procedures and estimates of accuracy and precision were discussed by *Huang and Frey* [2003]. The 2 sigma uncertainty for BHVO-2, which is analyzed as an unknown sample, is better than ±3%. Ten of the fourteen samples with REE-Y enrichment were not analyzed by ICP-MS but their trace element abundances were determined by XRF and Instrumental Neutron Activation Analysis (INAA) at USGS, Denver.

[55] Samples for Sr, Nd, Hf and Pb isotopic analyses were chosen so as to encompass the full range of compositions (Table 5). Two dive samples (T307R1 and R4) were analyzed at Carleton University on a Finnigan MAT261 multicollector mass spectrometer running in static mode. For these two samples, analyses were done on two powder splits. The Sr splits were washed for eight days in hot 6 M HCl, whereas the splits for Nd and Pb were washed in hot 1.5 M HCl overnight. Subsequently they were rinsed twice with ultra-pure H_2O before dissolution in HF-HNO_3. Information on methods, precision and accuracy for these two samples (T307R1 and R4), and values for standards analyzed at this facility, is given by *Cousens et al.* [2003].

[56] Hafnium isotopic analyses (and Nd isotopic ratios for acid-leached (in hot 6 M HCl) submarine samples T307R1, R2, R4, R6, R7 and R8) were determined at the Ecole Normale Supérieure in Lyon (ENSL) following the procedure described by *Blichert-Toft et al.* [1997]. Hafnium isotopic compositions were measured by MC-ICP-MS at ENSL using a Nu Plasma 500 HR coupled with a desolvating nebulizer Nu DSN-100. The analytical procedure was similar to that of *Blichert-Toft et al.* [1997] with the exception that potential W isobaric interferences on mass 180 were monitored on mass 183 instead of mass 182. The Faraday cups were positioned to collect masses 173 (Yb monitor; L3), 175 (Lu monitor; L2), 176 (Hf, Lu, Yb; L1), 177 (Hf; Ax), 178 (Hf; H1), 179 (Hf; H2), 180 (Hf, Ta, W; H3), 181 (Ta monitor; H4) and 183 (W Monitor; H5). On-line mass fractionation-corrected corrections for Yb, Lu, Ta and W isobaric interferences were either zero (Lu and Yb) or zero to negligible (Ta and W). Sixty ratios, in 3 blocks of 20 ratios each, were measured for each sample with an integration time of 10 seconds s per scan. In order to monitor machine performance, the JMC-475 Hf standard was analyzed systematically in alternation with samples and gave 0.282162 ± 0.000012 (2 sigma; n = 28) for $^{176}Hf/^{177}Hf$ during the three run session of the present samples, corresponding to an external reproducibility of 0.35ε (Tables 5 and 6). $^{176}Hf/^{177}Hf$ was normalized for mass fractionation relative to $^{176}Hf/^{177}Hf = 0.7325$ using an exponential law. Hafnium total procedural blanks were less than 20 pg for all sample batches. Uncertainties reported on Hf measured isotope ratios are in-run $2\sigma/\sqrt{n}$ analytical errors in last decimal place, where n is the number of measured isotope ratios.

[57] The Nd for the six samples analyzed at ENSL for their Nd isotope compositions was recovered from the CaMg-fluoride precipitates left over from the Hf separation chemistry and purified by a two-step procedure using first a cation-exchange column to separate the REE fraction and then an

Table A1. Glass Compositions for Dikes and Artifacts[a]

	Longitude	Latitude	SiO_2	TiO_2	Al_2O_3	FeO*	MnO	MgO	CaO	Na_2O	K_2O	P_2O_5	S	Total
Postshield-Stage Lavas														
Alkalic basalt														
89KAA-1 (dike)	−157.1915	21.2072	49.5	3.32	15.0	11.72	0.16	6.41	9.83	3.42	0.98	0.56	0.01	100.9
WM21R-5	−157.1505	21.1950	49.0	3.27	14.9	11.62	0.17	6.49	9.68	3.35	1.01	0.72	0.00	100.2
WM24-2	−157.1505	21.1950	48.8	3.23	14.4	11.76	0.17	6.49	9.67	3.34	0.97	0.58	0.01	99.4
WM24-14	−157.1505	21.1950	49.4	3.24	15.0	11.84	0.15	6.42	9.79	3.43	0.98	0.58	0.02	100.8
WM28-7	−157.1505	21.1950	48.5	3.22	14.6	11.45	0.16	6.41	9.64	3.41	1.01	0.63	0.01	99.0
WM28-17	−157.1505	21.1950	49.7	3.26	15.2	11.75	0.17	6.53	9.86	3.42	1.01	0.63	0.01	101.5
WM890-1	−157.1505	21.1950	49.0	3.30	14.9	11.80	0.17	6.50	9.82	3.36	1.00	0.64	0.01	100.5
Shield-Stage Lavas														
Tholeiite														
WMO-11 (dike)	−157.1484	21.1394	53.6	3.27	13.6	12.40	0.18	4.11	8.08	2.63	1.02	0.67	0.01	99.6
89FDD-1 (dike)	−157.1518	21.1367	51.4	2.55	14.5	11.20	0.16	6.70	10.26	2.24	0.51	0.30	0.01	99.8
WFD (dike)	−157.1505	21.1375	52.1	2.50	14.3	11.16	0.16	6.69	10.58	2.50	0.51	0.38	0.00	100.9
WFD-1 (dike)	−157.1505	21.1375	52.0	2.66	14.6	11.41	0.17	6.33	10.31	2.58	0.55	0.33	0.02	101.0
WM820-1	−157.1505	21.1950	52.0	2.87	14.1	11.66	0.18	4.99	8.81	2.76	0.84	0.49	0.02	98.7
WM820-2	−157.1505	21.1950	52.5	3.00	14.1	11.79	0.17	5.08	8.95	2.61	0.92	0.55	0.01	99.7
WM28-12	−157.1505	21.1950	51.5	3.32	13.7	13.36	0.19	5.13	9.12	2.80	0.78	0.52	0.02	100.4
WM24-1	−157.1505	21.1950	52.0	3.04	14.1	12.19	0.20	5.59	9.40	2.90	0.77	0.53	0.01	100.7
WM40-2	−157.1505	21.1950	51.2	2.86	13.9	12.13	0.18	5.87	9.83	2.62	0.55	0.40	0.02	99.6
WM28-20	−157.1505	21.1950	51.2	2.77	13.9	11.77	0.16	6.06	10.15	2.68	0.62	0.45	0.01	99.8
WM21-66B	−157.1505	21.1950	52.2	2.62	14.5	11.05	0.17	6.44	10.30	2.74	0.61	0.38	0.00	101.0
WM21-74	−157.1505	21.1950	51.4	2.56	14.4	10.95	0.17	6.36	10.00	2.68	0.57	0.34	0.01	99.4
WM24-3	−157.1505	21.1950	51.3	2.52	14.2	11.12	0.18	6.47	10.02	2.72	0.58	0.38	0.00	99.5
WM24-4	−157.1505	21.1950	51.7	2.61	14.2	11.00	0.19	6.38	10.13	2.67	0.59	0.36	0.01	99.8
WM24-6	−157.1505	21.1950	51.6	2.62	14.2	11.11	0.17	6.43	10.13	2.75	0.58	0.39	0.01	100.0
WM24-11	−157.1505	21.1950	51.9	2.57	14.6	11.03	0.17	6.41	10.12	2.73	0.59	0.38	0.01	100.5
WM28-3	−157.1505	21.1950	52.1	2.58	14.7	10.95	0.15	6.44	10.25	2.70	0.59	0.39	0.01	100.9
WM28-4	−157.1505	21.1950	51.5	2.58	14.2	10.97	0.17	6.40	10.04	2.66	0.60	0.35	0.00	99.5
WM28-6	−157.1505	21.1950	52.1	2.54	14.5	10.92	0.17	6.37	10.23	2.74	0.60	0.33	0.01	100.5
WM28-8	−157.1505	21.1950	52.0	2.58	14.4	10.90	0.16	6.44	10.26	2.72	0.61	0.35	0.01	100.4
WM28-9	−157.1505	21.1950	51.2	2.54	14.1	10.93	0.17	6.38	10.11	2.66	0.58	0.34	0.01	99.0
WM28-10	−157.1505	21.1950	52.0	2.63	14.2	10.84	0.15	6.35	10.27	2.76	0.60	0.36	0.01	100.2
WM28-11	−157.1505	21.1950	52.1	2.60	14.5	10.72	0.16	6.46	10.28	2.71	0.60	0.33	0.00	100.5
WM28-18	−157.1505	21.1950	52.1	2.67	14.5	10.80	0.17	6.47	10.28	2.82	0.62	0.36	0.01	100.8
WM28-21	−157.1505	21.1950	52.0	2.57	14.2	11.06	0.17	6.45	10.12	2.71	0.60	0.37	0.01	100.3
WM21-71	−157.1505	21.1950	51.6	2.50	14.3	11.56	0.16	6.50	10.22	2.57	0.47	0.32	0.01	100.2
WM24-12	−157.1505	21.1950	51.2	2.45	14.4	11.43	0.18	6.58	10.27	2.58	0.48	0.30	0.01	99.9
WM24-13	−157.1505	21.1950	51.4	2.49	14.6	10.96	0.16	6.53	10.47	2.60	0.51	0.29	0.01	100.0
WM21-66A	−157.1505	21.1950	50.9	2.51	14.1	10.84	0.18	6.70	10.25	2.52	0.56	0.36	0.00	98.9
WM21-69	−157.1505	21.1950	51.0	2.44	14.1	10.86	0.19	6.69	10.16	2.57	0.53	0.36	0.01	98.9
WM21-72	−157.1505	21.1950	50.9	2.50	14.1	10.86	0.17	6.77	10.27	2.55	0.52	0.34	0.01	99.0
WM21-73	−157.1505	21.1950	51.5	2.53	14.1	11.07	0.17	6.71	10.48	2.61	0.58	0.35	0.01	100.1
WM21R-1	−157.1505	21.1950	51.3	2.57	14.2	10.99	0.17	6.72	10.28	2.56	0.55	0.36	0.01	99.7
WM21R-3	−157.1505	21.1950	51.2	2.38	14.1	11.03	0.17	6.60	10.29	2.55	0.54	0.39	0.01	99.3
WM21R-4	−157.1505	21.1950	51.2	2.41	14.6	10.87	0.17	6.53	10.47	2.55	0.54	0.34	0.01	99.7
WM21R-6	−157.1505	21.1950	51.7	2.48	14.3	10.99	0.16	6.72	10.42	2.60	0.55	0.35	0.01	100.3
WM24-5	−157.1505	21.1950	51.2	2.50	14.2	11.19	0.16	6.74	10.61	2.46	0.46	0.33	0.01	99.9
WM24-7	−157.1505	21.1950	51.6	2.36	14.4	11.23	0.18	6.73	10.53	2.48	0.49	0.31	0.01	100.3
WM24-8	−157.1505	21.1950	51.4	2.50	14.4	11.04	0.18	6.79	10.32	2.51	0.54	0.28	0.00	100.0
WM24-10	−157.1505	21.1950	52.0	2.34	14.4	10.90	0.16	6.82	10.56	2.53	0.50	0.31	0.01	100.5
WM26-1	−157.1505	21.1950	51.1	2.40	14.2	10.83	0.18	6.67	10.29	2.55	0.53	0.34	0.00	99.1
WM26-2	−157.1505	21.1950	51.6	2.51	14.3	11.08	0.16	6.79	10.31	2.61	0.53	0.34	0.01	100.2
WM28-13	−157.1505	21.1950	50.9	2.56	14.4	11.22	0.18	6.88	9.96	2.58	0.57	0.37	0.01	99.6
WM28-14	−157.1505	21.1950	51.3	2.62	14.2	11.22	0.15	6.78	10.20	2.61	0.58	0.36	0.01	100.0
WM28-15	−157.1505	21.1950	51.6	2.54	14.7	11.15	0.17	6.44	10.53	2.53	0.51	0.31	0.00	100.5
WM21R-2	−157.1505	21.1950	51.6	2.42	14.6	10.83	0.16	6.52	10.68	2.62	0.52	0.35	0.01	100.3
WM21R-7	−157.1505	21.1950	50.9	2.38	14.7	10.86	0.18	6.50	10.40	2.53	0.52	0.37	0.01	99.4
WM28-1	−157.1505	21.1950	51.1	2.47	14.5	11.31	0.17	6.51	10.41	2.42	0.50	0.36	0.01	99.8
WM28-2	−157.1505	21.1950	51.6	2.58	14.3	11.37	0.15	6.53	10.51	2.53	0.49	0.34	0.01	100.4
WM28-16	−157.1505	21.1950	51.7	2.58	14.7	11.44	0.17	6.54	10.58	2.34	0.50	0.30	0.01	100.9

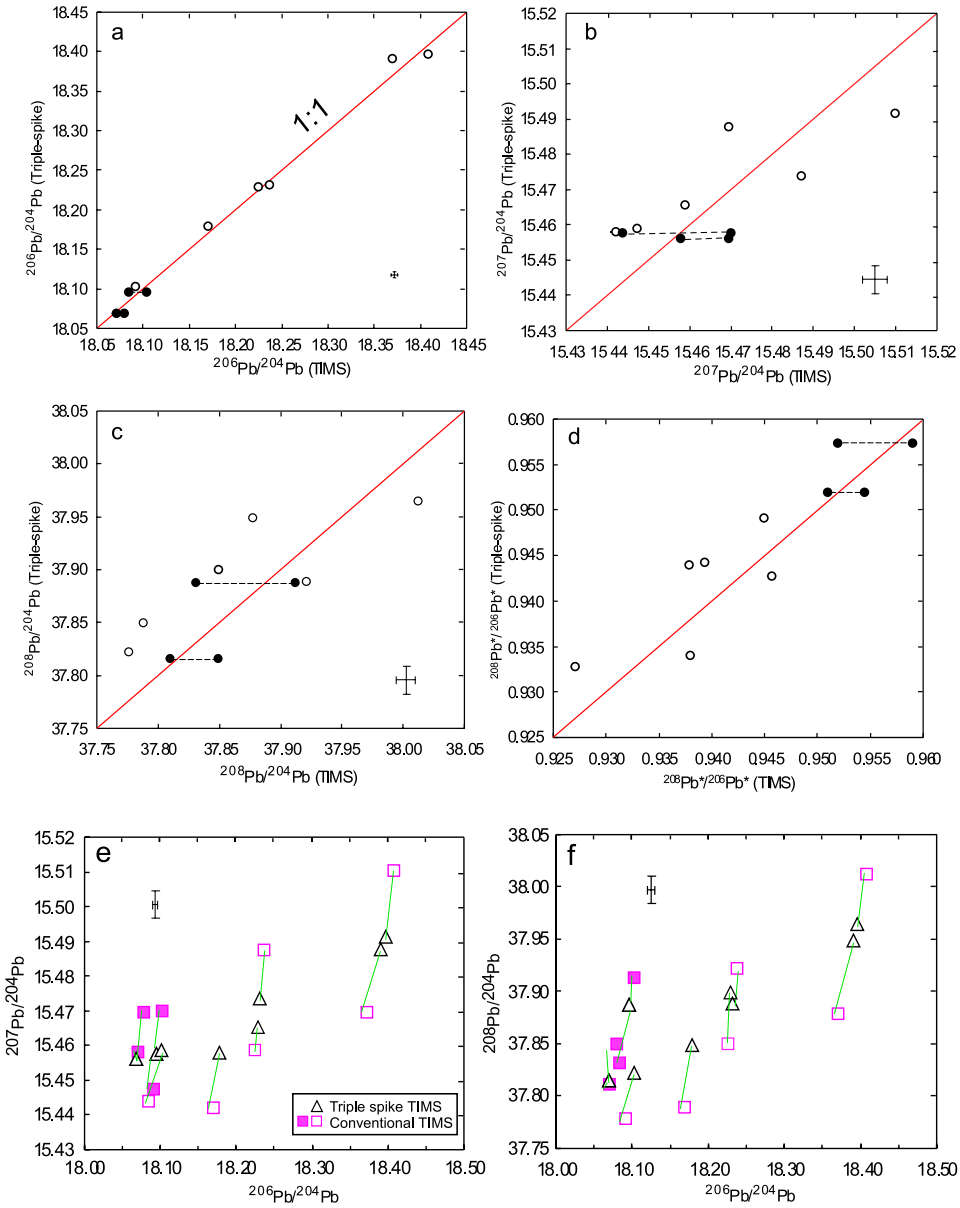

Figure A1. Comparison of Pb isotopic ratios analyzed by conventional TIMS and the triple-spike method. The 2 sigma errors shown are the maximum in-run uncertainties which are similar for conventional TIMS and triple-spike data. Both data sets are highly correlated for $^{206}Pb/^{204}Pb$, but they are more scattered for $^{207}Pb/^{204}Pb$ and $^{208}Pb/^{204}Pb$. Two samples which were analyzed in duplicate by conventional TIMS (filled symbols) are shown in the figures. The dashed lines connect the duplicates in Figures A1a, A1b, A1c, and A1d. The lines in Figures A1e and A1f link the different data for the same sample. Filled pink squares are TIMS duplicates.

HDEHP column to isolate Nd. Neodymium isotopic compositions likewise were measured by MC-ICP-MS at ENSL using the Nu Plasma HR coupled with a desolvating nebulizer Nu DSN-100 and the same approach as for the Hf isotopic measurements. The Faraday cups were positioned to collect masses 140 (Ce monitor; L3), 142 (Nd, Ce; L2), 143 (Nd; L1), 144 (Nd, Sm; Ax), 145 (Nd;

Notes to Table A1.

[a] Glass compositions are in wt%. Data from *Weisler and Clague* [1998]. See Figure 3 for sample locations. Except for glass on dikes, all data are for artifacts collected from the north coast near Moomomi (see Figure 3).

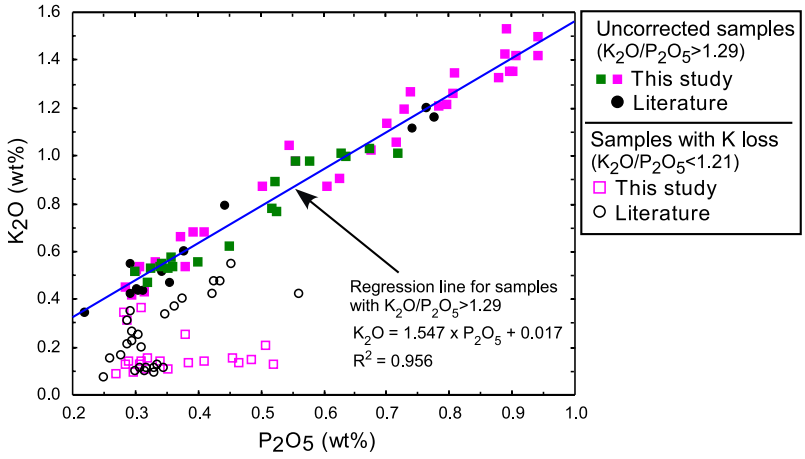

Figure A2. K_2O versus P_2O_5 for West Molokai whole rocks and glasses. All the glasses (green squares) and whole rocks with $K_2O/P_2O_5 > 1.29$ (filled pink squares and circles) define a strong positive trend, whereas whole rocks with $K_2O/P_2O_5 < 1.21$ (open squares and circles) are offset to lower K_2O at a given P_2O_5. We inferred that samples with $K_2O/P_2O_5 < 1.21$ have lost K; these samples were corrected for K loss by adding K_2O so that they plot on the regression line derived from the "normal" samples. Data sources: this study, *Macdonald and Katsura* [1964], and *Shinozaki et al.* [2002].

H1), 146 (Nd; H2), 147 (Sm monitor; H3), 148 (Nd, Sm; H4) and 150 (Nd, Sm; H5). Samarium isobaric interference corrections on Nd were zero. Our in-house JMC Nd standard (batch #801149A) was run in alternation with the samples and gave 0.512126 ± 0.000012 (2 sigma; n = 3) for $^{143}Nd/^{144}Nd$ during the single short run session of the present samples (Table 5), and corresponds within error to the accepted value of the La Jolla Nd standard of 0.511846 as determined by cross calibration measurements. $^{143}Nd/^{144}Nd$ was normalized for mass fractionation relative to $^{146}Nd/^{144}Nd = 0.7219$ using an exponential law. The Nd total procedural blank was less than 20 pg for the single sample batch analyzed in this study. Uncertainties reported on Nd measured isotope ratios are in-run 2σ analytical errors in last decimal place.

[58] Twelve samples were analyzed for Pb isotopic ratios by the triple-spike technique at the Max-Planck-Institut fur Chemie (MPI) following the procedure of *Abouchami et al.* [2000]. The average ratios measured for NBS-981 by the triple-spike method are $^{206}Pb/^{204}Pb = 16.9447 \pm 0.0015$, $^{207}Pb/^{204}Pb = 15.5024 \pm 0.0015$ and $^{208}Pb/^{204}Pb = 36.7350 \pm 0.0034$ (2 sigma) on the basis of 12 runs during the course of this study. The data reported in Table 5 were normalized to the values of *Galer and Abouchami* [1998]. Data obtained by the triple-spike method and conventional TIMS at MIT (see following text) have comparable machine in-run uncertainties. They agree within 0.1% for $^{206}Pb/^{204}Pb$ and the data sets are highly correlated (Table 5 and Figure A1a). For $^{207}Pb/^{204}Pb$ and $^{208}Pb/^{204}Pb$ both data sets agree within 0.2%, although they are more scattered which is likely due to the larger uncertainties in mass fractionation correction for conventional TIMS data (Figure A1).

[59] All other isotopic data were obtained at MIT using the following procedures. In order to avoid the effects of postmagmatic alteration on isotopic ratios, a 6.0 M HCl multistep acid leaching procedure was used prior to dissolving in HF-HNO_3 [*Xu et al.*, 2005]. After verification of complete dissolution, samples were evaporated and the residual cake was dissolved overnight in 1 mL 6.0 M HCl, and aliquots were taken for Sr (0.25 mL), Pb (0.25 mL) and Nd (0.5 mL) isotope analysis. The aliquots were dried on a hot plate. The Sr aliquot was dissolved using 0.5 mL concentrated 14 M HNO_3 and then fluxed on a hot plate for at least one hour before drying. Then 0.5 mL 3.5 M HNO_3 was added and digested for 24 hours. The Nd and Pb aliquots were dissolved using 3 mL 1 M HCl and 0.5 mL 1.1 M HBr, respectively, and digested for 24 hours.

[60] Sr was separated from other elements using 50 μL columns filled with Eichrome Sr-Spec resin. The Sr aliquot was loaded onto the column followed by rinsing with 1.2 mL 3.5 M HNO_3. Sr was then eluted with 800 μL MQ H_2O. A drop of 0.1 M H_3PO_4 was added to the eluate before drying.

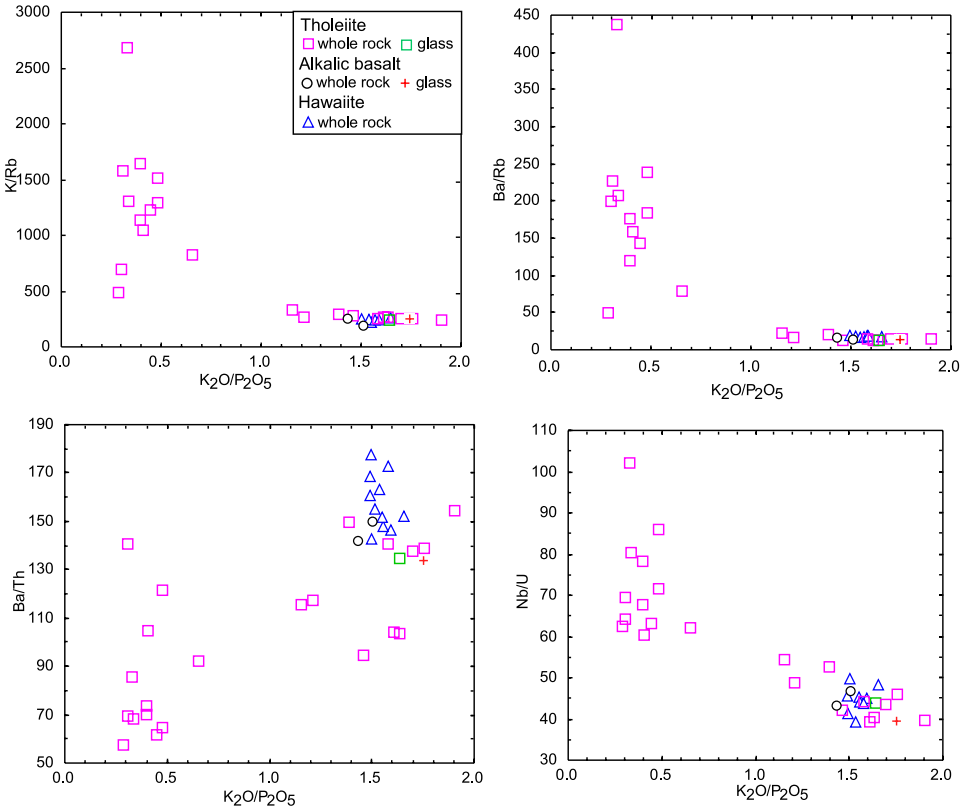

Figure A3. K_2O/P_2O_5 versus K/Rb, Ba/Rb, Ba/Th, and Nb/U for West Molokai lavas. Tholeiitic lavas with $K_2O/P_2O_5 < 1.3$ have experienced loss of K, Rb, U, and Ba (for some lavas) during postmagmatic alteration.

[61] Pb was separated by anion exchange using HBr. The Pb aliquot was loaded onto 120 μL columns containing Eichrom AG1-X8 anion exchange resin. The columns were then washed with 0.5 mL 1.1 M HBr and 0.5 mL 2 M HCl, and Pb was eluted with 1 mL 6 M HCl. A drop of 0.1 M H_3PO_4 was added to the eluate before drying. For Ca- and Mg-rich samples, this procedure was repeated to improve separation of Pb from Ca.

[62] Separation of Nd and Sm for isotopic analysis requires two ion exchange procedures. The first column separates out the rare earth elements from the bulk rock solution, whereas the second column separates Nd from the other rare earth elements. Rare earth element separation from bulk rock solution utilizes an 8 cm^3 column containing Bio-Rad AG® 50W-X8 resin. The Nd aliquot was loaded onto the column and washed by 12 mL 1 M HCl followed by 60 mL 3 M HCl, which removes the bulk of the Fe and Al in the solution, and then washed by 5 mL 3 M HNO_3, which removes the bulk of the Ba. The change from HCl to HNO_3 also allows some separation of Nd and Sm from Ce and La on the first column. The rare earth element concentrate was eluted with 30 mL 3M HNO_3 and dried down. The concentrate was dissolved in 100 μL 0.3 M HCl for the second column, on which Nd was separated from the other rare earth elements using 0.3 and 0.5 M HCl on a 5 cm^3 column filled with Eichrome LN-Spec resin.

[63] Sr, Nd and Pb were run on a thermal ionization multicollector mass spectrometer (GV Isoprobe-T) at MIT. Sr was loaded in phosphoric acid on Re filaments with $TaCl_5$ activator, and run in dynamic mode with an average ^{88}Sr signal of 3 V. Pb was loaded on Re filaments with phosphoric acid and silica gel, and run in static mode with an average ^{208}Pb signal of 1–1.5 V. Nd was loaded with phosphoric acid on the Re side filaments of a triple filament assembly, and run in dynamic mode as Nd metal with an average ^{142}Nd signal of 1–1.5 V. The blanks for Sr, Nd and Pb were 300 pg, 100 pg and 10 pg, respectively. See Table 5 footnotes for normalization procedures, precision estimates and data for Sr and Nd standards.

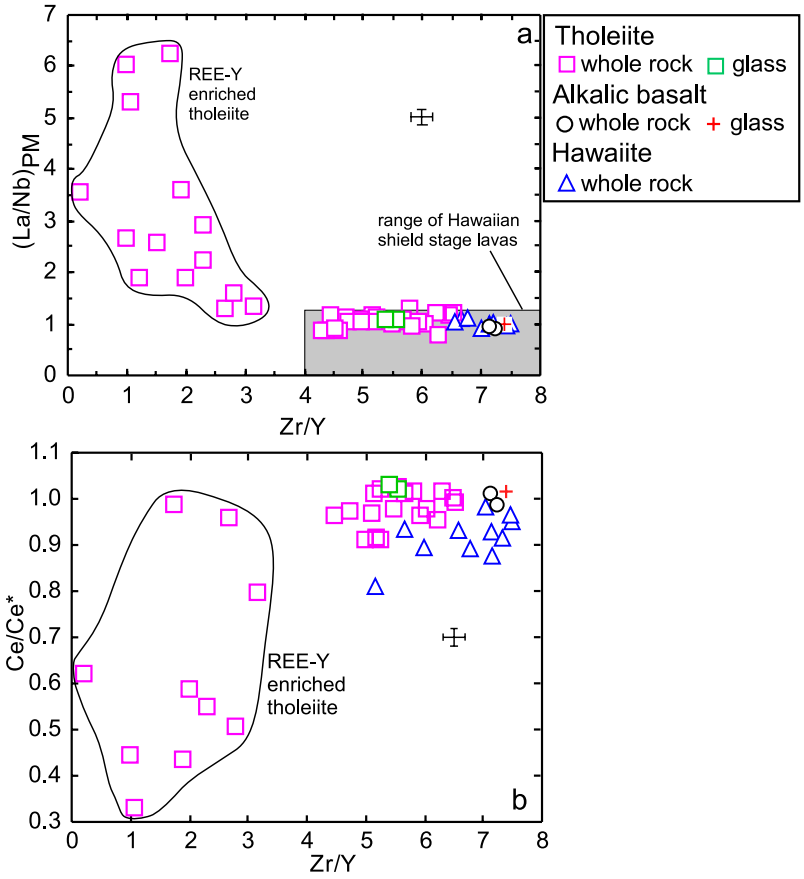

Figure A4. Zr/Y versus (a) $(La/Nb)_{PM}$ and (b) Ce/Ce* for West Molokai lavas. Subscript PM designates normalized to primitive mantle value of *Sun and McDonough* [1989]. Ce* is Ce abundance interpolated from primitive mantle normalized abundances of La and Nd. Some West Molokai lavas range to very low Zr/Y (<3.5) and $(La/Nb)_{PM}$ (>1.2) ratios, and these lavas are inferred to reflect a REE-Y enrichment process. Eight out of ten lavas with REE-Y enrichment also have a negative Ce anomaly (see Figure A5). Error bars shown are 2 sigma uncertainties. Data for Hawaiian shield-stage lavas from GEOROC (http://georoc.mpch-mainz.gwdg.de/georoc/).

[64] The Pb analyses are corrected for fractionation using the NBS-981 standard. The average ratios measured for NBS-981 are $^{206}Pb/^{204}Pb = 16.896 \pm 0.016$, $^{207}Pb/^{204}Pb = 15.437 \pm 0.022$ and $^{208}Pb/^{204}Pb = 36.527 \pm 0.070$ (2 sigma) on the basis of 61 runs during the course of this study. The MIT isotope laboratory routinely uses a fractionation correction of $0.12 \pm 0.03\%$/amu, based on the values of *Todt et al.* [1996]. Considering the uncertainties of in-run and mass fractionation correction, the 2 sigma reproducibility is better than 0.1% for $^{206}Pb/^{204}Pb$. One of the two full procedure duplicates agrees within 0.1% and the other agrees within 0.2% (Table 5); triple-spike data suggest that there is measurable sampling heterogeneity [*Abouchami et al.*, 2000]. The reported data in Table 5 are normalized to the values of *Galer and Abouchami* [1998] for NBS-981, which require a fractionation correction of 0.135%/amu, and are within the uncertainty of the routinely used fractionation corrections.

A2. Postmagmatic Alteration

[65] Except for historic eruptions Hawaiian subaerial lavas have been affected to variable extents by postmagmatic alteration; the effects of such alteration must be evaluated before using geochemical data to constrain magmatic processes and magma sources. The most common observation is that low-temperature, subaerial alteration in the Hawaiian environment results in loss of K, Rb, Ba and U [e.g., *Feigenson et al.*, 1983; *Frey et al.*, 1994]. We estimated K_2O loss by identifying samples with anomalously low K_2O/P_2O_5 (<1.29) (Figure A2); such samples range widely to anomalously high K/

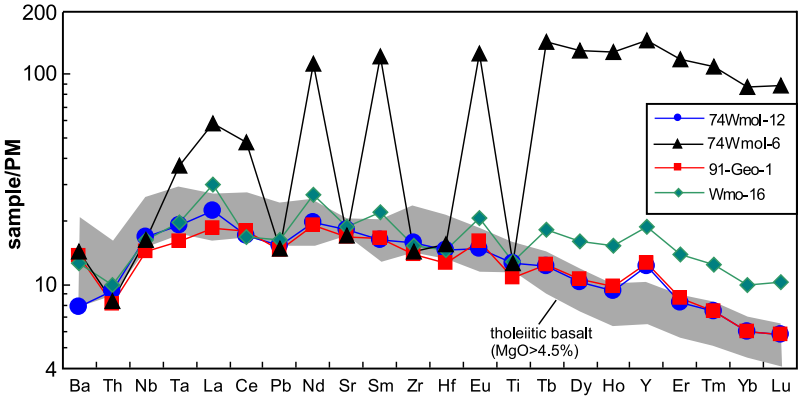

Figure A5. Incompatible trace element abundances in West Molokai tholeiitic shield lavas normalized to the primitive mantle [*Sun and McDonough*, 1989]. The gray field shows the range for 17 tholeiitic basalts; only lavas with >4.5% MgO analyzed by ICP-MS are shown. Data points are shown for samples with anomalous ratios involving rare earth elements (REE) and Y that are interpreted as an alteration feature [*Clague*, 1987]. Sample 74WMOL-6 is the most extreme example, but three additional samples have anomalously high La/Nb, Nd/Sr, Sm/Zr, Eu/Ti, and Y/Zr.

Rb (260 to 2669), Ba/Rb (15 to 436 relative to the 11.3 value of most fresh oceanic basalts [*Hofmann and White*, 1983]), Nb/U (49 to 102) and low Ba/Th (57 to 140) (Figure A3). In our isotopic analyses some samples with anomalous abundance ratios were included, but we used a multistep acid-leaching procedure in an effort to recover the isotopic characteristics of the magmas. The well-defined $^{87}Sr/^{86}Sr$ versus $^{143}Nd/^{144}Nd$ correlation (Figure 8a) suggests that the leaching was successful in removing the relatively high $^{87}Sr/^{86}Sr$ material caused by alteration [e.g., *Huang et al.*, 2005c].

[66] There are, however, other postmagmatic processes; in particular, some Hawaiian lavas have been enriched in REE and Y but typically not in other incompatible elements [e.g., *Clague*, 1987; *Fodor et al.*, 1989, 1992; *Frey et al.*, 1994]. Although the process is not well-understood, the REE and Y enrichment is apparently caused by formation of a groundmass rhabdophane-type phosphate [*Fodor et al.*, 1989; *Cotten et al.*, 1995]. This process can be recognized by anomalously high La/Nb and low Zr/Y, commonly accompanied by a relative depletion in Ce, which is inferred to reflect an oxidizing environment. Fourteen of 40 West Molokai tholeiitic whole rocks have La/Nb > 1.25 and Zr/Y < 3.5 (Figure A4). The dramatic effect of such alteration is evident on a mantle-normalized plot for incompatible element abundances (Figure A5). Although there is no strong evidence that this REE-Y enrichment affects isotopic ratios [*Clague*, 1987; *Cotten et al.*, 1995], i.e., the REE-Y mobilization and deposition is highly localized, we did not analyze these West Molokai lavas for isotopic ratios.

Acknowledgments

[67] G. X. thanks Frank Dudas for his help and guidance for the Sr, Nd, and Pb isotope analyses and column separations. Sam Bowring is thanked for providing financial support for the isotopic analyses at MIT. Rick Kayser is thanked for his assistance in ICP-MS analysis. F. Albarède, S. Galer, M. Garcia, and S. Huang are thanked for their comments and discussion. M. Bizimis, an anonymous reviewer, and V. Salters (editor) are thanked for their constructive reviews. Xu was supported by NSF grant EAR-0607895. D. A. C. was supported by a grant to MBARI from the David and Lucile Packard Foundation, which also supported the MBARI Hawaii expedition in 2001 when the submarine samples were expertly collected by the pilots of the ROV Tiburon. J. B. T. acknowledges financial support from INSU.

References

Abouchami, W., and F. A. Frey (2006), Temporal evolution of Pb isotopes in shield lavas from Haleakala Volcano, *Geophys. Res. Abstr.*, *8*, Abstract 03915.

Abouchami, W., S. J. G. Galer, and A. W. Hofmann (2000), High precision lead isotope systematics of lavas from the Hawaiian Scientific Drilling Project, *Chem. Geol.*, *169*, 187–209.

Abouchami, W., A. W. Hofmann, S. J. G. Galer, F. A. Frey, J. Eisele, and M. Feigenson (2005), Lead isotopes reveal bilateral asymmetry and vertical continuity in the Hawaiian mantle plume, *Nature*, *434*, 851–856.

Basu, A. R., and B. E. Faggart (1996), Temporal isotopic variations in the Hawaiian mantle plume: The Lanai anomaly, the Molokai Fracture Zone and a seawater-altered lithospheric

component in Hawaiian volcanism, in *Earth Processes: Reading the Isotopic Code*, *Geophys. Monogr. Ser.*, vol. 95, edited by A. R. Basu and S. R. Hart, pp. 149–159, AGU, Washington, D. C.

Bedard, J. H. (2005), Partitioning coefficients between olivine and silicate melts, *Lithos*, *83*, 394–419.

Bindeman, I. N., A. M. Davis, and M. J. Drake (1998), Ion microprobe study of plagioclase-basalt partition experiments at natural concentration levels of trace elements, *Geochim. Cosmochim. Acta*, *62*, 1175–1193.

Bizimis, M., G. Sen, V. J. M. Salters, and S. Keshav (2005), Hf-Nd-Sr isotope systematics of garnet pyroxenites from Salt Lake Crater, Oahu, Hawaii: Evidence for a depleted component in Hawaiian volcanism, *Geochim. Cosmochim. Acta*, *69*, 2629–2646.

Blichert-Toft, J., and F. Albarède (1999), Hf isotopic compositions of the Hawaii Scientific Drilling Project core and the source mineralogy of Hawaiian basalts, *Geophys. Res. Lett.*, *26*, 935–938.

Blichert-Toft, J., C. Chauvel, and F. Albarède (1997), Separation of Hf and Lu for high-precision isotope analysis of rock samples by magnetic sector multiple collector ICP-MS, *Contrib. Mineral. Petrol.*, *127*, 248–260.

Blichert-Toft, J., F. A. Frey, and F. Albarède (1999), Hf isotope evidence for pelagic sediments in the source of Hawaiian basalts, *Science*, *285*, 879–882.

Blichert-Toft, J., D. Weis, C. Maerschalk, A. Agranier, and F. Albarède (2003), Hawaiian hot spot dynamics as inferred from the Hf and Pb isotope evolution of Mauna Kea volcano, *Geochem. Geophys. Geosyst.*, *4*(2), 8704, doi:10.1029/2002GC000340.

Blundy, J., and J. Dalton (2000), Experimental comparison of trace element partitioning between clinopyroxene and melt in carbonate and silicate systems, and implications for mantle metasomatism, *Contrib. Mineral. Petrol.*, *139*, 356–371.

Bryce, J. G., D. J. DePaolo, and J. C. Lassiter (2005), Geochemical structure of the Hawaiian plume: Sr, Nd, and Os isotopes in the 2.8 km HSDP-2 section of Mauna Kea volcano, *Geochem. Geophys. Geosyst.*, *6*, Q09G18, doi:10.1029/2004GC000809.

Chen, C. Y., and F. A. Frey (1985), Trace-element and isotopic geochemistry of lavas from Haleakala Volcano, East Maui, Hawaii: Implications for the origin of Hawaiian basalts, *J. Geophys. Res.*, *90*, 8743–8768.

Chen, C. Y., F. Frey, J. M. Rhodes, and R. M. Easton (1996), Temporal geochemical evolution of Kilauea volcano: Comparison of Hilina and Puna basalt, in *Earth Processes: Reading the Isotopic Code*, *Geophys. Monogr. Ser.*, vol. 95, pp. 161–181, AGU, Washington, D. C.

Clague, D. A. (1987), Petrology of West Molokai Volcano, *Geol. Soc. Am. Abstr. Programs*, *19*, 366.

Clague, D. A., and G. B. Dalrymple (1987), The Hawaiian-Emperor volcanic chain: Part I: Geologic evolution, *U.S. Geol. Sury. Prof. Pap.*, *1350*, 5–54.

Clague, D. A., and F. A. Frey (1982), Petrology and trace-element geochemistry of the Honolulu volcanics, Oahu—Implications for the oceanic mantle below Hawaii, *J. Petrol.*, *23*, 447–504.

Clague, D. A., J. G. Moore, J. E. Dixon, and W. B. Friesen (1995), Petrology of submarine lavas from Kilaueas Puna Ridge, Hawaii, *J. Petrol.*, *36*, 299–349.

Cohen, A. S., R. K. Onions, and M. D. Kurz (1996), Chemical and isotopic variations in Mauna Loa tholeiites, *Earth Planet. Sci. Lett.*, *143*, 111–124.

Coombs, M. L., T. W. Sisson, and P. W. Lipman (2006), Growth history of Kilauea inferred from volatile concentrations in submarine-collected basalts, *J. Volcanol. Geotherm. Res.*, *151*, 19–49.

Cotten, J., A. Ledez, M. Bau, M. Caroff, R. C. Maury, P. Dulski, S. Fourcade, M. Bohn, and R. Brousse (1995), Origin of anomalous rare-earth element and yttrium enrichments in subaerially exposed basalts: Evidence from French Polynesia, *Chem. Geol.*, *119*, 115–138.

Cousens, B. L., D. A. Clague, and W. D. Sharp (2003), Chronology, chemistry, and origin of trachytes from Hualalai Volcano, Hawaii, *Geochem. Geophys. Geosyst.*, *4*(9), 1078, doi:10.1029/2003GC000560.

DePaolo, D., E. Stolper, D. Tomas, and M. O. Garcia (1999), Hawaii Scientific Drilling Project: Core logs and summarizing data, report, Calif. Inst. of Technol., Pasadena.

DePaolo, D. J., J. G. Bryce, A. Dodson, D. L. Shuster, and B. M. Kennedy (2001), Isotopic evolution of Mauna Loa and the chemical structure of the Hawaiian plume, *Geochem. Geophys. Geosyst.*, *2*(7), doi:10.1029/2000GC000139.

Dixon, J. E., D. A. Clague, and E. M. Stolper (1991), Degassing history of water, sulfur, and carbon in submarine lavas from Kilauea Volcano, Hawaii, *J. Geol.*, *99*, 371–394.

Eisele, J., W. Abouchami, S. J. G. Galer, and A. W. Hofmann (2003), The 320 kyr Pb isotope evolution of Mauna Kea lavas recorded in the HSDP-2 drill core, *Geochem. Geophys. Geosyst.*, *4*(5), 8710, doi:10.1029/2002GC000339.

Feigenson, M. D., A. W. Hofmann, and F. J. Spera (1983), Case studies on the origin of basalt II, The transition from tholeiitic to alkalic volcanism on Kohala Volcano, Hawaii, *Contrib. Mineral. Petrol.*, *V84*, 390–405.

Fekiacova, Z., W. Abouchami, S. J. G. Galer, M. Garcia, and A. W. Hofmann (2007), Temporal evolution of Koolau volcano: Inferences from isotope results on the Koolau Scientific Drilling Project (KSDP) and Honolulu Volcanics, *Earth Planet. Sci. Lett.*, doi:10.1016/j.epsl.2007.06.005, in press.

Fodor, R. V., D. P. Malta, G. R. Bauer, and R. S. Jacobs (1989), Microbeam analyses of rare-earth element phosphate in basalt from Kahoolawe Island, Hawaii, paper presented at the 24th Annual Conference of the Microbeam Analytical Society, San Francisco, Calif.

Fodor, R. V., F. A. Frey, G. R. Bauer, and D. A. Clague (1992), Ages, rare-earth element enrichment, and petrogenesis of tholeiitic and alkalic basalts from Kahoolawe Island, Hawaii, *Contrib. Mineral. Petrol.*, *110*, 442–462.

Frey, F. A., and J. M. Rhodes (1993), Intershield geochemical differences among Hawaiian volcanoes: Implications for source compositions, melting process and magma ascent paths, *Philos. Trans. R. Soc. London, Ser. A*, *342*, 121–136.

Frey, F. A., W. S. Wise, M. O. Garcia, H. West, S. T. Kwon, and A. Kennedy (1990), Evolution of Mauna-Kea Volcano, Hawaii: Petrologic and geochemical constraints on post-shield volcanism, *J. Geophys. Res.*, *95*, 1271–1300.

Frey, F. A., M. O. Garcia, W. S. Wise, A. Kennedy, P. Gurriet, and F. Albarède (1991), The evolution of Mauna Kea Volcano, Hawaii: Petrogenesis of tholeiitic and alkalic basalts, *J. Geophys. Res.*, *96*, 14,347–14,375.

Frey, F. A., M. O. Garcia, and M. F. Roden (1994), Geochemical characteristics of Koolau Volcano: Implications of intershield geochemical differences among Hawaiian volcanoes, *Geochim. Cosmochim. Acta*, *58*, 1441–1462.

Frey, F. A., S. Huang, J. Blichert-Toft, M. Regelous, and M. Boyet (2005), Origin of depleted components in basalt related to the Hawaiian hot spot: Evidence from isotopic and incompatible element ratios, *Geochem. Geophys. Geosyst.*, *6*, Q02L07, doi:10.1029/2004GC000757.

Gaffney, A. M., B. K. Nelson, and J. Blichert-Toft (2004), Geochemical constraints on the role of oceanic lithosphere

in intra-volcano heterogeneity at West Maui, Hawaii, *J. Petrol.*, *45*, 1663–1687.

Gaffney, A. M., B. K. Nelson, and J. Blichert-Toft (2005), Melting in the Hawaiian plume at 1–2 Ma as recorded at Maui Nui: The role of eclogite, peridotite, and source mixing, *Geochem. Geophys. Geosyst.*, *6*, Q10L11, doi:10.1029/2005GC000927.

Galer, S. J. G., and W. Abouchami (1998), Practical application of lead triple spiking for correction of instrumental mass discrimination, *Mineral. Mag.*, *62A*, 491–492.

Garcia, M. O. (1996), Petrography and olivine and glass chemistry of lavas from the Hawaii Scientific Drilling Project, *J. Geophys. Res.*, *101*, 11,701–11,713.

Garcia, M. O., D. W. Muenow, K. E. Aggrey, and J. R. Oneil (1989), Major element, volatile, and stable isotope geochemistry of Hawaiian submarine tholeiitic glasses, *J. Geophys. Res.*, *94*, 10,525–10,538.

Garcia, M. O., T. P. Hulsebosch, and J. M. Rhodes (1995), Olivine-rich submarine basalts from the southwest rift zone of Mauna Loa volcano: Implications for magmatic processes and geochemical evolution, in *Mauna Loa Revealed: Structure, Composition, History, and Hazards*, *Geophys. Monogr. Ser.*, vol. 92, edited by J. M. Rhodes and J. P. Lockwood, pp. 219–239, AGU, Washington, D. C.

Hammer, J. E., M. L. Coombs, P. J. Shamberger, and J.-I. Kimura (2006), Submarine sliver in North Kona: A window into the early magmatic and growth history of Hualalai Volcano, Hawaii, *J. Volcanol. Geotherm. Res.*, *151*, 157–188.

Hanano, D., D. Weis, S. Aciego, J. Scoates, and D. DePaolo (2005), Geochemical systematics of Hawaiian postshield lavas: Implications for the chemical structure of the Hawaiian mantle plume, *Eos Trans. AGU*, *86*(52), Fall Meet. Suppl., Abstract V41D-1497.

Haskins, E. H., and M. O. Garcia (2004), Scientific drilling reveals geochemical heterogeneity within the Ko'olau shield, Hawai'i, *Contrib. Mineral. Petrol.*, *147*, 162–188.

Hauri, E. H., J. C. Lassiter, and D. J. DePaolo (1996), Osmium isotope systematics of drilled lavas from Mauna Loa, Hawaii, *J. Geophys. Res.*, *101*, 11,793–11,806.

Helz, R. T., and T. L. Wright (1992), Differentiation and magma mixing on Kilauea East Rift Zone—A further look at the eruptions of 1955 and 1960. 1. The late 1955 lavas, *Bull. Volcanol.*, *54*, 361–384.

Herzberg, C. (2005), Mantle geochemistry: Big lessons from little droplets, *Nature*, *436*, 789–790.

Hieronymus, C. F., and D. Bercovici (2001), A theoretical model of hotspot volcanism: Control on volcanic spacing and patterns via magma dynamics and lithospheric stresses, *J. Geophys. Res.*, *106*, 683–702.

Hofmann, A. W. (2004), Sampling mantle heterogeneity through oceanic basalts: Isotopes and trace elements, in *Treatise on Geochemistry*, edited by H. D. Holland and K. K. Turekian, pp. 61–101, Elsevier, Oxford.

Hofmann, A. W., and W. M. White (1983), Ba, Rb and Cs in the Earth's mantle, *Z. Naturforsch. Sect. A J. Phys. Sci.*, *38*, 256–266.

Huang, S., and F. A. Frey (2003), Trace element abundances of Mauna Kea basalt from phase 2 of the Hawaii Scientific Drilling Project: Petrogenetic implications of correlations with major element content and isotopic ratios, *Geochem. Geophys. Geosyst.*, *4*(6), 8711, doi:10.1029/2002GC000322.

Huang, S., and F. A. Frey (2005a), The geochemical structure of the Hawaiian Plume, *Eos Trans. AGU*, *86*(52), Fall Meet. Suppl., Abstract V51A-1466.

Huang, S., and F. A. Frey (2005b), Recycled oceanic crust in the Hawaiian Plume: Evidence from temporal geochemical variations within the Koolau Shield, *Contrib. Mineral. Petrol.*, *149*, 556–575.

Huang, S., F. Frey, J. Blichert-Toft, R. V. Fodor, and G. Xu (2005a), Depleted rejuvenated-stage source component in Hawaiian shield-stage lavas, *Geochim. Cosmochim. Acta*, *69*, A104.

Huang, S., F. A. Frey, J. Blichert-Toft, R. V. Fodor, G. R. Bauer, and G. Xu (2005b), Enriched components in the Hawaiian plume: Evidence from Kahoolawe Volcano, Hawaii, *Geochem. Geophys. Geosyst.*, *6*, Q11006, doi:10.1029/2005GC001012.

Huang, S., M. Regelous, T. Thordarson, and F. A. Frey (2005c), Petrogenesis of lavas from Detroit Seamount: Geochemical differences between Emperor Chain and Hawaiian volcanoes, *Geochem. Geophys. Geosyst.*, *6*, Q01L06, doi:10.1029/2004GC000756.

Huang, S., M. Bizimis, R. V. Fodor, and G. R. Bauer (2006), Geochemical structure of the Hawaiian Plume: Constraints from the shield to postshield transition, *Eos Trans. AGU*, *87*(52), Fall Meet. Suppl., Abstract V13B-0665.

Ito, G., and J. J. Mahoney (2005), Flow and melting of a heterogeneous mantle: 1. Method and importance to the geochemistry of ocean island and mid-ocean ridge basalts, *Earth Planet. Sci. Lett.*, *230*, 29–46.

Jackson, D. E., E. A. Silver, and G. B. Dalrymple (1972), Hawaiian-Emperor chain and its relation to Cenozoic circumpacific tectonics, *Geol. Soc. Am. Bull.*, *83*, 601–618.

Jang, Y. D., and H. R. Naslund (2003), Major and trace element variation in ilmenite in the Skaergaard Intrusion: Petrologic implications, *Chem. Geol.*, *193*, 109–125.

Kennedy, A. K., S. T. Kwon, F. A. Frey, and H. B. West (1991), The isotopic composition of postshield lavas from Mauna-Kea Volcano, Hawaii, *Earth Planet. Sci. Lett.*, *103*, 339–353.

Kurz, M. D., T. C. Kenna, D. P. Kammer, J. M. Rhodes, and M. O. Garcia (1995), Isotopic evolution of Mauna Loa volcano: A view from the submarine Southwest Rift Zone, in *Mauna Loa Revealed: Structure, Composition, History, and Hazards*, *Geophys. Monogr. Ser.*, vol. 92, edited by J. M. Rhodes and J. P. Lockwood, pp. 289–306, AGU, Washington, D. C.

Kurz, M. D., J. Curtice, D. E. Lott, III, and A. Solow (2004), Rapid helium isotopic variability in Mauna Kea shield lavas from the Hawaiian Scientific Drilling Project, *Geochem. Geophys. Geosyst.*, *5*, Q04G14, doi:10.1029/2002GC000439.

Lassiter, J. C., D. J. DePaolo, and M. Tatsumoto (1996), Isotopic evolution of Mauna Kea volcano: Results from the initial phase of the Hawaii Scientific Drilling Project, *J. Geophys. Res.*, *101*, 11,769–11,780.

Macdonald, G. A., and T. Katsura (1964), Chemical compositional of Hawaiian lavas, *J. Petrol.*, *5*, 82–133.

McDougall, I. (1964), Potassium-argon ages from lavas of the Hawaiian Islands, *Geol. Soc. Am. Bull.*, *75*, 107–128.

Menard, H. W. (1962), Correlation between length and offset on very large wrench faults, *J. Geophys. Res.*, *67*, 4096–4098.

Moore, J. G., and D. A. Clague (1987), Coastal lava flows from Mauna Loa and Hualalai volcanoes, Kona, Hawaii, *Bull. Volcanol.*, *49*, 752–764.

Moore, J. G., and D. A. Clague (1992), Volcano growth and evolution of the island of Hawaii, *Geol. Soc. Am. Bull.*, *104*, 1471–1484.

Moore, J. G., and D. A. Clague (2002), Mapping the Nuuanu and Wailau landslides in Hawaii, in *Hawaiian Volcanoes: Deep Underwater Perspectives*, *Geophys. Monogr. Ser.*,

vol. 128, edited by E. Takahashi et al., pp. 223–244, AGU, Washington, D. C.

Moore, J. G., D. A. Clague, and W. R. Normark (1982), Diverse basalt types from Loihi Seamount, Hawaii, *Geology*, *10*, 88–92.

Moore, J. G., W. B. Bryan, M. H. Beeson, and W. R. Normark (1995), Giant blocks in the south Kona landslide, Hawaii, *Geology*, *23*, 125–128.

Morgan, J. K., D. A. Clague, D. C. Borchers, A. S. Davis, and K. L. Milliken (2007), Mauna Loa's submarine western flank: Landsliding, deep volcanic spreading, and hydrothermal alteration, *Geochem. Geophys. Geosyst.*, *8*, Q05002, doi:10.1029/2006GC001420.

Pietruszka, A. J., and M. O. Garcia (1999), The size and shape of Kilauea Volcano's summit magma storage reservoir: A geochemical probe, *Earth Planet. Sci. Lett.*, *167*, 311–320.

Price, J. P., and D. Elliott-Fisk (2004), Topographic history of the Maui Nui Complex, Hawaii, and its implications for biogeography, *Pac. Sci.*, *58*, 27–45.

Ren, Z. Y., S. Ingle, E. Takahashi, N. Hirano, and T. Hirata (2005), The chemical structure of the Hawaiian mantle plume, *Nature*, *436*, 837–840.

Ren, Z. Y., T. Shibata, M. Yoshikawa, K. T. M. Johnson, and E. Takahashi (2006), Isotope compositions of submarine Hana Ridge lavas, Haleakala volcano, Hawaii: Implications for source compositions, melting process and the structure of the Hawaiian plume, *J. Petrol.*, *47*, 255–275.

Rhodes, J. M. (1995), The 1852 and 1868 Mauna Loa picrite eruptions: Clues to parental magma compositions and the magmatic plumbing system, in *Mauna Loa Revealed: Structure, Composition, History, and Hazards*, *Geophys. Monogr. Ser.*, vol. 92, edited by J. M. Rhodes and J. P. Lockwood, pp. 241–262, AGU, Washington, D. C.

Rhodes, J. M. (1996), Geochemical stratigraphy of lava flows sampled by the Hawaii Scientific Drilling Project, *J. Geophys. Res.*, *101*, 11,729–11,746.

Rhodes, J. M., and S. R. Hart (1995), Episodic trace element and isotopic variations in historical Mauna Loa lavas: Implications for Magma and plume dynamics, in *Mauna Loa Revealed: Structure, Composition, History, and Hazards*, *Geophys. Monogr. Ser.*, vol. 92, edited by J. M. Rhodes and J. P. Lockwood, pp. 263–288, AGU, Washington, D. C.

Rhodes, J. M., and M. J. Vollinger (2004), Composition of basaltic lavas sampled by phase-2 of the Hawaii Scientific Drilling Project: Geochemical stratigraphy and magma types, *Geochem. Geophys. Geosyst.*, *5*, Q03G13, doi:10.1029/2002GC000434.

Robinson, J. E., and B. W. Eakins (2006), Calculated volumes of individual shield volcanoes at the young end of the Hawaiian Ridge, *J. Volcanol. Geotherm. Res.*, *151*, 309–317.

Roden, M. F., T. Trull, S. R. Hart, and F. A. Frey (1994), New He, Nd, Pb, and Sr isotopic constraints on the constitution of the Hawaiian Plume—Results from Koolau Volcano, Oahu, Hawaii, USA, *Geochim. Cosmochim. Acta*, *58*, 1431–1440.

Salters, V. J. M., J. Blichert-Toft, Z. Fekiacova, A. Sachi-Kocher, and M. Bizimis (2006), Isotope and trace element evidence for depleted lithosphere in the source of enriched Ko'olau basalts, *Contrib. Mineral. Petrol.*, *151*, 297–312.

Searle, R. C., R. T. Holcomb, J. B. Wilson, M. L. Holmes, R. J. Whittington, E. S. Kappel, B. A. McGregor, and A. N. Shor (1993), The Molokai Fracture Zone near Hawaii, and the Late Cretaceous change in Pacific/Farallon spreading direction, in *The Mesozoic Pacific: Geology, Tectonics, and Volcanism*, *Geophys. Monogr. Ser.*, vol. 77, edited by M. S. Pringle et al., pp. 155–169, AGU, Washington, D. C.

Shinozaki, K., Z.-Y. Ren, and E. Takahashi (2002), Geochemical and petrological characteristics of Nuuanu and Wailau landslides blocks, in *Hawaiian Volcanoes: Deep Underwater Perspectives*, *Geophys. Monogr. Ser.*, vol. 128, edited by E. Takahashi et al., pp. 297–310, AGU, Washington, D. C.

Sinton, J. M. (1987), Revision of stratigraphic nomenclature of Waianae Volcano, Oahu, Hawaii, *U.S. Geol. Surv. Bull.*, *1775A*, A9–A15.

Sisson, T. W., and P. W. Lipman (2002), Submarine alkalic through tholeiitic shield-stage development of Kilauea Volcano, Hawaii, in *Hawaiian Volcanoes: Deep Underwater Perspectives*, *Geophys. Monogr. Ser.*, vol. 128, edited by E. Takahashi et al., pp. 193–219, AGU, Washington, D. C.

Sobolev, A. V., A. W. Hofmann, S. V. Sobolev, and I. K. Nikogosian (2005), An olivine-free mantle source of Hawaiian shield basalts, *Nature*, *434*, 590–597.

Steiger, R. H., and E. Jager (1977), Subcommission on Geochronology—Convention on Use of Decay Constants in Geochronology and Cosmochronology, *Earth Planet. Sci. Lett.*, *36*, 359–362.

Stille, P., D. M. Unruh, and M. Tatsumoto (1986), Pb, Sr, Nd, and Hf isotopic constraints on the origin of Hawaiian basalts and evidence for a unique mantle source, *Geochim. Cosmochim. Acta*, *50*, 2303–2319.

Stolper, E., S. Sherman, M. Garcia, M. Baker, and C. Seaman (2004), Glass in the submarine section of the HSDP2 drill core, Hilo, Hawaii, *Geochem. Geophys. Geosyst.*, *5*, Q07G15, doi:10.1029/2003GC000553.

Stracke, A., V. J. M. Salters, and K. W. W. Sims (1999), Assessing the presence of garnet-pyroxenite in the mantle sources of basalts through combined hafnium-neodymium-thorium isotope systematics, *Geochem. Geophys. Geosyst.*, *1*(1), doi:10.1029/1999GC000013.

Sun, S.-S., and W. F. McDonough (1989), Chemical and isotopic systematics of oceanic basalts: Implications for mantle composition and processes, in *Magmatism in the Ocean Basins*, edited by A. D. Saunders and M. J. Norry, *Geol. Soc. Spec. Publ.*, *42*, 313–345.

Tanaka, R., E. Nakamura, and E. Takahashi (2002), Geochemical evolution of Koolau Volcano, Hawaii, in *Hawaiian Volcanoes: Deep Underwater Perspectives*, *Geophys. Monogr. Ser.*, vol. 128, edited by E. Takahashi et al., pp. 311–332, AGU, Washington, D. C.

Tatsumoto, M. (1978), Isotopic composition of lead in oceanic basalt and its implication to mantle evolution, *Earth Planet. Sci. Lett.*, *38*, 63–87.

ten Brink, U. S., and T. M. Brocher (1988), Multichannel seismic evidence for variations in crustal thickness across the Molokai Fracture Zone in the mid-Pacific, *J. Geophys. Res.*, *93*, 1119–1130.

Todt, W., R. A. Cliff, A. Hanser, and A. W. Hofmann (1996), Evaluation of a $^{202}Pb/^{205}Pb$ double spike for high-precision lead isotope analysis, in *Earth Processes: Reading the Isotopic Code*, *Geophys. Monogr. Ser.*, vol. 95, edited by A. Basu and S. R. Hart, pp. 429–437, AGU, Washington, D. C.

Wanless, V. D., M. O. Garcia, J. Michael Rhodes, D. Weis, and M. D. Norman (2006), Shield-stage alkalic volcanism on Mauna Loa Volcano, Hawaii, *J. Volcanol. Geotherm. Res.*, *151*, 141–155.

Weisler, M. I., and D. A. Clague (1998), Characterization of archaeological volcanic glass from Oceania: The utility of three techniques, in *Archaeological Obsidian Studies: Methods and Theory*, edited by M. S. Shackley, pp. 103–128, Plenum, New York.

Wessel, P., and L. Kroenke (1997), A geometric technique for relocating hotspots and refining absolute plate motions, *Nature*, *387*, 365–369.

West, H. B., D. C. Gerlach, W. P. Leeman, and M. O. Garcia (1987), Isotopic constraints on the origin of Hawaiian lavas from the Maui volcanic complex, Hawaii, *Nature*, *330*, 216–220.

West, H. B., M. O. Garcia, F. A. Frey, and A. Kennedy (1988), Nature and cause of compositional variation among the Alkalic Cap lavas of Mauna Kea Volcano, Hawaii, *Contrib. Mineral. Petrol.*, *100*, 383–397.

Xu, G., F. A. Frey, D. A. Clague, D. Weis, and M. H. Beeson (2005), East Molokai and other Kea-trend volcanoes: Magmatic processes and sources as they migrate away from the Hawaiian hot spot, *Geochem. Geophys. Geosyst.*, *6*, Q05008, doi:10.1029/2004GC000830.

Yang, H. J., F. A. Frey, J. M. Rhodes, and M. O. Garcia (1996), Evolution of Mauna Kea volcano: Inferences from lava compositions recovered in the Hawaii Scientific Drilling Project, *J. Geophys. Res.*, *101*, 11,747–11,767.

Yang, H. J., F. A. Frey, D. A. Clague, and M. O. Garcia (1999), Mineral chemistry of submarine lavas from Hilo Ridge, Hawaii: Implications for magmatic processes within Hawaiian rift zones, *Contrib. Mineral. Petrol.*, *135*, 355–372.

Zindler, A., H. Staudigel, and R. Batiza (1984), Isotope and trace element geochemistry of young Pacific seamounts: Implications for the scale of upper mantle heterogeneity, *Earth Planet. Sci. Lett.*, *70*, 175–195.